TECHNICAL UNIVERSITY OF MOLDOVA

As a manuscript
UDC 664:663.058.9:536.757:664-4

Alexei Baerle

PROLONGING THE FUNCTIONALITY OF BIOLOGICALLY ACTIVE COMPOUNDS IN FOOD COMPOSITIONS

253.06. Biological and Chemical Technologies in the Food Industry

Summary of the Doctor Habilitat Thesis in Engineering Sciences

Scientific consultant: **STURZA Rodica,**
Doctor Habilitat, Professor,
Correspondent Member of
Academy of Sciences of Moldova

Author: **BAERLE Alexei**

Chișinău, 2026

The Thesis was developed within the Doctoral School of the Technical University of Moldova, Faculty of Food Technology, Department of Oenology and Chemistry, Department of Food Products Technology.

Scientific consultant:
STURZA Rodica - Doctor Habilit in Technical Sciences, University Professor, ASM Corresponding Member

The Public Defence Committee authorized to organize the defence of the Habilitat Thesis was approved with the following composition:

Chairman:	***Balan Valerian***	Dr. Habil., Prof.
Reviewer:	***Arâcu Aculina***	Dr. Habil., Prof., Corr. Memb. ASM
Reviewer:	***Boincean Boris***	Dr. Habil., Prof., Corr. Memb. ASM
Reviewer:	***Siminiuc Rodica***	Dr. Habil., Assoc. Prof.
Reviewer:	***Balan Greta***	Dr. Habil., Assoc. Prof.
Member:	***Duca Gheorghe***	Dr. Habil., Prof., Acad. ASM
Member:	***Sturza Rodica***	Dr. Habil., Prof., Corr. Memb. ASM

The defense will take place on **28 May 2026,**
at the meeting of the Public Defence Committee for the Doctor Habilitat Thesis, Technical University of Moldova, at the following address: 9/9 Studenților Street, academic building no. 5, room 5-1, MD-2045, Chișinău, Republic of Moldova.

The Doctor Habilitat Thesis and its abstract may be consulted at the library of the Technical University of Moldova and on the website of the National Agency for Quality Assurance in Education and Research (ANACEC). (www.anacec.md).
The abstract was distributed on: 22 April 2026

Scientific consultant: STURZA Rodica

Author: BAERLE Alexei

ADNOTATION

BAERLE Alexei: **"Prolonging the Functionality of Biologically Active Compounds in Food Compositions". Doctor Habilitatus Thesis in Engineering Sciences.**

Thesis structure: Abstract (RO, EN), Introduction, 6 Chapters, General Conclusions and Recommendations, Bibliography of 424 titles. The core text of the Thesis comprises 169 pages and includes 88 figures and 40 tables. The results have been published in 49 scientific papers, including: 1 monograph; 4 chapters in edited volume; 5 articles indexed in Web of Science, PubMed, Scopus; 8 articles recognized by NAQAER (ANACEC); 9 patents.

Study field: 253.06 – Biological & chemical technologies in the food industry.

Keywords: anthocyanins, betanin, biopolymers, chalcones, combinatorics, entropy control, fermented dairy products, mathematical modeling, microencapsulation, phase diagrams, polyunsaturated lipids, stability of biological systems, thermodynamic functions.

Research goal: To elaborate and to validate innovative strategies for prolonging the functionality of biologically active compounds (BACs), through the integration of classical and modern instrumental methods by development of thermodynamic, statistical and combinatorial models, the design of patentable procedures for extracting of functional biopolymers, microencapsulation of lipids and fat-soluble vitamins, complexing pigments with biopolymers, as well as for monitoring of physico-chemical parameters relevant to food processing technologies.

Objectives: Clarify the mechanisms of BAC stabilization under physico-chemical and mechanical factors; to optimize extraction/separation procedures of BAC from vegetal sources; to adapt instrumental methods for monitoring BAC functionality in food systems; apply combinatorial and statistical modeling for multiphase systems; to identify biopolymer–BAC interactions; to validate the applicability of long-acting BAC; to develop technological solutions for the use of natural colorants in fermented foods; to analyze the role of physico-chemical phenomena in stabilization; to elaborate the microencapsulation technology; to demonstrate biosynthesis thermodynamic; to establish the causal link between thermodynamics of BAC accumulation and the maximization of food value; patent technological schemes for prolongation of foods functional activity.

Scientific novelty and originality. Here, the prolongation of BAC functionality in foods is represented as a counterpart of entropic control: hierarchization; removal of destabilizing compounds; antioxidant synergism; BAC-polymer complexation; microstructure formation. The points of novelty are: (1) new research protocols: electrochemical control of microencapsulation, polydispersity analysis, RGB profile determination, the hybrid use of instrumental techniques and mathematical modeling; (2) the

development of models combining chemical analysis and process simulation; (3) the evaluation of food quality in relation to BAC functionality.

Results obtained. Regression equations, thermodynamic paramrters, statistical and combinatorial models; interpretation of UV-Vis, FTIR-ATR spectra and HPLC/PDA chromatograms; CIE-Lab and RGB chromatic profiles; phase diagrams of protein–polyuronate compositions and W/O/W emulsions; stabilization mechanisms of biopolymer–pigment–water systems.

Theoretical significance: Reasoned clarification of certain controversial aspects in the thermodynamics of biological systems; demonstration of the usefulness of thought experiments in the study of food compositions; analysis of the limited efficacy of traditional methods for maintaining BAC functionality; elaboration of new operational systems and technological approaches to ensure extended functionality of BACs in food compositions; elucidation of stabilization mechanisms in structured systems.

Practical value: The results support the development of functional foods, the evaluation of BAC stability and food quality monitoring, contributing to more efficient food technologies and high-quality products, strengthening research infrastructure and TUM-industry partnerships, increasing the competitiveness of the Republic of Moldova on the European market.

Results implementation: Some results were implemented in the courses "Physical Chemistry" and „Biochemistry". 9 invention patents were granted.

ADNOTARE

BAERLE Alexei: „Prolongarea funcționalității compușilor biologic activi în compozițiile alimentare". Teza de doctor habilitat în științe inginerești.

Structura tezei: Adnotare (RO, EN), Introducere, 6 Capitole, Concluzii generale și Recomandări, Bibliografie din 424 titluri. Textul de bază a tezei 169 pagini, include 88 figuri și 40 tabele. Rezultatele obținute au fost publicate în 49 de lucrări științifice, dintre care: 1 monografie; 4 capitole în monografie colectivă; 5 articole clasate în baze Web of Science, PubMed, Scopus, 8 articole recunoscute de ANACEC în reviste de categorie B^+, 9 brevete.

Domeniul: 253.06 – Tehnologii biologice și chimice în industria alimentară.

Cuvinte-cheie: anti-entropie, antocieni, betanină, biopolimeri, chinocalcone, combinatorica, diagrame de stare, funcții termodinamice, entropie, lipide polinesaturate, microîncapsulare, modelarea matematică, produse acido-lactice, stabilitate sisteme biologice.

Scopul lucrării: Elaborarea și validarea strategiilor inovatoare de prolongare a funcționalității CBA, integrarea metodelor instrumentale clasice și moderne de cercetare, dezvoltarea modelelor termodinamice, statistice și combinatorice, elaborarea procedeelor brevetabile de extracție a biopolimerilor funcționali, de microîncapsulare a lipidelor și vitaminelor liposolubile, de complexare a coloranților cu biopolimeri, monitorizarea și controlul parametrilor fizico-chimici ai proceselor tehnologice relevante pentru industria alimentară.

Obiectivele: Precizarea mecanismelor de stabilizare a CBA sub acțiunea factorilor fizico-chimici și mecanici; optimizarea procedeelor de separare a CBA din surse vegetale; adaptarea metodelor instrumentale pentru monitorizarea funcționalității CBA în sisteme alimentare; modelarea combinatorică și statistică a sistemelor polifazice; identificarea interacțiunilor biopolimer-CBA; validarea aplicabilității CBA cu activitatea prolongată; adaptarea tehnologică a coloranților naturali în produse fermentate; analiza rolului fenomenelor fizico-chimice, elaborarea tehnologiei de microîncapsulare; demonstrarea aspectului termodinamic al biosintezei, stabilirea legăturii cauzale între termodinamica acumulării CBA și maximizarea valorii alimentelor; brevetarea procedeilor și schemelor tehnologice de prolongare a activității funcționale a CBA în alimente.
Noutatea și originalitatea: În premieră, prolongarea funcționalității CBA în alimente este reprezentată ca replica controlului entropic al proceselor: asamblarea ierarhiilor, îndepărtarea compușilor destabilizanți, sinergia antioxidanților, complexarea CBA cu biopolimeri, formarea microstructurilor. Noutatea se manifestă prin: 1) propunerea unor protocoale de cercetare noi: controlul electrochimic al microîncapsulării, analiza polidispersității, determinarea profilului RGB, utilizarea hibridă a tehnicilor instrumentale și a modelărilor statistico-matematice; 2) elaborarea modelelor integrate, care combină analiza chimică cu simularea proceselor; 3) definirea unor parametri de evaluare a calității alimentelor, raportați la funcționalitatea CBA.
Rezultatele obținute: ecuații de regresie, modele termodinamice, combinatorice, statistice; descifrările spectrelor (UV-Vis, FTIR-ATR) și cromatogramelor HPLC/PDA; profiluri cromatice CIE-Lab și RGB; diagramele de stare ale compozițiilor proteina-poliuronat, emulsiilor U/A/U; mecanismele de stabilizăre ale compozițiilor biopolimer-colorant-apă.
Semnificația teoretică: clarificarea argumentată a unor aspecte controversate ale termodinamicii sistemelor biologice, elucidarea cauzelor eficacității scăzute și potențialului limitat al unor metode tradiționale de asigurare a activității funcționale ale CBA, elaborarea noilor sisteme BY prolongare funcționalității CBA din compozițiile alimentare, elucidarea mecanismelor de stabilizare a CBA în diferite compoziții cu grad de structurizare ridicat.
Valoarea aplicativă: Rezultatele sunt valoroase pentru crearea alimentelor funcționale, evaluarea stabilității CBA și monitorizarea calității alimentelor, contribuind la tehnologii alimentare eficiente și produse de înaltă calitate, la consolidarea infrastructurii de cercetare și a parteneriatelor UTM–industrie, precum și la creșterea competitivității Republicii Moldova pe piața europeană.
Implementarea rezultatelor științifice: rezultatele au fost implementate în cursul „Chimie Fizică” și „Biochimie”. Pe tema tezei au fost eliberate 9 brevete de invenție.

CONCEPTUAL FRAMEWORK

Relevance and importance of the addressed topic. At the global level, a transition has occurred from infectious diseases to chronic non-communicable ones, closely associated with unbalanced nutrition poor in biologically active compounds (BAC). These compounds – anthocyanins, betalains, quinocalcones, polyunsaturated fatty acids, fibers, oligosaccharides – play an essential role in reducing oxidative stress and inflammation but are often unstable under processing and digestion conditions. The object of the research is the prolongation of BAC functionality in the food matrix through innovative technological solutions: multiphase microencapsulation, complexation with biopolymers, reorganization of aqueous phases and reduction of water activity. The structure of most BAC allows the application of UV-Vis methods, HPLC-PDA, RGB analysis, electrochemical techniques, and entropic/exergonic modelling, which make it possible to monitor BAC behavior under real and simulated conditions. The study results include patented technologies and contribute to the expansion of the portfolio of functional products, the valorization of plant resources, and the support of circular bioeconomy. The thesis is aligned with EU directions on public health and sustainability, proposing solutions transferable to the national and European food industry.

Aim of the thesis (general objective): To develop and validate innovative scientific and technological strategies for prolonging the functionality of biologically active compounds in model systems and food compositions, through the integration of classical and modern instrumental research methods, the development of mathematical models (thermodynamic, statistical and combinatorial), the elaboration of methods for extracting biopolymers with functional properties, for microencapsulating lipids and fat-soluble vitamins, for complexing natural colorants with biopolymers, and the monitoring and control of the physicochemical parameters of technological processes relevant to the food industry..

Objectives: The following operational objectives were formulated:

1. To clarify the mechanisms of destabilization/stabilization of biologically active compounds under the action of physicochemical and mechanical factors.
2. To develop and adapt advanced analytical methods (spectroscopic, chromatographic, electrochemical, hybrid) for real-time monitoring of the integrity and functional activity of BAC in model and real systems.
3. To optimize the procedures for obtaining BAC from plant sources, while maintaining their structural integrity and functional value in food products.
4. To develop and model - thermodynamically, combinatorially and statistically - polyphase systems: O/W/G emulsions and microcapsules; to obtain functional products with an optimized content of PUFAs.

5. To study and apply food biopolymers (alginate, hyaluronic acid, microcrystalline cellulose, etc.) as stabilizing agents for natural colorants, and to identify and explain beneficial or destabilizing interactions.
6. To obtain and validate the applicability of food supplements with high stability and prolonged activity in food media.
7. To adapt technologically natural colorants that are sensorially compatible with certain fermented products, to replace synthetic colorants.
8. To clarify and critically analyze the role of physicochemical phenomena in the microencapsulation process, and to improve the efficiency of microencapsulation technology.
9. To demonstrate the thermodynamic aspect of biosynthesis, establishing the causal relationship: thermodynamics of BAC accumulation => value of functional foods.
10. To develop and to patent procedures and technological schemes ensuring the prolongation of the functional activity of BACs in foods.

Hypothesis. It is assumed that the integration of classical and modern strategies for stabilizing biologically active compounds, including by modelling the influence of physicochemical factors, reducing system entropy, and applying microencapsulation and complexation procedures with biopolymers, will lead to the prolongation of the functionality of these compounds in foods. Process control by advanced analytical methods, matrix stabilization, and the targeted delivery effect will contribute to preserving the value of BAC under processing and consumption conditions.

Justification and synthesis of the research methodology. The research methodology integrated experimental techniques, mathematical models, and technological procedures for optimizing BAC stability. For qualitative and quantitative analysis, UV-Vis and HPLC/PDA ("DR 5000", "Shimadzu LC 2030", TUM), HPLC/MS ("Agilent 1260", UASVM Cluj) were used, selected for their high sensitivity to the chromophores of natural pigments. Polydispersity was analyzed by a new method combining image analysis with statistical-geometric calculations. For the study of BAC-biopolymer interactions, FTIR-ATR techniques ("Shimadzu Prestige 21", UASVM Cluj) were applied. CIE-Lab chromatic analysis ("Konica Minolta CR 400", TUM) was performed. A new RGB analysis method was also proposed. Control of microencapsulation was achieved using an integrated electrochemical system (multimeter, pH meter, thermostat, dispenser, stirrer), which allows real-time monitoring of essential parameters and elimination of intermediate stages. Process modelling was performed through thermodynamic and statistical calculations (the role of the hierarchical structure of food in BAC stability, the gelatin adsorption model) and combinatorial calculations (stability analysis of Oil/Water/Air systems). The methods were applied in vitro and on real systems (extracts, emulsions, dairy products).

Theoretical significance and scientific novelty are highlighted by:

- The prolongation of BAC functionality is correlated with their life cycle.
- Entropy reduction contributes to the prolongation of BAC functionality.
- The structuring of food systems ensures their anti-entropic stability.
- The reduction of entropy production can be achieved through the selective and extensive removal of destabilizing compounds, the synergistic antioxidants interaction, the BACs complexation with biopolymers, and the formation of ordered microstructures limiting systemic disorganization.

Research methods developed and applied for the first time:

- electrochemical control system for microencapsulation,
- method for analyzing the polydispersity of emulsions and suspensions,
- diversification of evaluation methods and increased accessibility of determining the chromatic aspect of samples in different phasic states,
- use of spectroscopic techniques, HPLC, and statistical-mathematical modelling for characterizing the stability of food systems.

Practical value. The high patentability of the obtained results suggests that they have practical value and can be applied for:

- the development of functional foods with stable BAC,
- the evaluation of the stability of colorants and antioxidants in foods,
- the use of the results in IT and AI platforms for quality monitoring,
- the diversification of local plant sources,
- policies for replacing synthetic additives with natural ingredients,
- the promotion of food education and conscious choice.

Approval of the thesis at national and international scientific forums. The main results of the thesis were presented and discussed at National and International Conferences.

International conferences held abroad: 11th International Symposium Euro-Aliment, 2023, Galați, România; Conference Euro-Aliment, the 10th International Symposium, 2021, Galați, România; 16th International Conference of Constructive Design and Technological Optimization in Machine Building Field, 2021, Bacău, România; 4th International Scientific Conference Agrobiodiversity Nutrition, Health and Quality of Human and Bees Life, 2019, Nitra, Slovak Republic.

International conferences held in the Republic of Moldova: International Conference Modern Technologies in The Food Industry, 2022, Chișinău, Republica Moldova; Conferința Intelligent Valorization of Agro-Food Industrial Wastes, 2021, Chișinău, Republica Moldova; International Conference Modern Technologies in the Food Industry, 2018, Chișinău, Republica Moldova. Likewise, the results of this thesis were also presented at national conferences: Technical and Scientific Conference of Students, Master's and Doctoral Students, 2021, Chisinau, RM (Diploma of the 3rd

degree); Technical and Scientific Conference of Students, Master's and Doctoral Students, 2019, Chisinau, Republic of Moldova (Diploma of the 2nd degree); Technical and Scientific Conference of Students, Master's and Doctoral Students, 2017, Chisinau, Republic of Moldova.

The results were also presented at a series of invention exhibitions: The 7th Innovation and Creative Education Fair for Youth ICE-USV. (Medalia de Bronz); Salonul Internațional al Cercetării Științifice, Inovării și Inventicii PRO INVENT, ediția a XX-a, 26-28 octombrie 2022, Cluj-Napoca, România (Medalia de Aur și Diploma de Apreciere de la Ministerul Sănătății al Republicii Moldova, Agenția Națională pentru Sănătate Publică); International Fair of Innovation and creative Education for Youth, ICE – USV, 5th Edition, 28-29 mai 2021, Suceava, România (Medalia de Bronz); Expoziţia Internaţională Specializată INFOINVENT, ediția a XVII-a, 17-20 noiembrie, 2021, Chișinău, Republica Moldova (Medalia de Bronz); European Exhibition of Creativity and Innovation, 13th edition - EUROINVENT, 22 mai, 2021, Iasi, Romania (Medalia de Aur); The 25th International Exhibition of Inventions, INVENTICA, ediția a XXV-a, 23-25 iunie, 2021, Iasi, Romania (Medalia de Argint); Salonul Internațional al Cercetării Științifice, Inovării și Inventicii PRO INVENT, ediția a XVIII-a, 18-20 noiembrie, 2020, Cluj-Napoca, România (Diploma de Excelență, Medalia de Aur și premiul „Augustin Maior").

Publications on the thesis topic: The obtained results were published in 49 works, including: 1 monograph; 4 chapters in a collective monograph prepared within the framework of State Project 20.80009.5107.09; 5 articles indexed in the scientometric databases Web of Science, PubMed and Scopus; 8 articles in journals indexed in databases accepted by NAQAER. Inventions, that were registered on the thesis topic – 9.

Summary of the thesis chapters. The thesis is presented on 169 pages of main text and includes the following sections: abstracts in Romanian and English, Introduction, 6 Chapters, 88 figures and 40 tables, General Conclusions and Recommendations. The Bibliography includes 424 references.

Introduction presents the scientific relevance of the thesis topic; the general objective (aim) of the thesis; the operational objectives; the general scientific hypothesis; the synthesis and justification of the research methodology; the theoretical significance and scientific novelty; the practical value of the thesis; the list of international and national forums and invention exhibitions where the thesis materials were presented; the description of publications; the summary of the chapters; and the keywords.

Keywords: *anthocyanins, betanin, biopolymers, chalcones, combinatorics, fermented dairy products, entropy control, mathematical modeling, microencapsulation, phase diagrams, polyunsaturated lipids, stability of biological systems, thermodynamic functions*.

1. PROBLEMS OF PROLONGING THE FUNCTIONALITY OF BAC IN BIOLOGICAL AND FOOD SYSTEMS

National (1) (2) (3) (4) etc. and international sources on the thesis topic are analyzed. The characteristics and challenges of the use of biologically active compounds in functional foods are presented. Their origin, structural diversity, and classification according to their effects are discussed. The lack of uniform terminology and the difficulties of implementing products containing BAC are emphasized. Methods for preventing lipid oxidation, the use of antioxidant compositions, and the formulation of balanced systems of saturated fatty acids, SFA / polyunsaturated fatty acids, PUFA are analyzed. Attention is drawn to the risks of hydrogenation, and the use of biopolymers as stabilizers is mentioned. Microencapsulation is described as a method for BAC protection: the types of microcapsules; wall materials; applicable techniques; limitations related to cost and sensory properties; BAC classification (1*, 13*)[1]. Problems of stability of certain polyphenols and natural colorants, influenced by pH, water activity, solvents, and the presence of polymers, are addressed.

Conclusions to Chapter 1

1. The need to develop foods containing biologically active compounds beneficial to human health is determined by population growth and by the demand for a higher quality of life. The deficiency of BAC in the daily diet is caused by intensive agriculture based on monocultures. The solution lies in the application of advanced technologies to produce functional foods whose chemical composition ensures positive physiological effects.
2. The production of foods with functional ingredients involves difficulties: the need for extensive research, consumer reluctance, complex legislative standards, high costs, and technological difficulties in ensuring BAC stability. Methods for prolonging the activity have not been studied in all necessary aspects. Data on the influence of food composition and physicochemical properties on the structure and function of BAC remain insufficient. There is a need to develop theoretical and practical principles for stabilizing their functionality in biological and food systems.
3. The traditional fortification methods, based on the addition of BAC without considering their interactions with the matrix, have reached their limits. The creation of efficient functional foods requires new approaches that ensure structural stability, protecting BAC from aggressive factors. The solutions include the structuring of systems with polyunsaturated fatty acids, the formation of biopolymer-BAC compositions, and procedures for microencapsulation of active ingredients.

[1] The * indicates the author's works included in the main material of the Thesis

2. MATERIALS AND METHODS

2.1. Characteristics of raw materials. For betanin production, red beet roots (*Beta vulgaris*) with intense and uniform coloration were used. The stratified thallus of seaweed (*Saccharina japonica*) served for the *in-situ* production of high-molecular-weight alginates. Safflower petals (*Carthamus tinctorius*) were collected in the fields of the IGFPP ASM, dried at 40°C, H_R < 5%, and stored in the dark. Flax seeds (*Linum usitatissimum*) with a high PUFA content were stored at 18°C. Walnuts (*Juglans regia*) were stored in perforated bags at 20°C and RH = 65%, then shelled manually. The kernels were inspected for the presence of pests and stored in PP containers. The oil and pomace were stored at 4°C (2*).

2.2. Characteristics of selected biopolymers. Solutions of pure **gelatin**, as well as the macromolecular complexes GelAlg and GelHur, were prepared using instant soluble food-grade gelatin. **Microcrystalline cellulose**: commercial preparations with a particle size of 50 μm ("Merck") and Flocel 102 ("Gujarat Microwax"), with <d> = 90 μm, ρ = 0.28...0.33 g·cm^{-3}, RH = 3...5%, were used. **Hyaluronic acid**. It is a linear polysaccharide containing *N*-acetylglucosamine units linked by β-1,4 and β-1,3 bridges. An accessible natural source of hyaluronic acid in concentrated form is the comb of the mature rooster, *Gallus gallus* L. *masculinum* (5).

Table 1. Characteristics of BAC, natural colorants

Description	Structure
Cyanidin **Cy, Cy**$^+$. Cation Cy$^+$: 271,2 D; CyCl: 306.7 D. UV-Vis, IR, ^{1}H-NMR. Hygroscopic red acicular crystals, soluble in alcohol and water, insoluble in $HCl_{(c)}$; > 99%	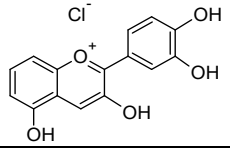
Cyanidine-3-glucosyl chloride. **CyGlu**, **Cy-3-O-Glu.** Cation CyGlu: 433,4 D; CyGluCl: 468,8 D; UV-Vis, IR, TLC. 10% aqueous concentrate, unstabl, 90...95% of Cy-3-Glu in DS	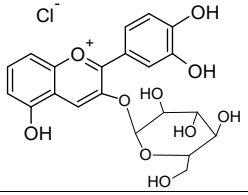
Betanina, E 162, **Bt;** 550,5 D; UV Vis, TLC. 10% extract in an EtOH : Aq mixture (40 : 60), in the presence of citric acid; > 95% betanin in the colorant mixture.	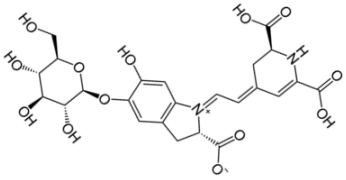

Yellow Food Dye from Safflor, **YFDS**: Hydroxisafflor Yellow A, HSYA, 612,5 D; Anhydrosafflor Yellow B, AHSYB, 1044,9 D; **Precarthamin**, PCrt, 956,8 D; HPLC/MS, HPLC/PDA, UV-Vis, RGB, CIELab. Yellow powder, moderately hygroscopic, > 90% quinochalcons.	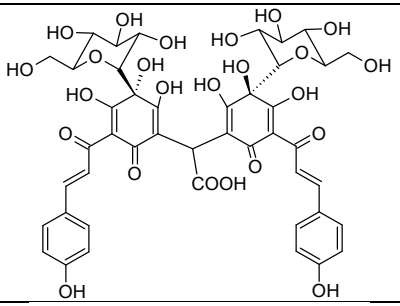
Carthamin, Isocarthamin – **Crt**, iCrt 910,8 D, Hydrocarthamin **Crt·H_2O** 928.8 - HPLC/PDA, UV-Vis, IR, RGB. Red powder, nearly non-hygroscopic, poorly soluble in Aq, moderately soluble in EtOH, readily in DMFA; > 99%	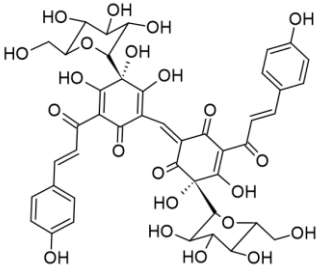
Complex of Carthamin with microcrystalline cellulose, CCC. HPLC/PDA, UV-Vis, IR, RGB. Non-hygroscopic magenta microcrystals. 10...25% Carthamin in the composition of the complex with cellulose (90...75% cellulose, respectively).	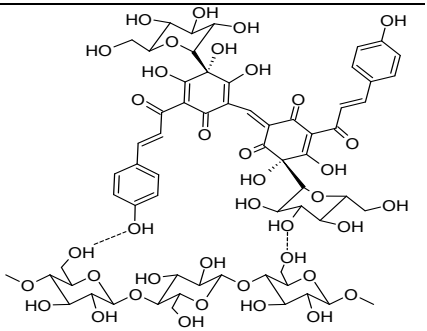

Table 2. Instruments used and brief characteristics of the method

Instrument	Description of the study object and method
pH measurement of BAC extracts, model systems, and food products.	
pH-150-MI „MinskNauch-Pribor". TUM	Combined electrode system "ESC-10603/7" (Ag/AgCl/KCl (saturated) // glass membrane, in automatic thermo-compensation mode (20…30°C).
Determination of water activity (a_w - metry) of powders	
LabSwiftAW. „Novasina AG" (Switzerland)	The water activity in the powder samples was recorded after 2 hours of exposure to air at a temperature of 24°C.

Viscometry of biopolymer solutions	
Ostwald viscosimeter Capillary diameter d <= 0.88 mm	**Mark–Houwink–Sakurada** intrinsic viscosity, [η], determination, at infinite dilution; calculation of the polymer viscosymetric molar mass using Equation 2.1: $M_{polymer} = ([\eta]/\mathrm{K})^{1/\alpha}$ (2.1)
CIELab colors codification	
Chroma Meter CR–400/410 „Konica Minolta" (Tokyo, Japan). TUM	The CIELab parameters (L* – lightness, a* – green-to-red coordinate, b* – blue-to-yellow coordinate) were measured in five replicates. The instrument was calibrated with white and black reference plates for homogenized samples. The color analysis of the two types of yogurt was performed based on variations in L*, a*, and b*, and by calculating the total color difference (ΔE*): $\Delta E^* = \sqrt{(L_i^* - L_o^*)^2 + (a_i^* - a_o^*)^2 + (b_i^* - b_o^*)^2}$ (2.2)
RGB coding for quinochalcone dyes and foods based on them	
Smartphone with 12…64 Mpixels camera	The images were picked under constant illumination (3000 ± 50 lx, using the "Lux Light Meter" application). The images were processed with "ImageColorPicker", and the RGB code was determined. The mean values <R>, <G>, <B> were obtained by analyzing at least 3 pixels.
UV-Vis Spectrophotometry	
Spectrophotometer UV-Vis "DR 5000". **"**Hach-Lange" (Germany-USA), TUM	Spectra were recorded in the 200...800 nm range, using a quartz or PS cells with l = 1.0 cm. To adjust the pH of the solutions subjected to spectrophotometry, hydrochloric acid (pH = 1...3), citric acid (pH = 3...6), sodium carbonate (pH = 6...10), and sodium and potassium hydroxides (pH = 6...12) were used.
FTIR-ATR Spectrometry	
"IR Prestige 21". "Shimadzu", (USA-Japan-Germany). UASVM Cluj	Powder samples were scanned at a resolution of 4 cm^{-1}, in the mode of 16 repeated scans, using the Attenuated Total Reflection (ATR) method on a diamond accessory, in the wave number range of 600...4000 cm^{-1}.
MS-coupled HPLC	
HPLC „Agilent 1200", MS „Agilent 6110" (USA). UASVM, Cluj	"Eclipse" C18 column (4.6 × 150 mm, 5 μm) at 25°C. Mass spectrum fragmentation by positive electrospray ionization, ESI(+), capillary voltage 3,000 V, at 350°C and a nitrogen flow rate of 8 $L \cdot min^{-1}$. Two energy levels were used to obtain 50 or 100 fragments in the m/z range 100...1000 Da (6).

PDA-coupled HPLC	
Cromatograf HPLC „LC 2030-C 3D-Plus”. „Shimadzu Corporation”, (USA-Japan-Germany). TUM	**Isocratic method:** “Phenomenex” C_{18} column (150 mm, 4.5 mm, 5 µm, pore size 0.08 µm). Eluent: H_2O : CH_3CN : CH3OH : TFA 59:30:10:1 (7). **Gradient method:** Variant 1: phase A: bidistilled water with 0.1% (v) CH_3COOH (HAc); phase B: acetonitrile with 0.1% HAc. Variant 2: phase A: bidistilled water with 0.1% (v) HAc; phase B: acetonitrile with 1.0% HAc. Eluent flow rate: 0.5 mL/min, 5% phase B; temperature 25 / 30°C; sampling: 12.5 Hz; cell temperature: 30 / 32°C. Gradient scheme, time / phase B: 0 min – 5%; 2 min – 5%; 18 min – 40%; 20 min – 90%; 24 min – 90%; 25 min – 5%; 30 min – 5% (flow).

2.3. Methods for optimizing data flow.

Construction of ternary diagrams $Y = f(X_1, X_2, X_3)$. Triangular diagrams were constructed to visualize the topology of the properties of ternary systems, using a limited number of experiments - 6...10. Each vertex of the Gibbs-Roseboom-Stocks triangle represents the maximum for components A, B, and C, and each lateral axis represents a binary composition expressed as a percentage. A line forming an angle of 60° with axis “a” represents the set of compositions with content *a*, %. Thus, the intersection point of the dotted lines in Fig. 1 has the coordinates 50:28:22%.

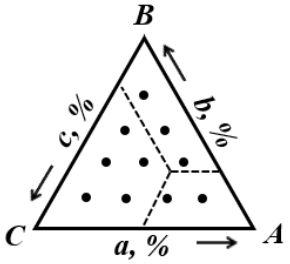

Fig.1. Roseboom triangle

Two-level linear factorial experiment. Regressions. In food systems, classical linear models (8) are sufficiently informative, requiring N = 2^j types of experiments for *j* factors in the Complete Factorial Experiment (CFE). The CFE matrix is transformed into an FFE matrix (Fractional Factorial Experiment, N = 2^j, where $j = j\Sigma - j\mathrm{S}$, $j\Sigma$ being the total number of influencing factors, of which *j*S were obtained by substituting interaction factors) (35*).

EFC 2^2: $Y = \beta_0 X_0 + \beta_1 X_1 + \beta_2 X_2 + \beta_{12} X_{12}$ (2.3)

EFF 2^{3-1}: $Y = \beta_0 X_0 + \beta_1 X_1 + \beta_2 X_2 + \beta_3 X_3$ (2.4)

EFC 2^3: $Y = \beta_0 X_0 + \beta_1 X_1 + \beta_2 X_2 + \beta_3 X_3 + \Sigma\beta_{kl} X_{kl} + \beta_{123} X_{123}$ (2.5)

EFF 2^{4-1}: $Y = \beta_0 X_0 + \beta_1 X_1 + \beta_2 X_2 + \beta_3 X_3 + \Sigma\beta_{kl} X_{kl} + \beta_4 X_4$ (2.6)

For some regressions obtained on the basis of spontaneous measurements, which had not been planned *a priori*, the Regression Analysis wizard was used: ***Excel Data Sheet*** → ***Data*** → ***Data Analysis*** → ***Regresion***

Determination of the polydispersity of emulsions and suspensions. The developed method is original and applicable to O/W emulsions, plant milk (19*), and microcapsule suspensions. The samples studied are photographed at a resolution of 12...64 MPx, with the camera installed in or aligned with the microscope eyepiece. The sample illumination mode is selected according to sample transparency. The objects are counted manually using enlarged and printed images. The object parameters are recalculated: mean diameter, fraction volume, and volume fraction:

$$V_i = \frac{\pi \cdot \overline{d_i}^3}{6} \quad (2.7) \qquad V_{\varphi_i} = N_i \cdot V_i \quad (2.8) \qquad \varphi_i = \frac{V_{\varphi i}}{\sum V} \quad (2.9)$$

where: $\boldsymbol{V_{\varphi i}}$ – volume of $\boldsymbol{i}$ fraction; $\boldsymbol{V_i}$ – the volume of a spherical object (microcapsule, emulsion droplet) with mean diameter $\boldsymbol{\overline{d}_i}$; $\boldsymbol{N_i}$ – the calculated number of objects in the fraction $\boldsymbol{i}$; $\boldsymbol{\varphi_i}$ – the volume fraction of micro-objects with mean diameter $\boldsymbol{\overline{d}_i}$; $\boldsymbol{\Sigma V}$ – total volume of all fractions.

Determination of certain BAC using a conventional standard. As a standard, an extract containing the compound in question or a relatively pure component with known optical parameters is used (i.e., CyGlu predominates in blackberry extract (9). Following UV-Vis and HPLC/PDA analysis:

$$C_{sample} = \frac{D \cdot A_{sample}}{\varepsilon \cdot l \cdot A_{con.st.}} = K \cdot \frac{A_{sample}}{A_{con.st.}} \quad (2.10)$$

where: $\mathbf{C_{sample}}$ – molarity of CBA in analyzed sample; **D** – optical density of CBA solution; **ε** – molar extinction; $L \cdot mol^{-1} \cdot cm^{-1}$ (from sources); **l** – optical way, cm; $\mathbf{A_{sample}}$ – pick area of CBA, $mAU \cdot s$. $\mathbf{A_{con.st.}}$ – conventional standard pick area, $mAU \cdot s$.

2.4. Operating and support systems.

System for operating filtration–sorption–elution processes. It represents an accessible analogue of preparative HPLC, consisting of a micro-pump capable of ensuring a constant mobile-phase flow rate of 0.1...10 $cm^3 \cdot min^{-1}$, and a thermostatable column connected to a pump thermostat.

Electrochemical system supporting the functionality of microcapsules. SSF-MC-EPC was developed for monitoring MC assembly processes (10*). SSF-MC-EPC allows the implementation and study of various processes in model systems having an easily measurable electrochemical response: resistance, conductivity, pH. The measured values serve for deciding the completion of one process and the beginning of another. SSF-MC-EPC enables the assembly of MC and the simultaneous measurement of supernatant conductivity without sample extraction. SSF-MC-EPC (Figure 2) is assembled on a magnetic stirrer with heating, 1. The reactor, 4, with a volume of 200...1000 cm^3, may be fitted with a cooling jacket. A thermometer, 5, a combined electrode, 8, connected to the pH meter, 3, and stainless-steel electrodes, 6 and 7, connected to the ohmmeter, 9, are immersed in the reactor. A constant position of electrodes 6 and 7 is ensured during the run, ideally throughout the entire experiment.

The disadvantage of the magnetic stirrer for electrochemical measurements is that it does not ensure a constant stirring rate, especially when the viscosity of the solutions changes, as occurs in systems and processes involving biopolymers. Replacing the magnetic stirrer with a mechanical stirrer solves the constant-rate problem but poses a risk to electrode integrity. The advantage of SSF-MC-CEP, as well as of other "multicooker"-type systems, lies in the fact that such systems can be implemented in underfunded laboratories.

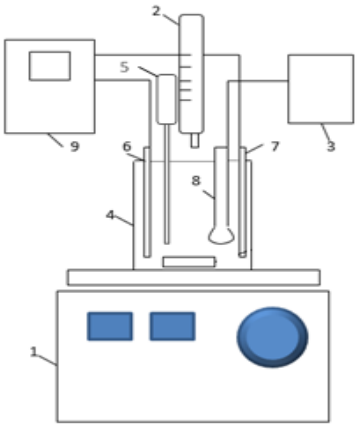

Fig.2. SSF-MC-EPC

Electrophoretic system. Electrophoresis makes it possible to determine the sign of the charge of a colloidal particle or micro-object that is mobile in an electrophoretic field. The second, more subtle and very important parameter is the electrokinetic potential, zeta, ζ, determined by the Helmholtz–Smoluchowski equation (10), (11):

$$\zeta = \frac{\eta \cdot V}{\varepsilon \cdot \varepsilon_0 \cdot H} = \frac{\eta \cdot l \cdot L}{\varepsilon \cdot \varepsilon_0 \cdot U \cdot \tau} \qquad (2.11)$$

where: η – water viscosity, $10^{-3} Pa \cdot s$; ε – water dielectric constant, 89; ε_0 – vacuum electric permitivity, $8{,}85 \cdot 10^{-12}\ F/m$; V – velocity, *m/s*; H– intensity of electric field, *V/m*; l – movement of colloidal particles, *m*; τ – time of electrophoresis, *s*; L – distance between electrodes (efficient tube length), *m* ; U – source voltage, *V* .

The electrophoretic device (Figure 3) includes: a) the voltage source "SPA-97" (Contragent Co, UA); b) tester "UT33C" (Shenzhen Sunkoo-Reid Electronic Ltd, CN); c) flat-surface electrodes, manually made of AISI 304 stainless steel; d) the "colloid / supernatant" interface (dispersion medium); e) a U-shaped tube with a diameter of 1...1.4 cm and an effective length of 15...25 cm; f) the direction of movement of particles with a net charge „-" (***A***) and „+" (***B***).

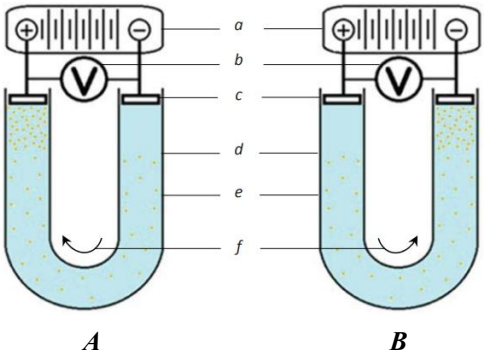

Fig.3. Electrophoresis system

System for color analysis based on red-green-blue (RGB) coding. *The* color of biologically active compounds is an important indication of their state and stability (11*). The CIELab method uses a virtual coordinate space (L, a, b), in which color is determined by the coordinates a and b, while L is lightness; L ∈ (−50; +50). Black corresponds to the coordinates L, a, b = −50, 0, 0, and white to L, a, b = +50, 0, 0. Especially for wet samples, a method was developed based on the use of the RGB code, directly compatible with the color tools in Microsoft Office. The RGB space is a cube in which the intensity of each component is represented by one byte of information (12). Figure 4 reflects the correlation between CIELab and RGB.

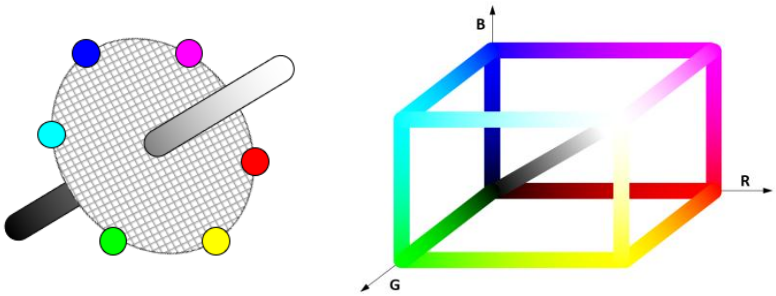

A ***B***

Fig.4. CIELab – RGB correlation:
A – CIELab: black (-50, 0, 0), grey (0, 0, 0), white (50, 0, 0);
B – RGB: black (0, 0, 0), white (255, 255, 255)

The analysis requires reproducible illumination conditions (3000 ± 50 lux) and image capture conditions (Fig.5). To reduce the color heterogeneity, RGB codes are recorded at 3 points forming a triangle. The meaning is rounded to an integer, since the RGB code is composed of integers (Red, 255:0:0; Green, 0:255:0; Blue, 0:0:255; Cyan, 0:255:255; Magenta, 255:0:255).

A ***B*** ***C*** ***D*** ***E***

Fig.5. RGB-code determination: ***A – LED 6400 K; B – illuminated object; C – smartphone; D – image; E – <RGB> code and <color>***

2.5. Statistical interpretation of experimental data

Estimation of measurement errors. In most experiments, the confidence level (certainty) accepted was P = 0.95. Indirect errors were calculated by the sum of squares of relative errors and by the method of partial derivatives:

$$\varepsilon_Y = \frac{\Delta Y}{\bar{Y}} = \sqrt{\sum_{i=1}^{j}\left(\frac{\Delta X_i}{\bar{X}}\right)^2} \quad (2.16) \qquad \Delta Y = \sqrt{\sum_{i=1}^{j}\left(\frac{\partial Y}{\partial X_i}\right)^2 \cdot \Delta X_i^{\,2}} \quad (2.19)$$

Statistical modelling. The "bag of balls" model makes it possible to calculate the probabilistic distribution of the system states according to Eq. 2.20...2.21:

$$P_{R/O} = \frac{N!}{N_R! \cdot N_O!} \quad (2.20) \qquad P^{\%}_{R/O} = \frac{P_{R/O}}{\sum P_i} \cdot 100\% \quad (2.21)$$

The curve $P_{R/O}{}^{\%} = f(N_R)$ describes the proportion of states of the model system.

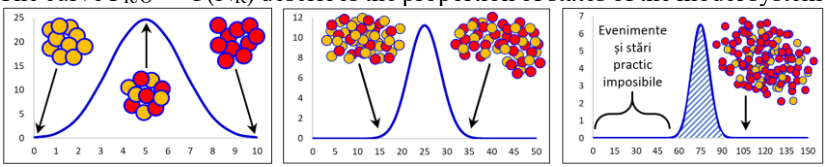

A *B* *C*

Fig. 6. $P^{\%} = f(n)$ repartition in model systems:
A – 10 particles; B – 50 particles; C – 150 particles

The ball model visualizes the irreversibility of processes: a perfectly ordered state is extremely unlikely, whereas disorganized states are far more probable.

Conclusions to Chapter 2.

1. The sources of BAC and biopolymers as *Saccharina* thallus, beet roots, walnut kernels, flax seeds, and safflower petals were used. The following were obtained: alginates; purified betacyanin and betaxanthin extracts; oil rich in ω3 and ω6; arabinoxylan; a mixture of yellow quinochalcones, YQCM; Carthamin, Crt; and the Carthamin-cellulose complex (CCC).
2. The study of functional food systems requires the combined use of instrumental methods (electrochemical, spectroscopic, HPLC), mental experiment and modelling methods (programmed/unprogrammed experiment, Box-Hunter regression analysis).
3. The limits of applicability of certain research methods were established. Two-level regressions are sufficiently informative. The UV-Vis spectra of BAC derive from chromophore and auxochrome groups that confer functionality. Therefore, UV-Vis spectroscopy is a universal method for studying BAC, and HPLC with a PDA detector is the optimal variant.
4. Analytical methods were developed: a constant-rate adsorption–elution system, an installation for the analysis of protein–polysaccharide systems by electrophoresis, an installation for obtaining MC by electrochemical control, a method for analyzing the polydispersity of O/W systems and MC suspensions, and the method for analyzing the "RGB" profile.

3. STABILIZATION AND PROLONGATION OF BAC FUNCTIONALITY IN FOOD SYSTEMS

3.1. Aspects of combining spectra and HPLC. The color of foods correlates with the presence of BAC with antioxidant activity (3*) (5*). The identification and separation of natural colorants are influenced by their interaction with biopolymers (23*) (40*).

3.2. Physicochemical factors and chalcone stability. Yellow quinochalcones from Safflower play an essential role in defense against pathogens (13) and exert beneficial effects on health (14).

Spectral characteristics of chalcones. Spectra are quantized and obey additive laws (15). The absorption maxima of the yellow quinochalcones HSYA, AHSYB, and Precarthamin fall within the range of 402...412 nm (16). UV-Vis absorbance for YQCM shows moderate dependence on pH (Fig. 7).

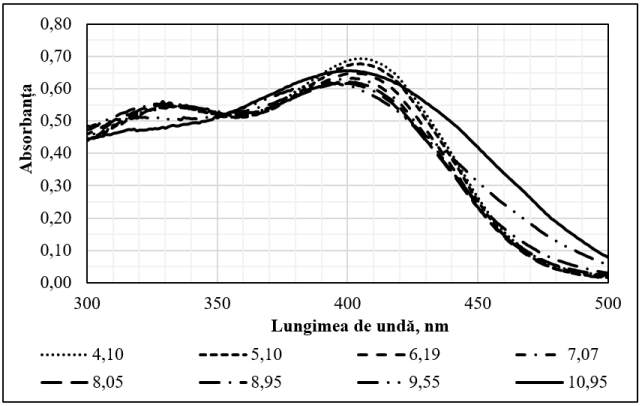

Fig. 7. Spectra of the 0.5% aqueous YFDS extract at different pH values

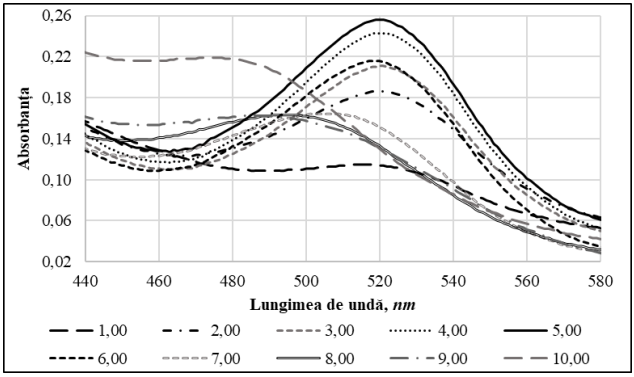

Fig. 8. pH and UV-Vis spectra of Carthamin, 10^{-5} mol·L^{-1}

The pH sensitivity of Carthamin is more pronounced than that of YFDS. At pH > 6, the maximum undergoes a hypsochromic shift up to 475 nm at pH 10 (Fig. 8). Foods are consumable within the pH 3.5...8.0. The ε = f (pH) is necessary for determining the optimal conditions for the colorants use:

$$\varepsilon(pH_i) = \frac{A(pH_i)}{C_M \cdot l} \qquad (3.1)$$

where: $A(pH_i)$ – experimental absorbances at the respectively pH_i, C_M – colorants molarity (recalculated into Precarthamin for yellow ones), l – optical way, 1 cm. Functions ε = f (pH) was founded using criteria: ***(1)*** minimal order of equation; ***(2)*** $R^2 > 0{,}97$. These two criteria satisfies 3rd order polynomial, giving an adequate model (Figure 9).

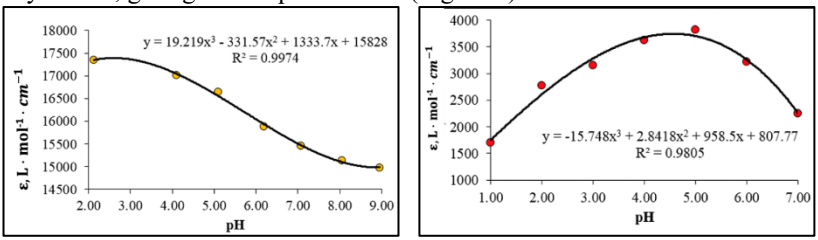

A ***B***

Fig. 9. Extinctions of chalcones in aqueous solutions as a function of pH: *A –YFDS, recalculated to Precarthamin; B – Carthamin*

Equations 3.3 make it possible to calculate the extinctions of the colorants for the range of pH corresponding to a wide variety of foods and beverages:

$$E_{YFDS} = 19{,}219\ (pH)^3 - 331{,}57\ (pH)^2 + 1333{,}7\ (pH) + 15828 \qquad (3.3.1)$$
$$R^2 = 0{,}9974\ ;\ pH \in (2;\ 9)\ ;\ \bar{\Delta}\varepsilon = 1{,}9 \cdot 10^2$$
$$\varepsilon_{Crt} = -\ 15{,}75\ (pH)^3 + 2{,}842\ (pH)^2 + 958{,}5\ (pH) + 807{,}8 \qquad (3.3.2)$$
$$R^2 = 0{,}9805;\ pH \in (1;\ 7)\ ;\ \bar{\Delta}\varepsilon = 1{,}6 \cdot 10^2$$
$$\varepsilon_{max}^{pH=2{,}5}(ACCG) = (173{,}0 \pm 1{,}9) \cdot 10^2\ L \cdot mol^{-1} \cdot cm^{-1} \qquad (3.4.1)$$
$$\varepsilon_{max}^{pH=4{,}5}(Crt) = (37{,}0 \pm 1{,}6) \cdot 10^2\ L \cdot mol^{-1} \cdot cm^{-1} \qquad (3.4.2)$$

The expression A = ε · C · l makes it possible to estimate the order of concentration of the red dye present in the form of swollen particles.

Table 3. Chalcones molarities in model systems

Quinocalconic colorant	Extinction, ε, $L \cdot mol^{-1} \cdot cm^{-1}$	M, $g \cdot mol^{-1}$	C_M^U, $mol \cdot L^{-1}$ A ≈ 0,2	C_M^I, $mol \cdot L^{-1}$ A ≈ 1,0
YFDS	17300	957	$1{,}2 \cdot 10^{-5}$	$5{,}8 \cdot 10^{-5}$
Carthamin	3700	911	$5{,}4 \cdot 10^{-5}$	$27 \cdot 10^{-5}$
CCC (~ 25% Crt)	3700	3644*	$5{,}4 \cdot 10^{-5}$	$27 \cdot 10^{-5}$

Note: C_M^U – estimative colorant molarity, necessary for easy coloration; C_M^I – molarity, necessary for deep coloration.

Table 3 allow estimating the dose of colorant administered in the food product, DC_{FP}, g · kg^{-1} (gram dye per kilogram product), necessary to color one kilogram or one liter of food product:

$$DC_{FP} = C_M^U \cdot M \quad (3.5)$$

Stability of chalcones as a function of pH. At pH 2.0...9.0, the color of the yellow chalcones remains practically unchanged. At pH > 9.5, the overall extinction in the 400...500 nm range increases. The Carthamin spectra varies as a function of pH (Fig. 8). At pH = 6.0, Δλ = -30...-40 nm: the red disappears. Carthamin is susceptible to considerable chromophore modifications (Fig. 10). The increase in absorption at λ = 390 nm in alkali is caused by the *p*-coumaroyl groups (17) at 6 and 6′. The *p*-coumaroyl groups are prone to phenol-quinone equilibria at pH > 10, undergoing oxidative degradation (18).

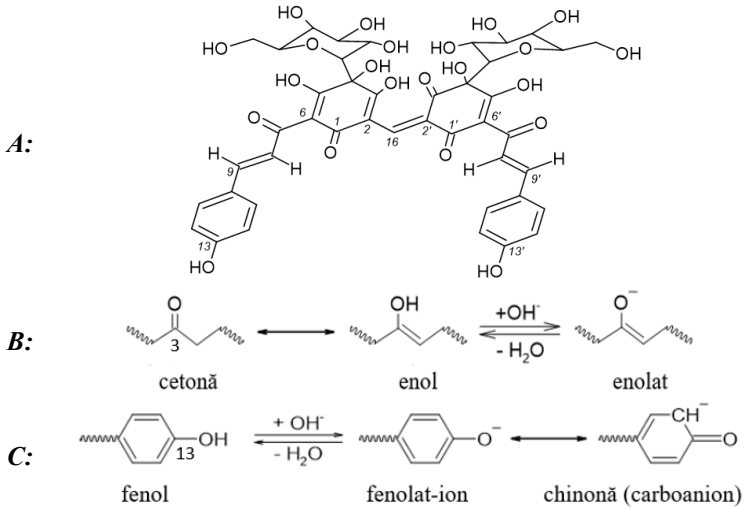

Fig.10. Carthamin. A: at pH 2.0...6.0; B: ketone-enol equilibria at pH 6.0...8.0; C: phenol-quinone equilibria at pH 8.0…11.0

Figure 11 presents the hydration process of Carthamin by anti-Markovnikov addition. Hydrogen is added to the less hydrogenated carbon 2′ due to the "-M" effect of the -CO- groups at positions 1′ and 3′ of Carthamin (19).

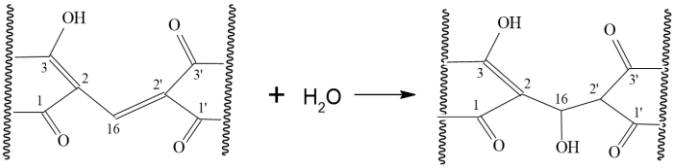

Fig.11. Yellow Hydrocarthamin (Crt·H₂O) formation

The structure of the Hydrocarthamin's chromophores is identical to that of these groups in the Precarthamin, λ_{max} = 410 nm. In weak base, Carthamin is hydrated. During the extraction of Carthamin from CCC, two peaks with similar spectra are observed, λ = 519 nm and λ = 521 nm (Figure 12).

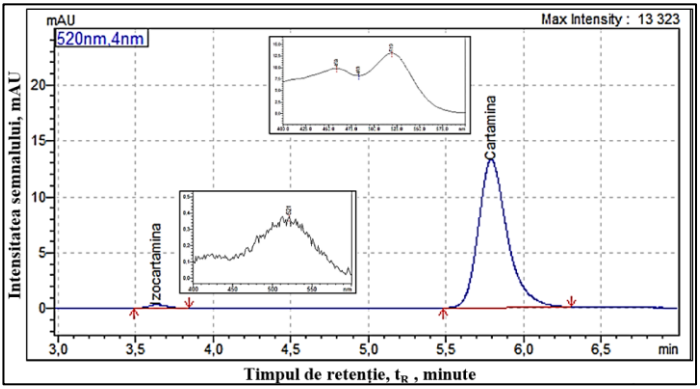

Fig.12. HPLC and UV-VIS/PDA spectra of two quinocalcones:
Isocarthamin (λ_{max} = 521 nm), Carthamin (λ_{max} = 519 nm)

Recent interpretations of the H^1-NMR and C^{13}-NMR spectra (20) confirm the "chicken cage" structure, as well as the fact that deprotonation occurs at 3 and 3′ positions due to keto-enol equilibrium. Isocarthamin is not even mentioned among the safflower pigments identified in different genotypes (21).

Kinetics of Carthamin decomposition. It was assumed that Carthamin degrades according to 1st-order kinetics. Carthamin was obtained by extraction from CCC with 1% Na_2CO_3 solution (32*), adjusted to pH 4.5, filtered, and injected. The rate constants were calculated as follows: $K_{I,278K} = 0{,}00357h^{-1}$ and $K_{I,293K} = 0{,}0835h^{-1}$. E_A = 142 ± 5 kJ corresponds to the process in a real solution and does not involve phenomena in the solid phase or at the interface.

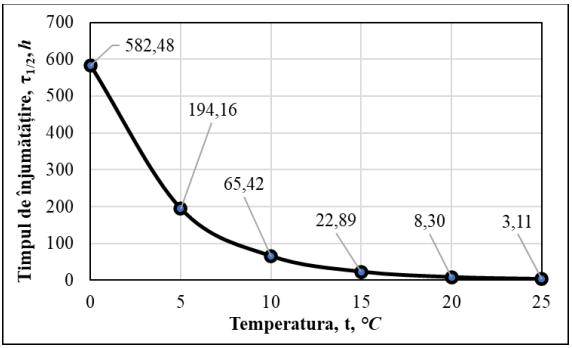

Fig.13. Function $\tau_{1/2}$ = f (t)

Carthamin is conventionally stable at temperatures below 10°C (Figure 13). Therefore, in the dissolved state it is not suitable for coloring beverages and other foods with a high water-content, especially since most such products are stored at room temperature.

Influence of UV on chalcone stability. The stability of a compound to UV radiation may serve as an additional, though not sufficient, indication of its stability in foods. YFDS and CCC were exposed to UV, 30 Wt, at an illumination intensity of 100 ± 2 lx, for 4 hours. YFDS samples, 0.100 ± 0.001 g, were dissolved, filtered through 0.22 μm PTFL, and injected immediately.

Table 4. Influence of UV radiation on the components of YFDS

Cod	Calcon	$\lambda_{max.}$, nm	R_T, min	C_{pCrt}, mg·g^{-1}	Δ, %
YFDS	***HSYA***	403	18,3	336 ± 11	-
	Unidentified	409	18,8	56,3 ± 1,7	-
	pCrt	411	20,0	309,5 ± 9,3	-
	AHSYB	411	22,0	248,4 ± 7,5	-
YFDS/UV	***HSYA***	403	18,2	347 ± 11	+ 3,4
	Unidentified	409	18,8	52,0 ± 1,6	- 7,7
	pCrt	409	20,0	292,7 ± 8,8	- 5,5
	AHSYB	410	22,0	258,1 ± 7,8	+ 3,9

Note: YFDS/UV – UV-irradiated YFDS; C_{pCrt} – chalcone concentration, mg·g^{-1} of pCrt; Δ – concentration shift after irradiation with UV.

Table 4 confirms that YFDS/UV undergoes no changes in chalcone composition. CCC samples, 0.100 ± 0.001 g, were extracted with Na_2CO_3 solution, the extracts were filtered through 0.22 μm PTFL, and injected.

Tabelul 5. Influence of UV radiation on the CCC

Cod	Calcon	λ(max), nm	Rt, min	Crt/CCC, mg·g^{-1}	% izomer
CCC	iCrt	513	6.13±0.05	~ 120	2.7±0.2
	Crt	519	8.84±0.05		97.3±0.2
CCC/UV	iCrt	522	6.13±0.05	~ 104	5.20±0.2
	Crt	520	8.84±0.05		94.80±0.2

Table 5 demonstrates the high sensitivity of Carthamin to UV radiation. Its concentration decreases from ~120 mg·g^{-1} to ~104 mg·g^{-1}, and the Crt/iCrt ratio changes. Thus, the proportion of Isocarthamin in CCC/UV increases to 5.20% compared with non-irradiated CCC, in which iCrt = 2.66%. Effects confirm the existence of an isomerization by means of Crt·(H_2O), in which C^{16} is sp^3.

3.3. Prolongation of lipid functionality.

The prevention of lipid degradation is a primary task in the development of long-life functional foods (22).

***Prevention of lipid oxidation using antioxidants*.** The UV-Vis spectra of walnut oils (WO) were analyzed (Figure 14). Walnut oils (**UN**), UN-PL-1 and

UN-PL-2, are commercial products declared as obtained by cold pressing. Walnut oil UN-UTM was obtained by cold pressing under laboratory conditions using a hydraulic press at 20 MPa.

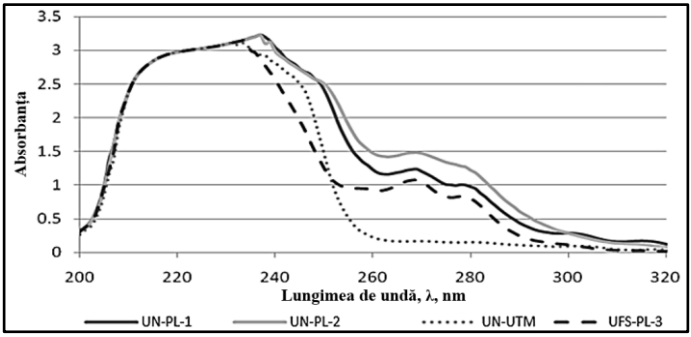

Fig.14. UV-spectra of oils

The UV spectra of oils from local producers show absorption at 270 and 280 nm, which may indicate the presence of liposoluble phenols. The UN-UTM sample, obtained by cold pressing, does not contain these bands. Accordingly, local producers process the oil with deviations from cold-pressing technology. The IR spectra of commercial oils show an increase in the contribution of the deformation vibrations of $-CH_3$ at 1380 cm^{-1} and of the deformation vibrations of -OH at 1410 cm^{-1}, which are signals of thermal treatment of the raw material (36*). Thus, UV and IR spectra are not sufficient for the reliable detection of oil adulteration but may serve as indicators of non-compliance with the production technology.

The influence of the following antioxidants on walnut oil was analyzed: DL-α-tocopherol, DLTP; ascorbyl palmitate, AAP; octyl gallate, OG. Analysis of the compositions showed that OG and AAP contribute to a decrease in the peroxide index, PI, and the *p*-anisidine index, PAI, of PUFA-rich oil (20*)

$$\overline{PI}_{14d}=3.06X_0-0.54X_1-0.24X_2-0.39X_3+0.27X_{12}+0.12X_{13}+0.08X_{23}+0.19X_{123}$$

$$\overline{PAI}_{75d}=2.04X_0-0.06X_1+0.20X_2-0.03X_3+0.00X_{12}-0.09X_{13}-0.07X_{23}+0.02X_{123}$$

The β coefficients reveal synergistic effects. The "controversial" DLTP (23), contributes to an increase in PAI directly and by interaction with AAP. The overall activity increases in the series DLTP < AAP < OG, which corresponds to the increase in surface activity and correlates with the other researchers (24).

Prolongation of PUFA functionality in lipid compositions. Lipid compositions with PUFA should pass into the liquid state at temperatures of 33...36°C, characteristic of the oral cavity (25). Fat polymorphism makes it possible to obtain lipid compositions with suitable texture and high stability during refrigerated storage, in which the fats with a high PUFA content become solid. In order to determine the influence of SFA and MUFA on melting

temperature, compositions containing walnut oil, stearic acid, and oleic acid were studied (Figure 15). Walnut oil compositions with 10...20% stearic acid and 10...30% oleic acid showed the required melting temperature. The obtained data can be used for developing the composition of PUFA-containing spreadable products. This approach is novel for lipid compositions, because co-crystallization of SFA with PUFA results in a food composition in which the components form a common solid lipid phase, more stable in its solid and ordered state against oxidative degradation than PUFA in the individual state. The dependence of the process effect on the cooling rate (and not only on the fact of cooling itself) indicates that the entropic factor plays a significant role. In the case of triglycerides with PUFA residues, an apparently paradoxical situation arises: the low entropy of the acid residue causes disorder (high entropy) at the level of the lipid phase. The double-bonds imposed rigidity is an obstacle to the solidification of fats. Thus, it is thermodynamically impossible to manufacture a spread exclusively from PUFA-rich oils.

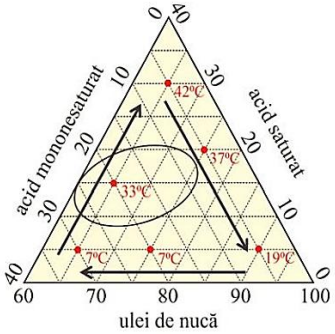

Fig.15. State diagram of WO-HStearate-HOleate system

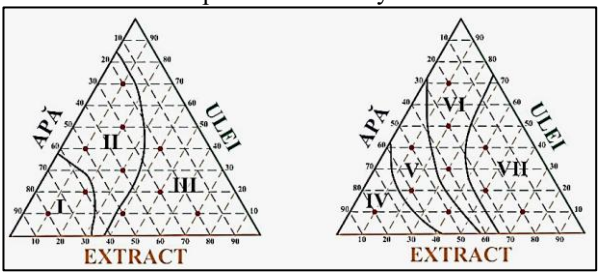

A ***B***

Fig.16. State diagrams of a ternary system GTEO – WO – Water

Lipid foods also contain an aqueous phase, influencing their stability (30*). Assuming the stabilizing role of green tea leaf extract in oil (GTEO = EFCVU), GTEO-WO(UN)-Water (APĂ) systems were formulated. Emulsions are formed (Figure 16, A): I - direct O/W; II - triple O/W/O, the most unstable type; III - inverse W/O. The W/O emulsion is structurally similar to spread, being of practical interest. A correlation was established between phase composition and kinetic stability, highlighting zones IV, V, VI, and VII (Figure 16, B): IV - very low-stability emulsions ($\tau_{1/2} < 1$ min); V - low-stability emulsions ($\tau_{1/2} = 2...4$ min); VI - relatively stable emulsions

($\tau_{1/2}$ = 4...7 min); VII - fairly stable emulsions ($\tau_{1/2}$ > 7min). The stable compositions are: water, 0...30%; WO, 0...50%; GTEO, 30...100% ("high"). Surface-active compounds of GTEO promote the stability of O/W emulsions. The physicochemical principles underlying the structural stability of spreads and margarines differ. Margarines are obtained by transforming PUFA into saturated FA and by isomerizing PUFA from the *cis* to the *trans*- form. *Trans* molecules, being more ordered than *cis*- ones, crystallize at lower temperatures. The spread stability is ensured by phenomena at the interface and within the "O" & "W" phases, repeating natural stabilization mechanisms. ***Combinatorics of spread stability.*** In spreads, the lipid phase contains crystals of 0.01...2.00 μm and an amorphous phase. Such a system is weakly stable to temperature fluctuations. The aqueous (W) and gaseous ("gas", G) phases form bubbles and droplets of 20...30 μm (26), affecting the rheological, physicochemical, and sensory properties of the spread, as well as the functional properties of BAC (27). The walnut-oil spread was obtained according to (46*), in the presence of colorants and lecithin. The lipid (O), aqueous (W), and air ("gas", G) phases are in contact with each other in all possible combinations (28). To clarify the structure and characterize BAC stability in the spread, combinatorics was used (29). It was postulated that all phases constituting the spread are formed by geometric bodies identical in shape and volume. Considering the principle of minimum energy, hexagonal representation in 2D space is more appropriate (Figure 17).

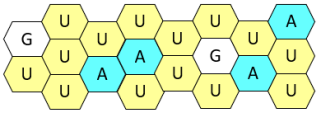

Fig. 17. Model of three-phase emulsion O/W/G (U/A/G) 7v : 2v : 1v

Φ_U , Φ_A and Φ_G are the volume fractions of oil, water, and air in the spread:

$$\Phi_U + \Phi_A + \Phi_G = 1 \qquad (3.9)$$

The lipid (U) content is regulated by the mass fraction, Ω_U, %, while the density of oil is about 0.925 g·cm^{-3}. The density of air is practically equal to 0.00 g·cm^{-3}; accordingly, the volume of entrapped air does not affect the mass of the spread, but decreases the volume fractions of oil and water:

$$\Phi_G = \Phi_G, \% / 100\% \qquad (3.10)$$

$$\Phi_U = \{1 - \Phi_G) \cdot \{\Omega_U / 0{,}925\} / \{\Omega_U / 0{,}925 + 100 - \Omega_U\} \qquad (3.11)$$

$$\Phi_A = \{1 - \Phi_G) \cdot \{100 - \Omega_U\} / \{\Omega_U / 0{,}925 + 100 - \Omega_U\} \qquad (3.12)$$

For infinite of hexagons, the probabilities of contact between identical phases, X, and between different, X and Y, are respectively equal to:

$S_{X/X} = \Phi_X \cdot \Phi_X$ (3.13) $S_{X/Y} = \Phi_X \cdot \Phi_Y$ (3.14)

The difference lies in the fact that the surface-active compounds (SAC) will concentrate at the interface. Then, the mass fraction of SAC at the interface:

$$\Omega(AAS)_{X/Y} = S_{X/Y} / (S_{U/A} + S_{U/G} + S_{A/G}) \qquad (3.15)$$

Table 6. Interfaces in the O/W/G system - combinatorial model

Ω(U) :Ω(A) : Φ(G)	$\Omega(AAS)_{U/A}$	$\Omega(AAS)_{U/G}$	$\Omega(AAS)_{A/G}$	AAS inutil
Real spreads				
72 m : 28 m : 1 v	0,951	0,036	0,013	5%
72 m : 28 m : 3 v	0,863	0,101	0,036	14%
82 m : 18 m : 1 v	0,933	0,056	0,011	7%
82 m : 18 m : 3 v	0,819	0,150	0,031	18%
Combinatorial model				
76.4 m : 23.6 m : 10 v (7 v : 2 v : 1 v)	0.609 15 (0.652)	0.304 8 (0.348)	0.087 1 (0.043)	39%

Note: data calculated by the author based on Equations (3.9)...(3.15).

3%-aeration leads to the use of 14...18% of SAC for the useless "stabilization" of air bubbles. Therefore, the prolongation of PUFA functionality in spread-type compositions can be ensured by structural homogeneity and a reduced air fraction. The hexagonal model makes it possible to estimate the value of the percolation threshold $\Phi_{U(PP)}$ At P = 0.999 for the event that no lipid hexagon remains surrounded only by water and gas, $\Phi_{U(PP)}$ is 68.4%, and in the spread the lipid phase (72/82%) is continuous. The developed model demonstrates that the formation of structures with two continuous and mutually interpenetrating phases is impossible.

3.4. Technology for obtaining spread with polyunsaturated fatty acids.

Using the patented procedure (46*) (Figure 18), samples were prepared with a content of 20...50% PUFA of the total fat amount in the spread.

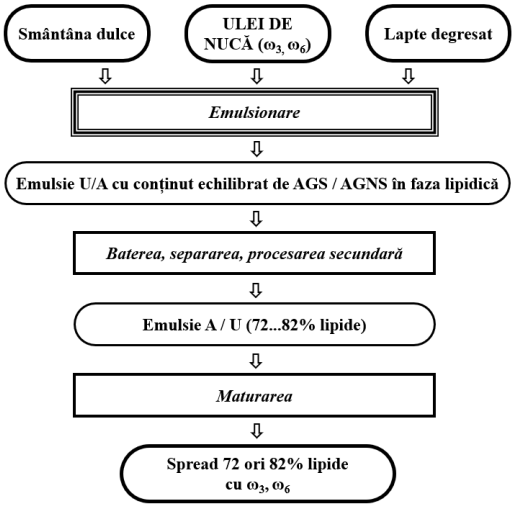

Fig.18. Technological scheme for producing spread with BAC.

The procedure for obtaining spread enriched with PUFA is based on the formation and controlled inversion of the emulsion, followed by structuring of the lipid phase. Sweet cream (30...35% fat), skimmed milk, and walnut oil are brought to temperatures of 40...55°C, after prior pasteurization (85...95°C, 15...30 s) and cooling to the emulsification temperature. Walnut oil is introduced at 35...45°C. Emulsification is carried out at 45...60°C at 1500...3000 rpm, followed by two-stage homogenization (at 10...20 MPa and 2...5 MPa), resulting in an O/W emulsion. By cooling to 8...14°C and mechanical churning (30...60 rpm, 10...20 min), coalescence and buttermilk separation occur, leading to lipid concentration up to 72...82% and emulsion inversion into W/O. Final structuring of the product is carried out in equipment with intensive cooling and controlled shear of the scraped-surface heat exchanger type, at 8...10°C and 200...600 rpm, where crystallization of the solid fat fraction is induced. Maturation at 4...8°C for 12...24 h ensures spreadability, structural stability, and resistance to phase separation. The result is a spread with 72...82% lipids, a stable W/O structure, a balanced SFA/PUFA lipid profile, and a functional contribution of ω3 and ω6 fatty acids, which naturally varies linearly as a function of the amount of introduced PUFA (Table 7). At the same time, the dependence of the thermostability coefficient is not linear, falling within the values qualified as “good” (0.86...1.00) and “satisfactory” (0.70...0.85), established for cow butter (30).

Table 7. Spread thermostability (T) vs composition (25)

Walnut oil	SFA	MUFA	PUFA	ω6 : ω3	T
20	55	28	17	14.3 : 1.7	0.93 ± 0.01
30	**51**	**25**	**23**	**20.3 : 2.4**	**0.88 ± 0.01**
40	**47**	**23**	**30**	**26.4 : 3.2**	**0.88 ± 0.01**
50	43	20	36	32.5 : 3.9	0.71 ± 0.02

The major risk to spread stability is posed not by PUFA, but by the aqueous phase, which constitutes 18...28% of the spread mass (15*), in correlation with the combinatorial model. The destabilizing role of water in food products, including those with a secondary aqueous phase, is confirmed. The rationale for prolonging the physiological activity of PUFA through their incorporation into spread-type products is thus confirmed.

Conclusions to Chapter 3

1. Reduction of aw is essential for stabilizing phenolic compounds and lipids both in aqueous systems and in media with organic solvents. Red colorants (anthocyanins, betalain, quinochalcones) are prone to degradation in aqueous medium. Anthocyanins are transformed into thermodynamically more stable chalcones, which constitutes an argument for the use of chalcones as pigment alternatives.

2. The stability of red Carthamin is lower than that of yellow chalcones ($\tau_{1/2}$ = 8.3 h at 20°C and 3.1 h at 25°C). However, compared with anthocyanins, Carthamin maintains its red color over a wider pH range (1...6 vs. 2...4), offering a relevant practical advantage, although increasing the kinetic stability of Carthamin remains necessary.
3. In polyphase O/W and W/O emulsions, water intensifies the oxidation of PUFA-rich lipids by facilitating oxygen permeability and reducing lipid stability, which is also confirmed by the combinatorial model of the Oil/Water/Air system. Prolongation of PUFA functionality is possible only in structured systems, where ω3/ω6 acids co-structure with SFA.
4. A technological scheme was developed for producing spread with a balanced PUFA profile. Integration of ω3/ω6 into a butter-like structure makes it possible to valorize plant sources, increase BAC stability, and obtain a spreadable product with high functional value.

4. PROLONGATION OF BAC FUNCTIONALITY IN SYSTEMS AND COMPOSITIONS WITH FUNCTIONAL POLYMERS

4.1. Chemical and technological characteristics of selected biopolymers.

Aspects of the stabilization of colorants with polysaccharides and polyols are examined: alginate, hyaluronic acid, arabinoxylan, inulin, polyvinyl alcohol.

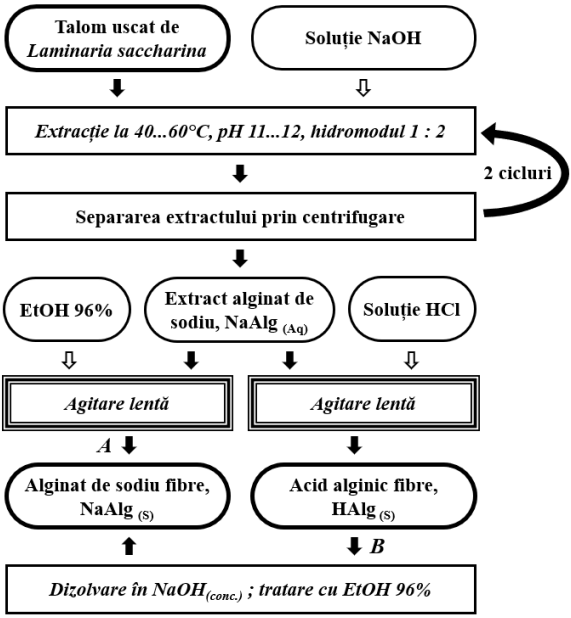

Fig.19. Isolation of sodium alginate and alginic acid

Technology for the isolation and stabilization of native alginate. Alginate processing leads to a 2...5-fold decrease in molecular mass (31) and requires rigorous pH control, unlike methods for the isolation of uncharged polysaccharides (49*). It was necessary to develop a procedure for isolating alginates in the native state, with maximum molar mass (47*). The technology (Figure 19) consists in extraction of the thallus with dilute NaOH and separation of alginate fibers with an excess of ethanol. Extraction takes place at 40...60°C, at pH 11...12, with a hydro module of 1:2...1:3. The extract is transformed into the final product by the short way (Figure 19, A) - treatment with a threefold excess of EtOH. Variant B includes obtaining HAlg by treating Alg^- with HCl. The HAlg gummy mass is washed and dissolved cold in NaOH, forming a concentrated NaAlg solution, which is precipitated with EtOH. The advantage of way "B" is obtaining fibers. The Alg yield reaches 25g / 100g.

Technology of arabinoxylan and PUFA isolation and stabilization. Flax seeds, *Linum usitatissimum*, represent a concentrate of BAC (21*, 27*). The technical problem lies in separating components of opposite polarity from the same batch of seeds (Figure 20).

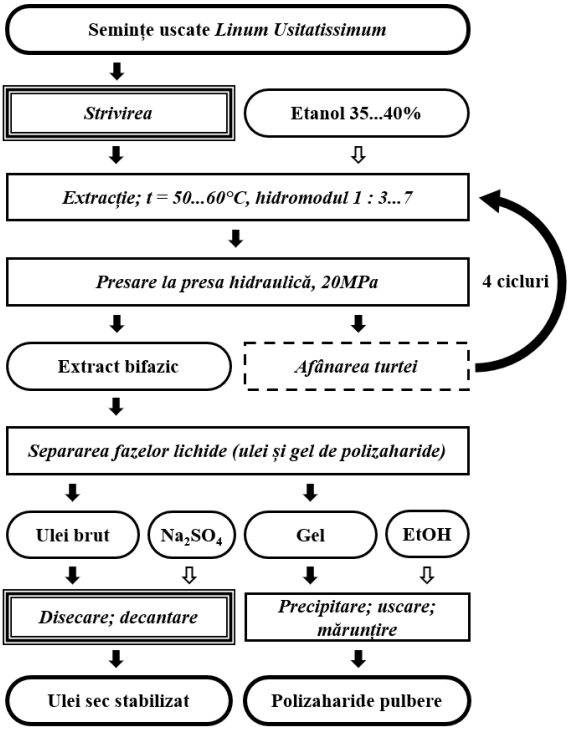

Fig.20. Obtaining oil and polysaccharides from *Linum* seeds

The procedure for obtaining arabinoxylan in fiber form is patented (25*, 44*). Crushing, unlike fine grinding, limits the mechanical destruction of mucilage structures and reduces the formation of stable oil/water emulsions (33*). Crushing preserves phase separability and reduces contact between PUFA and water. This contributes to BAC stabilization. Extraction is carried out with 35...40% EtOH, heated to 50...60°C, at a hydro-module of 1:7, ensuring mass transfer between the matrix and the hydroalcoholic phase without formation of a stable O/W emulsion. Upon repetition of the cycle, the hydro module is reduced to 1:3. At ≈ 20 MPa, simultaneous expulsion of the liquid phases occurs, reducing the liquid content in the cake to approximately 40...50%. The cycle is repeated four times. The biphasic mixture is separated into oil and polysaccharides, which are dehydrated and precipitated, respectively.

4.2. Stabilization of red colorants by biopolymers. An CFE[3] (8) was performed using deproteinized hyaluronic acid (5), cyanidin chloride (32), and betanin preparations purified by preparative chromatography (28*, 39*). The "CyCl / HHur-PVOH-Inu" were prepared. CyCl was 10 mg·L^{-1}, PVOH is polyvinyl alcohol. Spectra were recorded at 24 and 72 hours (Figure 21)

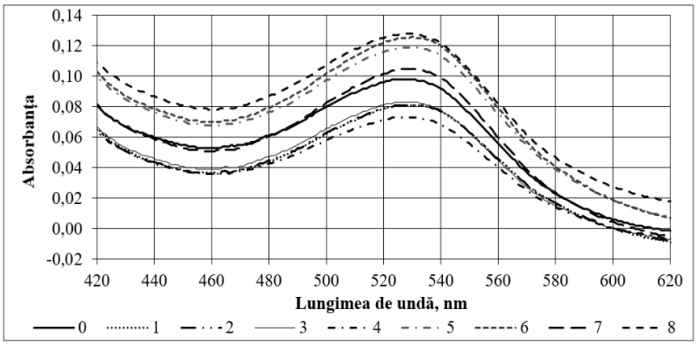

Fig.21. CyCl (0) and CyCl / HHur-PVOH-In spectra after 72h

A regression equation was calculated for $A_{Cy,24}$ – the absorbance value of the solutions at 530 nm, 24 hours after the start of the cyanidin experiment:

$A_{Cy,24,530} = 0.54X_0 - \mathbf{0.03}\boldsymbol{X_1} + 0.00X_2 - 0.01X_3 - 0.01X_{12} + 0.00X_{13} - 0.01X_{23} - 0.01X_{123}$

The coefficient of influence b_1 associated with X_1 is the largest in absolute value, whereas the values of all the other coefficients are much smaller, 0.00...0.01. The spectra are divided into two groups: one with spectra lower than that of the control sample, including samples 5...8, and another with more intense spectra of samples 1...4. This effect is also confirmed by the regressions modelling the optical density in the 280 nm region, at band II: $\mathbf{A_{Cy,24,280}}$:

$A_{Cy,24,280} = 0.83X_0 + \mathbf{0.12}\boldsymbol{X_1} - 0.01X_2 - 0.00X_3 - \mathbf{0.02}\boldsymbol{X_{12}} + 0.00X_{13} - 0.01X_{23} - \mathbf{0.02}\boldsymbol{X_{123}}$

The equation indicates the dominant influence of factor X_1 - the concentration of HHur on the spectrum. The increase in absorbance corresponds to

anthocyanin polycondensation products. The direct factors, X_2 and X_3, are smaller than the interaction ones. After 2 days, a decrease in flavylium absorbance at 530nm and an increase in the absorbance of anthocyanin transformation products below 300nm, giving the regressions for $\mathbf{A_{Cy,72,530}}$:

$\mathbf{A_{Cy,72,530}} = 0.10X_0 - \mathbf{0.02}\boldsymbol{X_1} + 0.00X_2 - 0.00X_3 - 0.00X_{12} + 0.01X_{13} + 0.00X_{23} - 0.00X_{123}$

The negative influence of hyaluronic acid on the CyCl stability was confirmed. It was demonstrated that inulin and PVA, both individually and through interaction with other factors, do not influence the stability of cyanidin.

Biopolymers influence on betanin. The betanin was prepared by extraction of red beet with an EtOH : water mixture (2:1), preparative chromatography of the obtained extract, extraction of the betanin band from the paper with the same ethanol : water mixture (2:1), vacuum distillation of ethanol (<50°C, rotary evaporator, P < 0.01 MPa), filtration of the concentrate through activated carbon, stabilization by acids to pH 2.50, followed by performing EFC 2^3 for the model systems "Bt / HHur–PVOH–Inu". Spectra were recorded after 48 hours, the response being A^{48h}_{535nm}, yielding the regression:

$A^{48h}_{535nm} = \mathbf{0.99}\boldsymbol{X_0} + \mathbf{0.05}\boldsymbol{X_1} + \mathbf{0.03}\boldsymbol{X_2} - 0.01X_3 + \mathbf{0.03}\boldsymbol{X_{12}} + 0.00X_{13} - 0.00X_{23} - 0.00X_{123}$

The equation shows the stabilizing influence of PVA (X_2). The interaction factor of the "hyaluronic acid – PHOH" tandem, X_{12}, is also highlighted. The factors HHur, PVOH, and HHur–PVOH stabilize betanin. For verification, control experiments were carried out with increasing concentrations of HHur, ΔC(HHur) = 0.004%, to which cyanidin chloride and betanin were added.

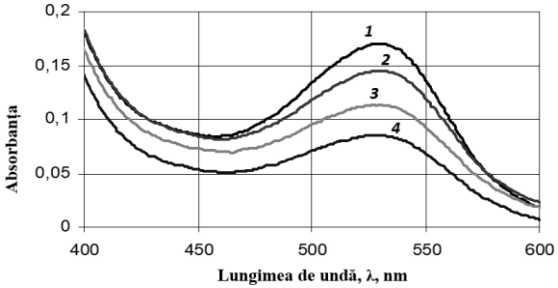

Fig.22. HHur influence on CyCl: 1...4 - 0.004...0.016% HHur

The spectra of the model systems were recorded after 24 hours (Figure 22). With increasing HHur concentration, the absorbance of anthocyanin at 530 nm decreases linearly. Under identical conditions, the UV spectra of betanin solutions do not show significant differences for 2...3 weeks. Solutions with ω(HHur) = 0.028...0.032% retain their red color upon heating. Thus, HHur destabilizes cyanidin and stabilizes betanin. Betanin stability is positively influenced by PVOH (a surface-active agent), and by the common influence factor of HHur and PVOH, which is of practical importance (37*).

4.3. Structure and properties of the Carthamin–cellulose complex.

The stabilizing effect of cellulose on Carthamin is known as the "Saito effect" (33), in contrast to the low stability of Carthamin demonstrated in its aqueous solutions (2*, 4*). Carthamin is poorly soluble in water: it precipitates in slightly acidified solutions at concentrations $>10^{-4}$ mol/L (>0.01%). At concentrations of 10^{-5} mol/L, Carthamin solutions retain aggregative stability but rapidly lose color. Carthamin is extracted from petals with bases, forming orange extracts. At the same time, in alkaline medium, the tense three-dimensional structure of cellulose fibers transforms into a relaxed linear amorphous one (34). The interaction between Carthamin and cellulose was studied by FTIR, RGB with water activity (a_W) measurement methods (8*). The relatively low solubility of Carthamin and the formation of a solid phase in water and slightly acidic media require modification of HPLC chromatographic protocols. When the mobile phase is rich in water, solid inclusions of Carthamin may form on C_{18}-type HPLC columns, leading to column blockage and analysis failure. It was established that if the mobile phase contains 10...40% organic solvent and a strong acid, solid carthamin formation and column blockage do not occur. The HPLC method reveals two Quinochalcones, referred to as Carthamin (Crt) and Isocarthamin (iCrt). The red color is due to a bulky chromophore with 17 conjugated electron pairs, to which C-glucosyl groups are attached, whose auxochromic influence has not been reported in the analyzed literature. In the examined sources, the term "Carthamin" refers to the form in which the chalcone groups are located on the same side of the zigzag 6-1-2-16-2′-1′-6′ (Figure 23, A).

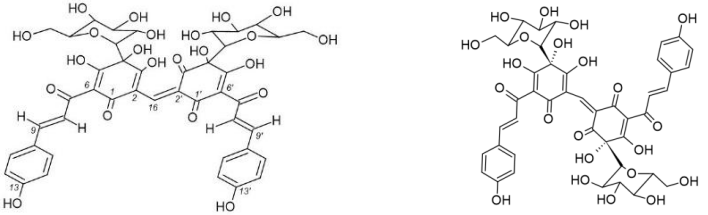

A ***B***

Fig.23. Structure of red quinochalcones: *A – Carthamin ("chicken-cage" conformation); B – Isocarthamin ("quadrocopter" conformation)*

The spectra of the isomers are very similar, with absorption maxima at 519 and 521 nm, respectively. Such a small difference does not allow definitive assignment of *cis*- or *trans*- structure; neither HPLC/PDA nor HPLC/MS can distinguish these structures in aqueous solution. However, molecules with predominantly lipophilic character are retained more efficiently on C_{18} (35). This supports the *cis*- configuration of the base quinochalcone. The direct conversion of Crt to iCrt by rotation around the C^2–C^{16} axis is forbidden (19).

Stability of the Carthamin–cellulose complex. In aqueous medium, carthamin transforms into an unidentified yellow product with an absorption maximum at λ_{max} = 404nm, corresponding to a quinochalcone. Degradation is indicated by a decrease in optical density at 519...520nm. The shoulder at 404nm, visible in the spectra of partially degraded Carthamin, corresponds to a newly pronounced peak after chromatography (Figure 24, B). Absorption with a maximum at 404 nm is also characteristic of Precarthamin, which contains 2 non-conjugated C-glucosyl quinochalcone fragments separated by 2 single bonds (7).

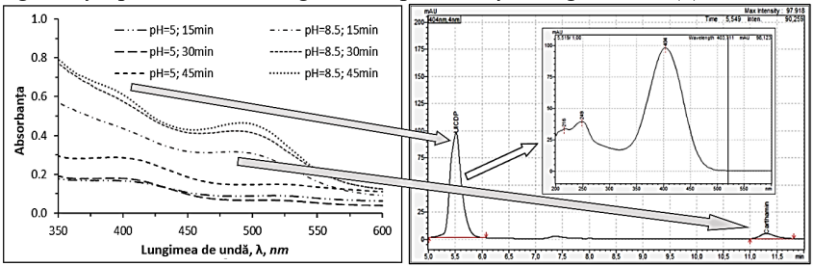

A *B*

Fig.24. Carthamin degradation: ***A – signals of Carthamin and the unidentified yellow chalcone; B – the peak at 404 nm and the UV-Vis/PDA spectrum of the unidentified quinochalcone***

Since Carthamin is highly unstable in aqueous solutions, it begins to decompose at the moment of extraction from the cellulose phase. The degradation of Carthamin in aqueous solutions occurs so rapidly that direct evaluation of its concentration immediately after extraction from cellulose, by measuring absorbance at 520 nm, becomes practically impossible. Classical UV-Vis spectra of Crt extracts from cellulose indicate the presence of undegraded Crt as well as derivatives, manifested by an increase in absorbance at 404 nm (Figure 24, *A*). The absorption maximum (or shoulder) at 404 nm, generated by the formation of Carthamin degradation products, is sufficiently distant from the absorption maximum of Carthamin.

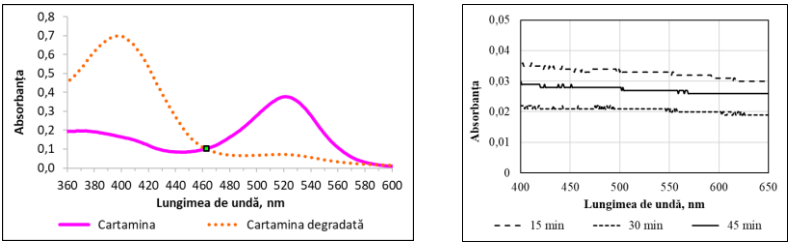

A *B*

Fig.25. Analysis of Carthamin extracts from CCC:
A – isosbestic point; B – absorbance due to diffraction on the polymer

The isosbestic point at 462 nm allows calculation of the total amount of Crt extracted from CCC. The extracts exhibit additional absorbance in the form of a plateau across the entire visible wavelength range, characteristic of UV-Vis spectra of polymers (18*). To account for the contribution of microparticles of swollen cellulose, the absorbance at 600 nm was measured (Figure 25, B). The preservation of CCC color at temperatures from 60°C to 80°C enables its practical use as a food colorant. This statement is particularly relevant for dairy products, which are pasteurized within this temperature range. Table 8 demonstrates that the Carthamin-cellulose complex is stable under the specified conditions. Thus, the parameter S_{CCC} exceeds 90% at pH of 3.9...5.0 and at temperatures of 50...60°C, provided that the exposure time is 30 minutes. Extraction of Crt from the cellulose phase into solution is well expressed even under static conditions, without stirring, at pH = 8,5 : over 50% Crt are extracted from CCC, în 15 minutes, at 50°C.

Table 8. Stability of CCC, S_{CCC}, *%* (ratio of intact Crt)

Temperature, ºC	**τ, *min***	**pH = 3,9**	**pH = 5,0**	**pH = 8,5**
	15	96,1 ± 0,5	93,8 ± 0,8	59,6 ± 4,8
50	30	94,6 ± 0,7	92,1 ± 1,0	47,6 ± 6,3
	45	94,0 ± 0,7	89,9 ± 1,2	43,3 ± 6,8
Temperature, ºC	**τ, *min***	**pH = 4,0**	**pH = 5,0**	**pH = 6,0**
	15	94,6 ± 0,7	91,8 ± 1,0	84,3 ± 1,9
60	30	93,4 ± 0,8	90,8 ± 1,1	82,0 ± 2,1
	45	89,3 ± 1,3	79,0 ± 2,5	88,8 ± 1,3
	15	93,8 ± 0,8	89,7 ± 1,3	77,0 ± 2,7
70	30	92,7 ± 0,9	88,9 ± 1,3	-
	45	92,1 ± 1,0	87,8 ± 1,5	72,8 ± 3,2

Note: pH modelled at (25 ± 2)°C

During the treatment of CCC at pH 3.0 to 6.0, the color of the solid phase does not change, while the extract becomes yellow; extraction of Carthamin induces irreversible transformations of the chromophore, which occur only in the aqueous phase, following regressions:

$$\mathbf{E_{60°C} = -3,51 + 0,06\tau + 1,15pH}, \qquad (4.1)$$

$$\mathbf{E_{70°C} = -6,47 + 0,07\tau + 1,92pH}, \qquad (4.2)$$

Equations (4.1) and (4.2) are valid in the pH range 3.9...6.0, which corresponds to a wide variety of foods. At 60°C, the percentage of Carthamin extraction from the cellulose phase is less than 5% if the extraction time does not exceed 27 minutes. At 70°C, 5% of Crt is extracted at pH = 5.4 within 15 minutes.
From Equations (4.1) and (4.2), it follows that for the use of CCC in food processing, the pH should not exceed 5.0. Processing at 60°C should last up to 30 minutes, and at 70°C up to 15 minutes. Hypothetically, the decomposition of Crt in CCC follows first-order kinetics (Figure 26).

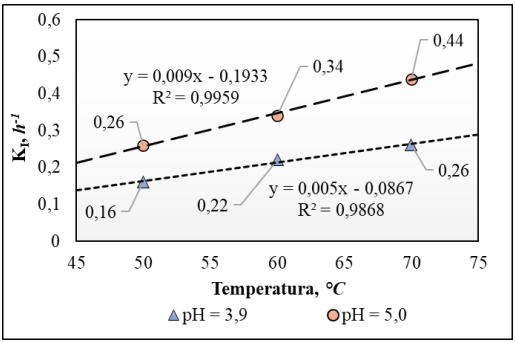

Fig.26. K_I of Crt *in nascendi* degradation after 15 min. treatment

The values of E_A for Carthamin decomposition at pH = 3.9 and pH = 5.0 were 22.4 kJ and 24.2 kJ, respectively. This is an argument that the decomposition of Carthamin from CCC takes place at the cellulose/solution interface, *in nascendi*, when Carthamin is no longer part of CCC but is already in the solution. The ratio $K_{I,T(Aq)}$ / $K_{I,T(CCC)}$characterizes how many times CCC is more stable than free Carthamin present in the aqueous phase (Table 9).

Table 9. Relative stability (α) of Crt in the phase CCC / in solution

Temperature, °C	50,0 ± 0,5	60,0 ± 0,5	70,0 ± 0,5
$\mathbf{K_{I,T(Aq)}}$	19 ± 4	93 ± 16	417 ± 71
$\mathbf{K_{I,T(CCC)}}$	0,26 ± 0,01	0,34 ± 0,02	0,44 ± 0,02
$\mathbf{\alpha = K_{I,T(Aq)} / K_{I,T(CCC)}}$	73 ± 13	273 ± 47	$(9,5 \pm 1,7) \cdot 10^2$

With increasing temperature, the relative stability of Crt in the cellulose phase, **"α"**, increases. This is another argument that Crt decomposition occurs at the moment of extraction into the solution. It is well known that water determines the stability and longevity of the entire system. In the context of the presumed practical use of Carthamin for food coloring, analysis of the chromatic parameters in the aqueous phase and in the swollen CCC phase, corresponding to its state in foods, is of interest. Depending on pH, aqueous Carthamin solutions are grouped into at least four color-shades (Table 10). The value of the green component ("G") decreases significantly in the pH 3...6, with an increase in the red ("R") and blue ("B") components. The predominance of the "R" component in the RGB profile of Carthamin solutions within the indicated pH range corresponds to the absorption maximum at 470...520 nm. Swollen CCC samples were obtained by preparing suspensions of the CCC complex (weighed dry, 0.1 g) in model solutions of the respective pH, stirring for 15 min, washing with the same solution, and separating the swollen CCC. The chromophore of the Crt molecule behaves differently in the aqueous phase and in the cellulose phase. At pH > 6, Crt in the swollen cellulose phase is purple.

Table 10. RGB-data for Carthamin and CCC

pH	10	9	8	7	6	5	4	3	2	1
Carthamin in solutions										
<R>	232	233	229	234	241	240	232	230	228	224
<G>	176	165	167	161	143	133	130	137	147	176
<B>	84	102	118	123	141	141	136	139	135	128
Swollen Carthamin-cellulose complex										
<R>	144	97	86	82	89	136	132	123	135	128
<G>	90	41	20	19	21	14	6	8	7	11
<B>	139	79	59	62	65	37	31	29	36	39

At the same pH, Crt in water exhibits orange shades. At pH = 1.0...5.0, swollen CCC samples display a magenta-bordeaux color. The *p*-hydroxyphenyl groups, formally attached at positions 9 and 9′ of Crt, are analogues of the *p*-cresol molecule. Therefore, for Crt, a correlation is expected between pH corresponding to the phenol-quinone transformations of *p*-cresol and the experimentally determined color transition interval (CTI) of Carthamin. For *p*-cresol, pKa = 10.2 (36). The pH_{CTI} for the *p*-cresolic fragment of Crt lies within the pH = 9.2...11.2, corresponding to the color change of Crt solutions from pink to orange at pH ≈ 10. In Figure 27, the C^1-C^{16} and $C^{1'}$-C^{16} bonds in acidic Hydrocarthamin (HCA) and basic Hydrocarthamin (HCB) are highlighted by dotted lines. Unlike the anhydrous forms of acidic Carthamin (CA) and basic Carthamin (CB), the C^{16} atom in HCA and HCB is in the sp^3 state, allowing rotation of the chalcone fragments. Using as precedent the blocking effect of anthocyanins in the cation-exchanger (37), it was hypothesized that in the cellulose the rotation of Crt is restricted, whereas rotation proceeds freely in water. In this case, tautomeric equilibria lead to different color forms of Crt in water and in cellulose, which is indeed observed experimentally.

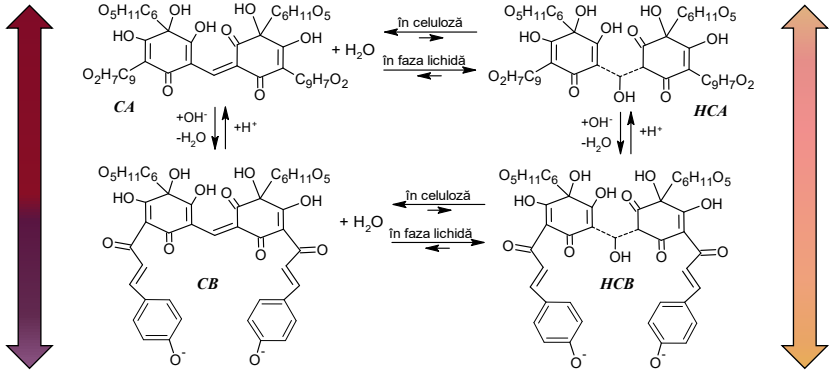

Fig.27. Color transitions of Carthamin in cellulose / water: CA - acidic Crt; HCA - acidic Crt · H_2O; CB - basic Crt; HCB - basic Crt · H_2O

Anhydrous Carthamin may pass into the hydrated state with M = 928 g·mol (38). This transition, accompanied by a change in the hybridization state of the C^{16} from sp^2 to sp^3, makes rotation of the quinochalcone groups possible.

Mechanism of Crt stabilization in the cellulose phase. In the FTIR spectra of CCC (Figure 28), weak bands are recorded at frequencies of 2340 and 2360 cm^{-1}, which are observed neither in the spectra of cellulose nor in the spectra of Crt. The appearance of new bands indicates a strong interaction between cellulose and Carthamin. This represents an independent instrumental indication which, together with the kinetic parameters, is interpreted as an argument in favor of complex formation rather than a simple mixture of Carthamin with cellulose.

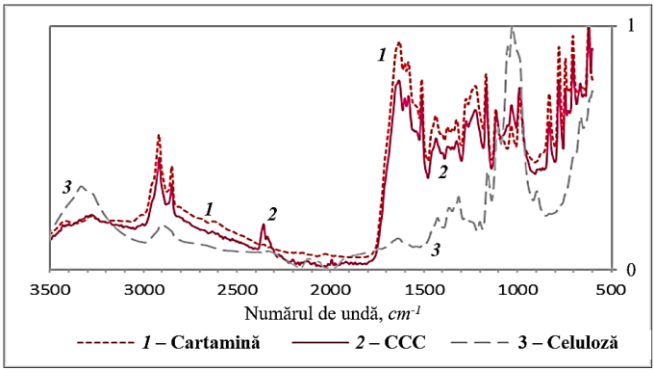

Fig.28. FTIR/ATR normalized spectra

Other effects were also observed in the FTIR spectra. The cellulose spectrum contains a broad band at 3330 cm^{-1}, attributed to intermolecular hydrogen bonds. The CCC spectrum in the 3200...3500 cm^{-1} frequency range is practically identical to the spectrum of Crt powder. This similarity is explained by the fixation of Carthamin molecules in the solid phase formed by cellulose macromolecules through the formation of dye-polymer hydrogen bonds. As a result of this complexation, the FTIR spectrum of CCC shows a decrease in the contribution of hydrogen bonds, –OH···HO–, between cellulose macromolecules. According to recent data, the band of intermolecular hydrogen bonds corresponds to the frequency 3370 cm^{-1} (39). Thus, according to the FTIR data, adsorption of Carthamin on cellulose leads to reorientation of the intermolecular hydrogen bonds of cellulose toward Carthamin. The results obtained both from RGB profile analysis and from interpretation of the FTIR-ATR spectra demonstrate that Carthamin molecules are rigidly fixed on cellulose. The molecular model of the complex is presented in Figure 29. As a result of this rigid fixation, it is assumed that even in the case of hydration, the Carthamin molecule loses the ability of free internal rotation along the C^1-C^{16} and C^{16}-$C^{1'}$ bonds. This assumption is partially confirmed by the smaller number of

color shades of the Carthamin-cellulose complex compared with free Carthamin in solution phase.

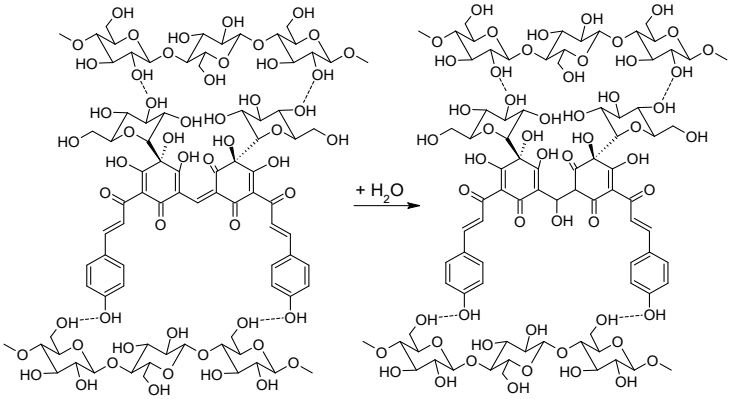

Fig.29. Blocking of the Hydrocarthamin internal rotation in CCC

Blocking of rotations in the Hydrocarthamin molecule explains the disappearance of semitones. The stability of RGB values of the Carthamin–cellulose complex in the wet state, compared with real Carthamin solution, correlates with data reported by other researchers. It has been reported that sugar solutions provide a measurable increase in the stability of quinochalcones from Safflower (40). The stabilizing effect can be explained by competition for water molecules (41) (31*). The values of water activity, a_W, were measured for cellulose, Carthamin, and CCC samples (8*): a_W (CCC) = 0.53 ± 0.01; a_W (cellulose) = 0.52 ± 0.01; a_W (Carthamin) = 0.50 ± 0.01. The higher water activity of CCC confirms the rearrangement of hydrogen bonds (Cel)–OH···HO–(Cel) and (Crt)–OH···HO–(Crt), with the formation of (Cel)–OH···HO–(Crt) bonds. Reducing the risk of pathogen contamination necessitates the development of colorants resistant to thermal treatment. To determine the thermal stability of dry CCC, samples with Crt/CCC = 120 mg/g and mass 0.100 ± 0.001 g were thermostated (Δt = ±0.2°C), then extracted with 1% Na_2CO_3 and immediately chromatographed. By regression analysis, Equation (4.4) was derived:

$$iCrt_{\%} = 1{,}9107 - 0{,}0023\ t + 0{,}0054\ \tau \qquad \Delta\beta = 0{,}15 \qquad (4.4)$$

where: **iCrt%** - Isocarthamin, %; **t** – temperature, °C; **τ** – treatment time, min. The values of the **β**-coefficients in Equation (4.4) demonstrate that the iCrt content decreases moderately with increasing temperature but increases with longer heating of CCC. The non-correlation between Crt/iCrt and heating time confirms that, in CCC powder, formation of the intermediate does not occur.

4.4. Technology for obtaining/prolonging functionality of the YFDS/Crt.

✓ The overall objective is to ensure the applicability of the colorants in industrial foods and in public catering. The operational objectives are:

- ✓ reduction of acid-base, oxidative, and enzymatic degradation;
- ✓ ensuring coloration of semi-finished products and foods with these dyes;
- ✓ achieving aggregative and structural stability of the colorants in foods;

Table 11. Parameters of fabrication system for YFDS and CCC

Holon	Settled Input/Output parameters of the technological system
Safflower petals	✓ "Mature" petals (red in color). ✓ Total quinochalcone content in petals: 25 ± 5% of DM. ✓ Absolute moisture content of petals: 4 ± 1%.
Technological line	✓ Ensures obtaining the red colorant (CCC) and the Yellow Food Dye from Safflower (YFDS) from the same batch of raw material. ✓ Line capacity: 50 ± 10 kg of petals per production cycle. three cycles of approximately two hours per shift (eight hours). ✓ Overall extraction–separation–packaging yield: 85 ± 5%.
Final product (colorants)	✓ Pink-magenta colorant, CCC, insoluble powder, Carthamin content from 10% (pink) to 25% (magenta), packaged in 10 ± 1 g units. ✓ YFDS – paste, 30...35% DM, or powder, 95...97% DM.

Using the specifications in Table 11, the production scheme of the colorants was developed (Figure 30).

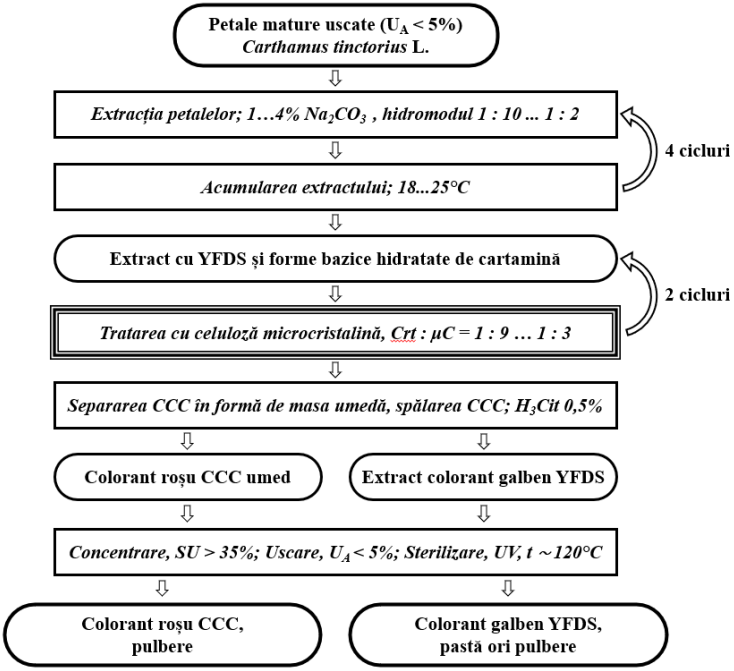

Fig.30. Technological scheme for quinocalconic colorants fabrication

Dried mature petals (H_A < 5%) are subjected to alkaline extraction with 1...4% Na_2CO_3, at a hydro module of 1:10...1:2, in four cycles, with extract accumulation at 18...25°C, yielding an extract containing YFDS and hydrated basic forms of Carthamin. The extract is treated twice with microcrystalline cellulose (Crt:μC = 1:9...1:3), followed by separation of the CCC complex in the form of a wet mass and washing with 0.5% citric acid solution, resulting in two fractions: red colorant CCC and YFDS extract. The fractions are concentrated (DM > 35%), dried to MC < 5%, and sterilized (UV, 120°C), yielding CCC powder and YFDS, paste or powder. A mass ratio Crt:μC within 1:9...1:3 leads to the production of CCC with a Carthamin content of 10...25%. Since the instability of Carthamin in the dissolved state has been demonstrated, the presence of traces of Crt in YFDS destabilizes the food system. Therefore, treatment with microcrystalline cellulose is crucial both for obtaining CCC and for the quality and prolongation of YFDS functionality (42*, 45*).

Coloring power may be expressed as the minimum amount of colorant that produces the required color and is measured in grams of colorant per liter or kilogram of product, $g \cdot L^{-1}$ or $g \cdot kg^{-1}$. The optimal amount of colorant is determined based on the absorbance of sufficiently colored solutions, A = 0.20...2.00 at l = 1 cm. Solutions with A < 0.20 have indistinct shades. At A > 2.00, the color becomes unnatural. Prediction of the required amount of YFDS is possible by direct application of the Lambert-Beer Law. Color perception in semi-opaque systems is formed in a 0.05 cm layer. The extinction of the YFDS colorant, calculated with reference to Precarthamin (PCrt), is 16500 $L \cdot mol^{-1} \cdot cm^{-1}$ at pH = 5.00. The calculated YFDS amount per 1 kg of product:

$$m_{YFDS} = \frac{A}{\varepsilon \cdot l} \cdot M_{PCrt} = \frac{A \cdot 957\ g \cdot mol^{-1}}{0{,}05\ cm \cdot 16500\ L \cdot cm^{-1} \cdot mol^{-1}} = 1{,}16 \cdot A \qquad (4.5)$$

From Equation (4.5), the mass of YFDS for A ∈ (0.20; 2.00) is estimated at 0.25 to 3.0 $g \cdot L^{-1}$ (Figure 32). Based on the extinction of Carthamin, 3800 $L \cdot mol^{-1} \cdot cm^{-1}$, and the mass fraction of Crt in CCC, 10...25%, it is concluded that for red coloration, the mass of CCC must be about 5...10 times greater than in the case of YFDS, amounting to 4...16 $g \cdot kg^{-1}$ of solid product (Figure 31).

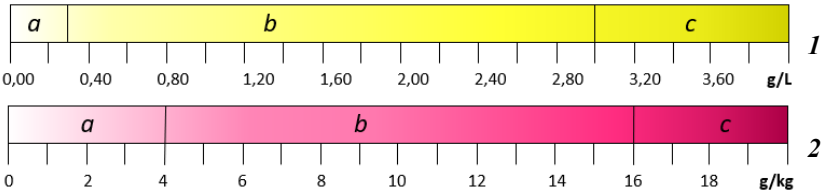

Fig.31. Reference scale for colorant dosages of YFDS (1) and CCC (2): a - in a lightly colored product; b - in an optimally colored product; c - in an overcolored product or with excessive colorant

Color formation in real systems depends on the food texture, co-pigmentation, and the physical parameters of the manufacturing. Depending on the stability of the dye to physicochemical factors, its addition may be carried out either during the formation of the food composition (preferably) or before packaging. Yogurt samples were produced using our method (4*, 41*), with YFDS added at the final stage of processing. The colors of the yogurt samples were evaluated using the CIELab technique, taking yogurt without added color as the reference. The coordinates L*, a*, and b* were determined (Table 12).

Table 12. CIELab for yogurt with YFDS

Denumirea	**0%**	**0,1%**	**0,2%**	**0,3%**	**0,4%**
Lightness, L*	75,1	75,3	**74,8**	**74,4**	74,6
Red-Green, a*	-2,9	-4,2	**-4,7**	**-5,2**	-5,2
Yellow-Cyan, b*	9,1	13,3	**15,5**	**18,0**	18,4
Shift color, ΔE	---	4,4	**6,7**	**9,2**	9,6
DM, %	11,7 ± 0,1	11,8 ± 0,1	11,9 ± 0,2	12,0 ± 0,2	12,1 ± 0,2
Fats, %	3,00 ± 0,11	2,97 ± 0,10	2,96 ± 0,09	2,96 ± 0,09	2,96 ± 0,09
pH	4,40 ± 0,03	4,41 ± 0,03	4,46 ± 0,03	4,48 ± 0,03	4,44 ± 0,03
η, Pa·s	3,31 ± 0,17	3,90 ± 0,20	3,84 ± 0,19	3,93 ± 0,20	3,97 ± 0,18
Syneresis, %	70,86 ± 0,71	66,31 ± 0,67	62,84 ± 0,63	60,78 ± 0,61	61,65 ± 0,62
Sensorial	4,8 ± 0,2	4,2 ± 0,4	4,4 ± 0,3	4,6 ± 0,2	4,9 ± 0,1

From Table 12, it follows that the reasonable YFDS content is 0.2...0.3%, respectively 2...3 g of colorant per 1 kg of yogurt. Exceeding this amount does not lead to substantial changes in the chromatic parameters a*, b*, and ΔE. When the YFDS content increases from 0.3 to 0.4%, the parameter ΔE increases by only 0.4 units, which is not perceived by the naked eye (42).
The data obtained correlate well with the estimated model based on extinction values, Figure 31. Yogurt samples containing 3 and 4 g YFDS / kg of yogurt were monitored during storage by measuring chromatic parameters (12*). Yogurt with tartrazine, E 102, was used as the control (Table 13).

Table 13. Variation of CIE-Lab parameters of yogurts with colorants

Colorant	**0,3% YFDS**		**0,4% YFDS**		**0,1% Tartrazine**	
Depozitare, days	**0**	**28**	**0**	**28**	**0**	**28**
Lightness, L*	74,4	74,6	74,6	74,0	75,2	75,5
Red-Green, a*	-5,2	-5,1	-5,2	-5,3	-5,8	-5,9
Yellow-Cyan, b*	18,0	18,0	18,4	18,9	18,3	18,6

Table 13 reflects the chromatic stability of yogurt with YFDS as an integral food system. The color of the yogurt remains practically constant throughout the entire monitoring period. Upon centrifugation, the yogurt separates into three phases: protein, aqueous, and lipid. The colored aqueous phase is filtered through a 0.45 μm PTFE filter. In Figure 32, quinochalcones are visualized after 7 days of storage, recorded at $\lambda = 404$ nm, average for chalcones (26*).

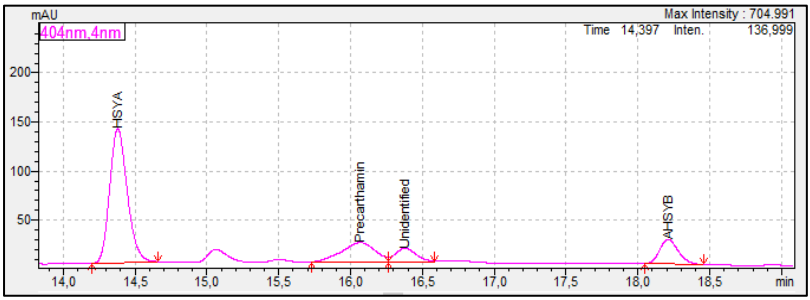

Fig.32. Quinochalcones identified in yogurt with YFDS after 7 days

The data obtained from processing the peak area of Hydroxysafflor Yellow A, HSYA; Anhydrosafflor Yellow B, AHSYB; Precarthamin, PCrt - demonstrate a constant chalcone ratio throughout the storage period, mg/100 g yogurt: HSYA (248 ± 9); PCrt (72 ± 3); unidentified (32 ± 2); AHSYB (48 ± 2).

The chromatic parameter ΔE characterizes the magnitude (but not the direction) of the color change vector and, in the case of chemical degradation, could indicate visible changes in chromatic parameters, particularly lightness. However, ΔE does not exceed 0.8 units over 4 weeks. Thus, YFDS does not fade and maintains its function - product coloration throughout the storage period, being an excellent natural substitute for Tartrazine.

Conclusions to Chapter 4

1. Technologies were developed for obtaining high-molecular-weight biopolymers. Arabinoxylan is extracted from the same batch of *Linum* seeds from which oil rich in polyunsaturated fatty acids is obtained.
2. It was demonstrated that biopolymers prolong BAC functionality. Inulin, HHur, alginates, and PVOH act as factors of protection or destabilization, depending on the structure of the colorant and the nature of the biopolymer.
3. Hyaluronic acid destabilizes anthocyanins, accelerating their degradation in aqueous solutions. Betanin, in contrast, is stabilized by HHur and PVOH at HHur > 0.03%, indicating potential for synergistic applications.
4. Carthamin (a quinochalcone from safflower), unstable in water, forms a stable edible complex with cellulose (CCC). Complexation protects the pigment against temperature and pH; stability is maximal at pH 3.9–5.0 and T < 60°C, allowing its use in acid-lactic products.
5. UV-Vis, FTIR, CIE-Lab, and RGB studies confirm significant differences between the behavior of colorants in aqueous solutions and in polymer matrices, highlighting the role of biopolymers in their stabilization. On this basis, technologies were developed to obtain the colorants YFDS and CCC for acidic food applications (pH < 5), including fruit yogurts.

5. PROLONGATION OF BIOLOGICALLY ACTIVE COMPOUNDS FUNCTIONALITY THROUGH MICROENCAPSULATION

Edible microcapsules are systems whose complex structural and functional organization is ensured by biopolymers, including proteins, which form compositions with polymers from other classes. Protein–polysaccharide systems are of interest as structural elements for microencapsulation (1*, 13*).

5.1. Mechanism of gelatin adsorption at the O/W interface.

The hydrophilic/phobic properties of proteins influence the self-assembly of biomolecules (43). The proline composition of gelatin differs from that of other proteins. In myofibrils, hydrophobic proline predominates (1.3...5.7%), while hydroxyproline is absent. In contrast, gelatin contains about 15% hydroxyproline (2). Of interest are the physicochemical processes that lead to the fixation of gelatin macromolecules at the interface of oil droplets in O/W emulsions - the precursors of microcapsules. A model was proposed to estimate the overall hydrophobicity, $HPhob_{\Sigma}$, expressing the proteins affinity for the oil.

- For amino acids, except for proline and hydroxyproline isomers:

$$M(R) = M(AAR) - M(NH_2 - \dot{C}H - COOH) = M(AAR) - 74) \quad (5.1)$$

- Only for proline and hydroxyproline isomers:

$$M(R) = M(AAR) - M(\dot{N}H - \dot{C}H - COOH) = M(AAR) - 73) \quad (5.2)$$

$$\omega(R) = \frac{M(R) \cdot \omega(AAR)}{M(AAR-Aq)} \quad (5.3)$$

$$HPhob_{\Sigma} = \sum \omega\,(R)_{HPhob} \quad (5.4)$$

where: M(R) - molar mass of the side chain; M(AAR) - molar mass of the amino acid; M(AAR-Aq) - molar mass of the amino acid residue in the polypeptide or protein; ω(R) - mass fraction of the side chain in the polypeptide/protein; $\omega(R)_{Phob}$ - mass fraction of hydrophobic side chains; ω(AAR) – mass fraction of the amino acid in the protein; $HPhob_{\Sigma}$ – total hydrophobicity; $HPhil_{\Sigma}$ - total hydrophilicity (Table 14).

Table 14.1. Composition of gelatin in hydrophilic side-groups

Acid, -phil	Cod	ω_{AAR}	M_{AAR}	M_{AAR-Aq}	M(R)	ω(R)
Arginine	Arg, R	10,0	174	156	100	6,4
Aspartic acid	Asp, D	6,7	133	115	59	3,4
Hydroxylysine	Hyl, hK	1,3	162	144	88	0,8
Hydroxyproline	Hyp, hP	14,7	131	113	58*	7,5
Histidine	His, H	0,7	155	137	81	0,4
Glutamic acid	Glu, E	11,8	147	129	73	6,7
Lysine	Lys, K	4,0	146	128	72	2,3
Serine	Ser, S	3,1	105	87	31	1,1
Tyrosine	Tyr, Y	0,4	181	163	107	0,3
Threonine	Thr, T	2,2	119	101	45	1,0
Hydrophilic acids:		**54**			**$HPhil_{\Sigma}$, %**	**29.9**

Table 14.1. Composition of gelatin in hydrophobic side-groups

Acid, -phob	Cod	ω_{AAR}	M_{AAR}	$M_{AAR\text{-}Aq}$	M(R)	ω(R)
Alanine	Ala, A	9,0	89	71	15	1,9
Valine	Val, V	2,5	117	99	43	1,1
Glycine	Gly, G	26,0	75	57	1	0,5
Isoleucine	Ile, I	1,0	131	113	57	0,5
Leucine	Leu, L	5,3	131	113	57	2,7
Methionine	Met, M	0,6	149	131	75	0,3
Proline	Pro, P	0,0	115	97	42	0,0
Tryptophan	Trp, W	0,0	204	186	130	0,0
Phenylalanine	Phe, F	2,5	165	147	91	1,5
Cysteine	Cys, C	0,0	121	103	47	0,0
Hydrophobic acids:		**46**			**$HPhob_{\Sigma}$, %:**	**8,5**
Total acids:		**100**			**Side-groups weight, %:**	**38,4**

Note: Data in columns 4...7 are calculated by the author, Equations (5.1)...(5.4).

The hydrophobicity of gelatin, 46%, calculated as the simple sum of amino acids, is much lower within the proposed model, when the contributions of hydrophobic side chains are considered: $HPhob_{\Sigma}$ = 8.5%. The absence of hydrophobic proline and the presence of hydrophilic hydroxyprolines reduce the hydrophobicity of gelatin twofold compared with other proteins. The structural arrangement of protein molecules into coils is typical only in the vicinity of the isoelectric point, IEP. Measurements of the electrokinetic potential ζ and the diagram of the GelAlg system demonstrate that the IEP is not suitable for the formation of stable microcapsule walls (9*). MC formation occurs at (IEP – pH) ≈ 1.0...1.5, when gelatin is a predominantly positively charged zwitter-ion, denoted $Gel^{+>-}$. The macromolecule does not lose its flexibility, not being transformed into a polycation or polyanion (44), and the accumulation of gelatin at the O/W **is not** coacervation. Formation of a gelatin layer on the lipid surface is determined by adsorption of lipophilic side groups (Figure 33), when gelatin molecules are in non-rigid conformations.

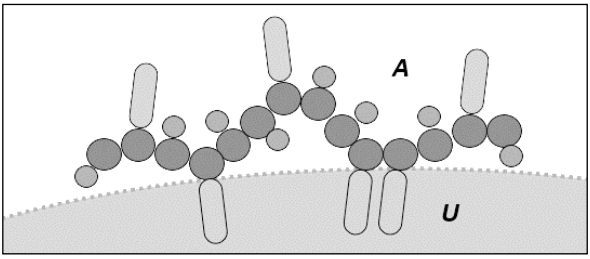

Group of $-NH-\dot{C}H-COO-$ or $-\dot{N}-\dot{C}H-COO-$ (Proline)
Hydrophilic side-group Hydrophobic side-group

Fig.33. Adsorption of the gelatin macromolecule on an oil droplet

From the small number of hydrophobic groups, which constitute only about 8.5% of the total mass of gelatin, not all participate in the adsorption; thus, at the O/W interface, what really forms are not a coacervate but a thin layer, which with reservation can be termed a “MC wall” and requires strengthening.

5.2. Development and interpretation of the GelAlg state diagram.

Systems were created in which the gelatin concentration is 1...3%, and the mGel/mAlg ratio varies from 1 to 90 (9*). The factors were predefined, the electrophoretic parameters of these systems were measured, and electrokinetic potentials were calculated in the case of sol formation. The results of the calculations using Equations (2.1) and (5.6) are presented in Table 15.

Table 15. Colloid type and ζ-potential in the Gelatin-Alginate system

m_{Gel}/m_{Alg}	**1.1**	**2.5**	**4.3**	**6.7**	**10**	**15**	**23**	**40**	**90**
$\log_{10}(m_{Gel}/m_{Alg})$	0.04	0.40	0.63	0.83	1.00	1.18	1.37	1.60	1.95
n_{Gel} / n_{Alg}	8	18	30	47	70	105	162	281	632
$M_{GelAlg}\cdot10^{-6}$, D	0.75	1.25	1.89	2.75	3.93	5.71	8.57	14.6	32.5
pH	**colloid: sol, if ζ, mV, is indicated. Δζ = ± 3.0 mV**								
4.5	Viscous solution						-41	-32.0	+14.5
4.0	-34	-40	-23	suspension of floccules			+17	gel	
3.5	-38	-35	-26	-20	+9	+12	+17	+29	gel

At low pH, electrophoresis is naturally disturbed by electrolysis. Therefore, a method was developed to visually assess the sign of the electric charges of the complexes (Figure 34).

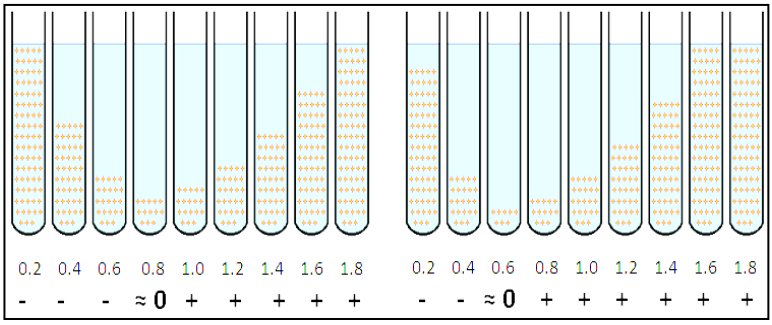

Fig.34. Sedimentation equilibria in the GelAlg system: function of $\log_{10}(m_{Gel}/m_{Alg})$ and particle charge sign: *A – at pH 3,0 ; B – at pH 2,5*

In the GelAlg colloids, obtained at pH 3.0 and at pH 2.5, a persistent equilibrium forms for 3...5 days. The sign of the solid phase is appreciated from the appearance of the series (figure 34). Thus, combining electrophoresis with visual control of the state of the colloids at low pH, the conditions of $GelAlg^0$ formation at different pH were studied (Table 16).

Table 16. Parameters of the neutral complex $GelAlg^0$ at different pH

pH	4.5	4.0	3.5	3.0	2.5
$\log_{10}(m_{Gel}/m_{Alg})$	1.7	1.1	0.9	0.80	0.60
m_{Gel}/m_{Alg}	50.1	12.6	7.9	6.3	4.0
n_{Gel} / n_{Alg}	352	89	56	44	28
$M_{GelAlg^0} \cdot 10^{-6}$, D	18.2	4.86	3.18	2.61	1.79

The neutrality point moves to lower values of the mGel/mAlg ratio, when the pH decreases. At the same time, at pH values close to the IEP a very small amount of polyuronic salts causes the formation of the GelAlg solid phase. The phase diagram of the gelatin polyuronate system, built in the coordinates "Gelatina/Polyuronate Ratio = f (pH)" (figure 35), represents the conceptualization of the laws in Table 15 and Table 16. The diagram is of great practical interest for controlling the interaction processes between gelatin and salts of polyuronic acids or other polyanions, which are used in microencapsulation techniques. At least 6 domains are highlighted.

Domain I corresponds to the mutual repulsion of the Gel– and Alg– anions. Most of Domain I is located at pH > 5, above the IEP of gelatin. At the ratio mGel/mAlg ≈ 1, the boundary of this domain drops to lower pH values (4.50…4.00), due to the excess of alginate and the formation of negatively charged complexes**. Domain II** corresponds to the formation of negatively charged particles, $GelAlg^-$ (or $GelHUr^-$). Uronic acids, alginic and hyaluronic, have anionic form at pH > 3.5, compensating for the positive charges of gelatin zwitterions. **Domain III** is like that of **II**: Excess gelatin $Gel^{+>-}$, determines the overall positive charge of the colloids in the form of flocs and Gel^+Alg soils, which sediment slowly.

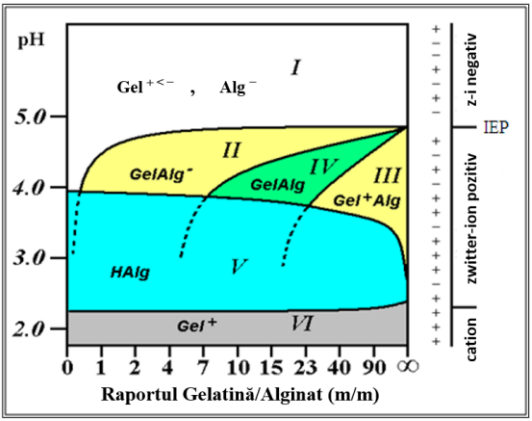

Fig.35. State diagram of the GelAlg system in the coordinates "Complex type = f (Gel/Alg ratio, pH)"

Domain IV is characterized by the formation of $GelAlg^0$ flocs, which settle rapidly. The charge of GelAlg complexes tends to zero as the mGel / mAlg ratio increases and the pH approaches the IEP. The formation of $GelAlg^0$ is contraindicated for MC walls. **Domain V**. At pH < 4, gelatin solutions acquire a transparency, inherent to real solutions, due to the stretching of the molecules following intramolecular repulsion. At pH < 3.5, the polyuronates precipitate in the form of the respective acids, $pK_{acid} \approx 3.5$ (45). **Domain VI** corresponds to pH values < 2, with solid HAlg or HHUr, gelatin representing the Gel^+ polycation. In **Domain VI**, the formation of $GelAlg^+$ is impossible.

5.3. Microencapsulation technology and microcapsule stability control.

The U/A emulsion with the characteristics necessary for initiating the formation of microcapsules is formed by mixing the oil phase, subjected to microencapsulation, with 3…4% gelatin solutions, the pH of which is 2.5…4.0 (48*). This range can be extended to pH = 1.5…5.0 for microcapsules with GelHur walls. Citric acid contributes to the consolidation of protein layers on the surface of oil droplets, generating up to seven hydrogen bonds (46). The formation of the emulsion requires compliance with temperatures of 50…60°C, rarely 60…80°C, $\Delta\tau = \pm 2.0$°C, due to the sensitivity of interfacial processes and the instability of CBA to heating. After the formation of the emulsion, its slow cooling to 15…20°C follows (Table 17).

Table 17. Interaction of factors in the microencapsulation process

↓entropy,↑microencapsulation efficiency	**Regime "V-t-τ"**	**Replica of the studied system**
	Low stirring speed (25...75 rpm) in all stages and at all thermal regimes	Formation of unstable emulsion with large oil droplets (50...100 μm), decreased yield
	High speed (300...450 rpm) of stirring at all stages of microencapsulation	Formation of free gelatin scales that do not participate in the formation of MC walls
	Slow decrease in stirring speed followed by sudden decrease in temperature	Destruction of MC by forming three separate phases: oil, water and gelatin scales
	Slow decrease in temperature, concomitant with gradual decrease in stirring speed	**Formation of "proto-MC" (stable), lack of separate oil and gelatin phases**

The stirring speed has a significant influence on different stages of the microencapsulation process and needs to be monitored. It has been observed that a sudden decrease in the speed of rotation can cause phase coalescence and microencapsulation failure. Good results were obtained when the stirring speed slowly decreased from 300...450 rpm to 25...75 rpm, simultaneously with the slow cooling of the mixture from 60...90°C to 15...20°C (Table 19). The efficiency of microencapsulation increases with decreasing entropy.

Formation of MC walls. The consolidation of MC walls is studied with SSF-MC-EPC (fig. 2), obtaining the electrochemical profile, fig. 36 (16*).

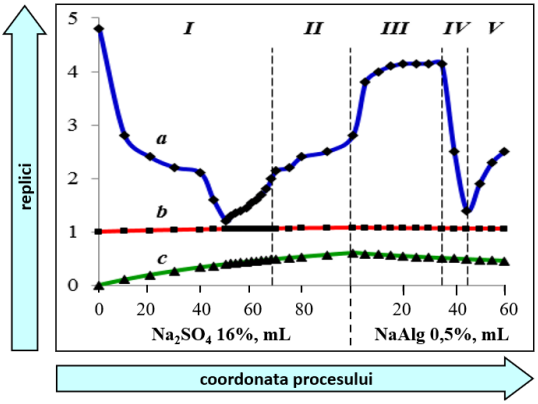

Fig.36. Interaction Gelatine-Na_2SO_4-Alginate. Replicates*: a – resistance, kΩ; b – density, g·mL^{-1}; c – C_M Na_2SO_4, mol·L^{-1}; Stages: I – gelatin dehydration; II – $Gel^{+>}$ deposition on the droplet surface; III – $GelAlg^+$ complex formation; IV – $GelAlg^0$ formation; V – $GelAlg^-$ formation*

The formation of the condensed phase, corresponding to the formation of microcapsule walls, occurs by expelling excess water from gelatin by dehydration with sodium sulfate, the concentration of which, according to SSF-MC-EPC data, is 6…7%. Interactions of sodium sulfate with water can cause syneresis of the gel, which forms the MC wall. The influence of Na_2SO_4 on the dynamics of consolidation of MC membranes has been studied (38*). The maximally strong state of the wall corresponds to Na_2SO_4 concentrations ranging from 5.4…6.4%. These data fall, in a direct sense, within the range determined using SSF-MC-EPC. After establishing the equilibrium between the microcapsule wall and the supernatant, the desiccant will be distributed between these two phases. Na_2SO_4 contributes to the self-compression of the gel. Ensuring the edibility of microcapsules involves removing excess desiccant. Dialysis and electrodialysis through cellulose film are effective for removing excess desiccant from the supernatant with microcapsules. Electrodialysis is performed with monitoring of conductivity, avoiding complete removal of Na_2SO_4 from the MC walls. Substitution of the supernatant with a medium, in which the desiccant is absent, will cause its diffusion (extraction), which will lead to destabilization and damage of the MC wall. Therefore, exceeding the electrodialysis time leads to destabilization of the walls and release of the contents. Studies of the Gelatin – Gum Arabic system confirm that the qualifiers “thick” and “strong” are not synonymous for the walls of microcapsules. The study of the Gelatin – Gum Arabic (GA)

system showed that the efficiency (yield) of microencapsulation practically does not depend on the overall mass fraction of the wall, increasing with increasing the Gelatin/Gum Arabic ratio (47). The stability of the wall is also strongly influenced by the density factor. Adsorbed biopolymers reduce the surface tension at the U/A interface by almost twofold (48). It is considered that the oil droplet can maintain only a thin, practically monomolecular layer of biopolymer on the surface (49). The densities of lipids, proteins and carbohydrates are reported as 0.9 : 2 : 1.5, which represents a destabilizing factor. The thick layer of biopolymer is torn off the droplet surface by gravitational stratification, causing the destruction of the MC.

Technological scheme of lipid microencapsulation with CBA. The scheme for obtaining MC with lipid content (48*) is presented in figure 37.

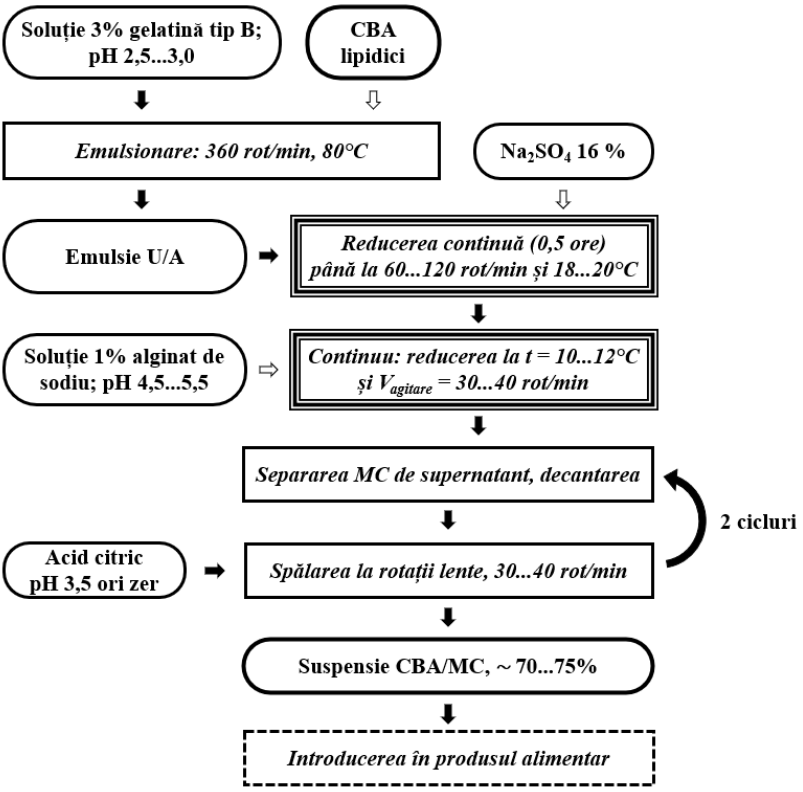

Fig. 37. Technological scheme for obtaining tank-type MC

The stages of slow administration, 0.5...2.0 mL·min^{-1} (referring to 100 mL gelatin), are denoted by (⇩). A 3% gelatin "B" solution with a pH 2.5...3.0 is

prepared by dissolving the gelatin in hot water and adjusting the pH with citric acid, and, if necessary, hydrochloric acid. The gelatin solution is introduced into the reactor with a stirrer and heating and cooling system. Under intense stirring, 360 rpm and at t = 60...80°C, the lipid phase, subjected to microencapsulation, is slowly introduced into the gelatin solution. After obtaining the emulsion, a 16% Na sulfate solution is slowly introduced into the reactor. At the same time, during the administration of Na sulfate, within 0.5...1.0 h, the stirring speed is still reduced to 60...120 rpm, and the temperature to 18...20°C. At this stage, the lipid droplet is covered with a wall of condensed gelatin, but this wall is unstable. The MC with gelatin walls begin to release the lipid phase 15...20 min. after stopping the agitation. Overnight, the proto-MC undergoes total syneresis. Therefore, the formation of a resistant wall follows immediately after the proto-MC formation stage. After finishing the administration of Na_2SO_4, a 1% NaAlg solution, adjusted to pH 4.5...6.5 with NaOH and/or citric acid, are gradually dropped into the reactor. The slow administration of NaAlg occurs simultaneously with the reduction of the temperature to 10...12°C and the stirring speed to 30...40 rpm. A wall of $GelAlg^+$ is formed around the lipid droplet, which ensures the prolongation of the functionality of the CBA. The obtained MC are separated from the supernatant by rapid decantation and rinsed with citric acid solution pH = 3.5. The cycle is repeated twice. Washing can be performed with dairy whey. The MC concentrate contains approx. 60...70% MC. Being separated from the supernatant, it becomes impossible to distribute MC uniformly in the food. The washing step of the proto-MC with gelatin walls can be omitted, and the obtained proto-MC are immediately treated with 1...2% polyuronates, or the extract (5...15%), obtained from the corresponding raw material: *Saccharina japonica* or *Gallus domesticus* (47*,48*) (50). Removal by decantation of the supernatant, followed by dialysis or electrodialysis of the MC until the conductivity of the washing water is about 10^{-3} $Sm \cdot m^{-1}$, causes the MC suspension to lose its bitter taste, MC becoming suitable for food.

Aggregative MC stability during electrophoresis. MC were subjected to electrophoresis and polydispersity analysis, equations (2.7)...(2.9). The presence of Na_2SO_4 requires purification of microcapsules by dialysis or electrodialysis through cellulose foil membranes. Dialysis continues until the conductivity of the washing water reaches 10^{-3} $Sm \cdot m^{-1}$. The dialysate (microcapsule suspension) is subjected to electrophoresis, using the following parameters: graphite / stainless steel electrodes; cathode-anode distance: 10/25cm; voltage: 10/100V; field intensity: 100/400$V \cdot m^{-1}$. At the anode (+), the destruction of MC was not observed even after 10...20 min. of electrophoresis. At the cathode, the large MCs were deformed and even broken (figure 38, B). Oil appears in the cathodic space, indicating the destruction of the MC by the interaction of their walls with the products of water electrolysis:

OH- at the cathode and H+ at the anode. Since it is not possible to measure the pH in the vicinity of the flat electrode, the pH was estimated from Faraday's Law, for I = 100 mA, τ = 15 min. In this case, $pH_{anode} \approx 3$, $pH_{cathode} \approx 11$.

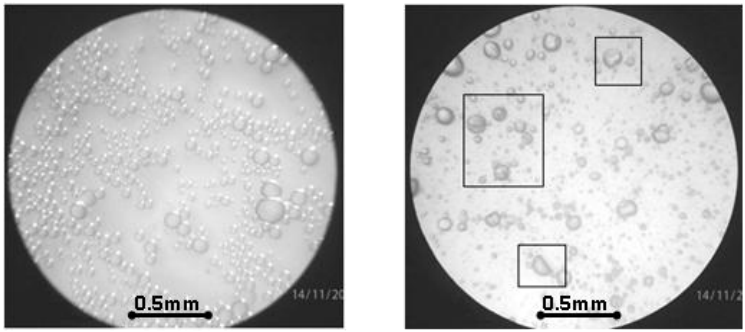

A *B*

Fig.38. MC with GelHur walls after electrophoresis: A – at the anode; B – at the cathode, deformed and broken MCs are outlined

Protein-polyuronate systems are stable at pH ≈ 2...5 (51) (9*). At the cathode (OH^-), as the pH increases, the destruction of the microcapsule walls occurs: $GelAlg + nOH^- \rightarrow Gel^- + Alg^-$. The high stability of the microcapsules in the anodic space is confirmed by the data for the polydispersity of the samples (figure 39). The maximum of the MC distribution curve, taken *in nascendi* directly from the reactor, is located at 75...100μm, being shifted towards small diameters. The polydispersity curve of MC extracted from the anodic space is like the respective curve of the MC sample, taken from the surface of the dialyzed suspension. In both cases the maximum is located at <d> ≈ 125μm.

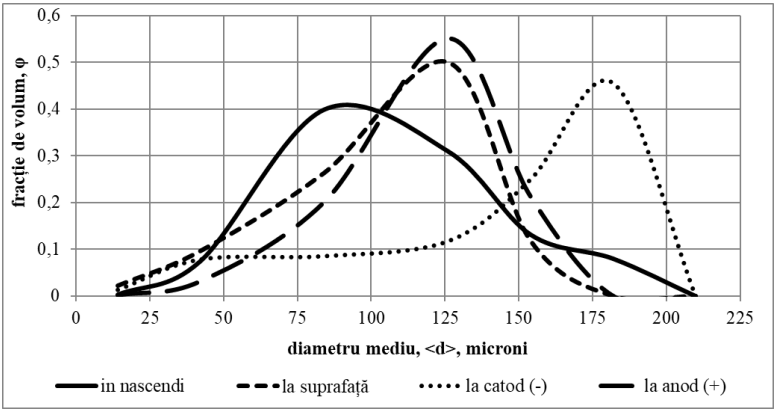

Fig.39. Statistical distributions of microcapsules in electrophoresis

This is also confirmed by the appearance of MC polydispersity in the cathodic space, which is shifted towards larger diameters. Fraction, which moves from the cathode to the anode, consists of MC of d < 35μm (figure 40). The effect of MC migration during electrophoresis is of interest for the separation of stable fractions in the formulation of targeted delivery systems.

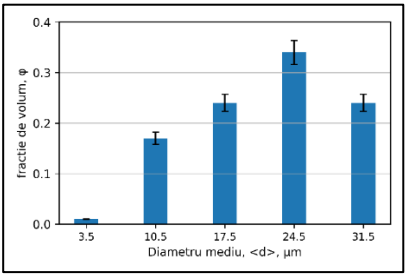

Fig.40. MC polydispersity, anode

MC in the human digestive system (HDS) model. The HDS is divided into three zones – functional cavities with secretory glands. Enzyme activity, pH, residence time in the HDS zone differ substantially (Table 18).

Table 18. Areas of the human digestive system (52)

Zona SDU	pH	Active enzymes	τ, *h*
Oral cavity	6,5...7,5	α-amylases: ptyalin, maltase	0,01
Pharynx, esophagus	6,0...7,0	α-amylases: ptyalin, maltase	0,02
Stomach	0,9...1,1	maltase, proteases, gelatinase	1...2
Small intestine	7,0...7,5	peptidases, lipases, nucleases	3...5
Large intestine	8,5...9,0	peptidases, lipases, nucleases	4...6

Multifactorial modeling of the conditions of the human digestive system (HDS) was carried out in a functional control system (FCS). FCS-HDS contains chemical, mechanical (administration speed), physic-chemical (setting and control of t, pH), electrochemical control elements (figure 41).

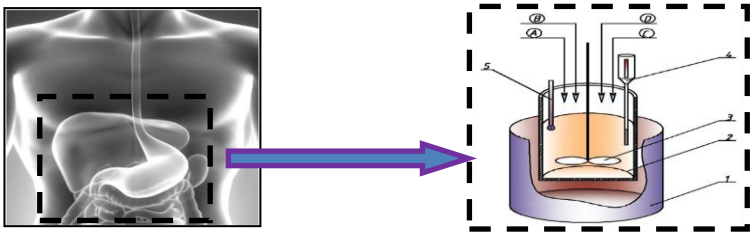

Fig.41. Model FCS-HDS: ***1 – thermostat; 2 – „stomach"; 3 – low-velocity stirrer ; 4 – thermometer; 5 – electrodes; a – HCl; b – enzymes; c – MC; D – $NaHCO_3$***

The microcapsules were introduced into the SCF-SDU and subjected to treatments corresponding to the physicochemical parameters indicated in Table 20. After the treatments, the integrity of the microcapsules was analyzed as a function of their polydispersity. The digestive process begins in the oral cavity under the action of enzymes from the α-amylase group, which hydrolyze amylopectin (53). Alpha-amylase in slabber does not hydrolyze alginate with bonds and cellulose (31). Physiological studies show that chewing practically

produces particles of about 500 μm, respectively, particles with a diameter smaller than 2...50 μm are not destroyed (54). In a strongly acidic environment, in the presence of enzymes, at 37°C and slow stirring, no destruction of MC was observed, regardless of MC size. Rapid MC damage is observed under conditions of duodenum. Being placed here, MC no longer exist after five minutes, returning to the O/W emulsion, which undergoes coalescence. Modeling the passage of MC through the HDS demonstrated that BAC encapsulated in MCs with GelAlg and GelHur walls reach the intestine intact, where release content. Thus, by using MCs with GelAlg and GelHur walls, PUFA are delivered to the small intestine, achieving the "targeted delivery" principle, and microencapsulation ensures the prolongation of functionality.

5.4. Technology of dairy products with microencapsulated BAC.

Dairy products are characterized by the seasonal content of BAC, respectively, the seasonal character will also have their functionality. In many cases, traditional methods cannot ensure the preservation of the biological and vitamin activity of biologically active compounds in food systems.

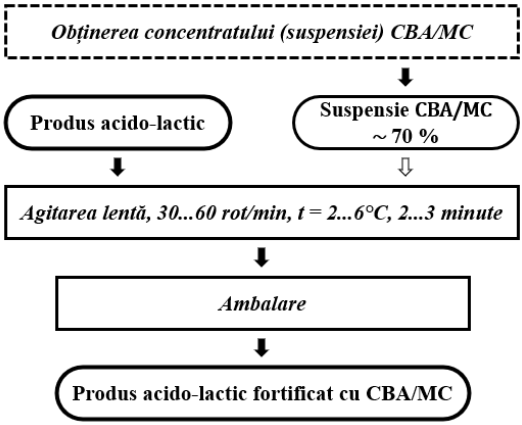

Fig.42. Scheme of administration of MC suspension with biologically active lipid compounds in lactic acid products (sour cream, kefir)

Lactic acid products are suitable for incorporation of MC with CBA, due to the comfortable pH ≈ 4 for GelAlg walls. Microcapsules, obtained according to (48*), are to be immediately introduced into the lactic acid product (figure 42). Two types of microcapsules, MC1 and MC2, were obtained. For the preparation of the MC core content, the commercial β carotene concentrate 0.837 ± 0.002% ("Bosko", Russia) was used, which corresponds to the solubility limit of carotenes in fats (55). The concentrate was diluted with refined sunflower oil to bring the β carotene content to values of 0.17 ± 0.01% or 0.21 ± 0.01% (Table 19).

Table 19. Characteristics of MC with vitaminized microencapsulated oil

MC	d, *μм*	<d>, *μм*	R_U, *μм*	βC in oil, *%*	UMV/MC	βC în MC, *mg/100g*
MC_1	5...50	10	4,63 ± 0,08	0,17 ± 0,01	0,77 ± 0,04	129 ± 7
MC_2	2...20	5	2,13 ± 0,08	0,21 ± 0,01	0,62 ± 0,04	130 ± 9

Note: d – diameter range; <d> – average diameter of MC; R_U – internal radius of MC core; L – MC wall thickness; βC – β-carotene; UMV/MC – mass fraction of vitaminized microencapsulated oil in MC.

Products used were milk 2.5%, cream 10%, K0 – kefir 0%, K2.5 – kefir 2.5%, S10 – sour cream 10%, S20 – sour cream 20% fat. MC were introduced in a ratio of 2.5 g per 100 g of product, respectively (3.3 ± 0.3) mg of β carotene, amount ≈ 1/3 of the RDA (56). Incorporation of MC in milk and cream led to the formation of layers and clots. Kefir and sour cream proved to be suitable for MC. Destruction of MC is not observed for 2...4 weeks, exceeding the shelf life of the product (17*). Destruction occurs after microbiological degradation of the product, accompanied by enzymatic and oxidative damage to the GelAlg shells. Incorporation of MC1 causes a deterioration in texture and appearance. In kefir K0, MC forms a separate phase. MC2 with a diameter range of 2...20 microns are uniformly distributed in kefir K2.5, as well as in cream S10 and S20, and in kefir K0 it is stratified. Therefore, the factors influencing the uniform distribution of MC are texture, fat content, viscosity of the food, and MC diameter. The densities are still in favor of the predominant effect of texture (Table 20). The physicochemical parameters and nutritional value of PAL before and after the introduction of microcapsules with walnut oil and β-carotene differ significantly.

Table 20. Characteristics of foods without and with MC2

Product	ρ, *g/cm³*	pH	Pr.,*%*	Fat,*%*	HC,*%*	DF,*%*	*kJ/100g*
K0	1,02 ± 0,01	4,32 ± 0,03	3,0	0,0	4,0	0,0	119
K0 + MC			3,3	1,5	3,9	0,1	179
K2,5	1,03 ± 0,01	4,49 ± 0,03	2,8	2,5	4,7	0,0	220
K2,5 + MC			3,1	4,0	4,6	0,1	280
S10	1,07 ± 0,01	4,36 ± 0,03	3,0	10,0	2,9	0,0	470
S10 + MC			3,3	11,3	2,8	0,1	523
S20	1,04 ± 0,01	4,27 ± 0,03	2,8	20,0	2,9	0,0	837
S20 + MC			3,1	21,0	2,8	0,1	878

The use of MC, in addition to vitaminization, contributes to the increase of proteins by 1.3%; fats by 1.0...1.5%; dietary fibers (DF) by 0.1%. Carbohydrates (HC) decrease slightly. Biphasic matrices with high viscosity (kefir, sour cream, mayonnaise, sauces) will contribute to the uniform distribution of MC. Contrary to expectation, the density of the medium does not affect the structural uniformity of the lactic acid product with MC. Microcapsules of 2...20 μm do not affect the food sensory properties.

Conclusions to Chapter 5

1. The coacervation model does not reflect the true mechanism of MC wall formation. The share of hydrophobic groups effectively adsorbed by the lipid phase is about 8.5% of the gelatin mass. The MC wall formation is due to adsorption and electrostatic repulsion.
2. The state diagram of the GelAlg system was constructed, which tracks the phase state depending on the mass ratio of the components and pH. The conditions in the IEP correspond to the destabilization of the MC walls.
3. The electrochemical system allows monitoring of the stages of microencapsulation. The charge of the MC walls is caused by the electrostatic interaction between biopolymers and the formation of HDS. Moderate charge provides GelAlg walls with high aggregative stability.
4. The technology of PUFA microencapsulation in tank MCs was developed, optimized by electrochemical control and reducing intermediate steps, ensuring BAC protection and compatibility with food.
5. The HDS model shows MCs are activated in the duodenum. The MCs obtained by the developed technology contribute to the prolongation of the physiological properties of PUFA in fermented dairy products.

6. ASPECTS OF THERMODYNAMICS OF BIOLOGICALLY ACTIVE COMPOUNDS

Food is the successor of biological systems, bearing the imprint of the thermodynamics of processes from plant and animal raw materials.

6.1. Model of stabilization of nutritional compounds and CBA.

Organisms are dynamic, allostatic or heterostatic systems at certain stages. The set of **closed** Hess processes forms an **open** biological system. Biosynthesis includes the raw material access from the environment ***(A)***, the formation of organic product ***(B)***, the elimination of O_2 ***(C)*** into the environment ***(D)***.

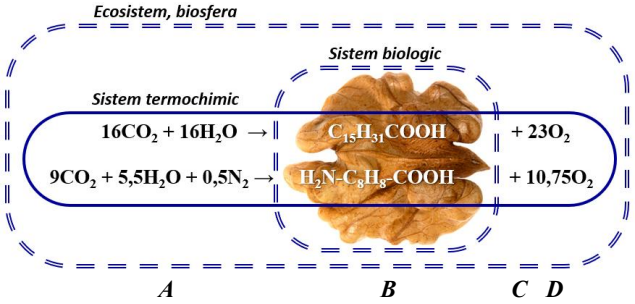

Fig.43. States of thermochemical–biological–ecosystem systems: ***A – initial of eco- and thermochemical systems; B – final of the biological system; C – final of the thermochemical system; D ~{B + C – A} – final of the ecosystem***

Biosynthesis is energy efficient if the synthesized compounds are endothermic with respect to the starting material. The EE_{BS} characterizes the energy efficiency of biosynthesis and represents the ratio of the standard enthalpy of biosynthesis of the compound from H_2O, CO_2 and N_2, ΔH^{θ}_{BS}, to the relation $\Delta H^{\theta}_{BS} - \Delta H^{\theta}_{f}$, where ΔH^{θ}_{f} is enthalpy of formation.

$$EE_{BS} = \frac{\Delta H^{\theta}_{BS}}{\Delta H^{\theta}_{BS} - \Delta H^{\theta}_{f}} \cdot 100\% \quad (6.1)$$

$$\Delta H_{BS} = - \Delta H_{combustion} \quad (6.2)$$

The EE_{BS} value for linoleic acid is 94.6%. From Equations (6.1)...(6.2) for phenylalanine, EE_{BS} ($C_9H_{11}NO_2$) = 91%. At first glance, this value is not much lower than the EE_{BS} for unsaturated fatty acid. But in fact, the lag of about 4% between EE_{BS} (amino acid) and EE_{BS} (PUFA) is significant. Reaching the latter %-s of the yield requires even greater effort => low exergonic efficiency (57).

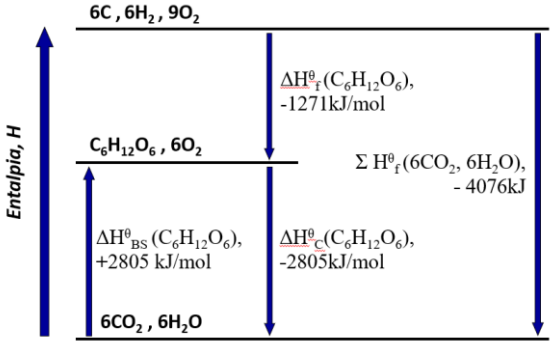

Fig.46. Diagrama entalpică de biosinteză a glucozei

For glucose, EE_{BS} ($C_6H_{12}O_6$) = 69%, which is very low compared to the respective values for fatty acids and amino acids (Figure 46). The EE_{BS} values demonstrate that in the biosynthesis of carbohydrates, energy accumulation occurs much more easily than in the biosynthesis of fats and amino acids, i.e. carbohydrates have high exergonic efficiency (58). The data on the EE_{BS} value for nitrogenous bases - carriers of hereditary information - are also of interest. For thiamine, EE_{BS} = 83.5%. Adenine, the only nitrogenous base without oxygen, is an endothermic compound with $\Delta H^{\theta}_{f} = +\ 95\ kJ \cdot mol^{-1}$. The calculated EE^{BS} value for adenine $C_5H_5N_5$ is 103%, i.e., adenine is richer in energy than the mixture of simple substances C, H_2 and N_2. The disadvantage of EE_{BS} is also because entropy is not considered for its determination.

$$\Delta G^{\theta}_{BS} = \Delta H^{\theta}_{BS} - T\Delta S^{\theta}_{BS} \quad (6.3)$$

The value of $\mathbf{\Delta G_{BS}^{sp}}$, expressed in $kJ \cdot kg^{-1}$, represents the value of the Gibbs potential of the biosynthetic production process of one kg of a nutrient

compound from CO_2, H_2O and N_2, in a feasible way, and can also be called the "specific biosynthetic work" of the nutrient:

$$\Delta G_{BS}^{sp} = \frac{\Delta G_{BS}^{\theta}}{M} \cdot 1000 = \frac{\Delta H_{BS}^{\theta} - T\Delta S_{BS}^{\theta}}{M} \cdot 1000. \qquad (6.4)$$

Generalizing the EE_{BS} and ΔG_{BS}^{sp} values for different compounds leads to an impressive series, which characterizes the specific work, i.e., the biosynthesis efficiency (i.e., the exergonic **inefficiency**) of the "bricks of life" (Table 21).

Table 21. Thermodynamic parameters for nutritional compounds

D	Sugars	Nucleotides	Amino Acids	Fat Acids
ΔH_f^{θ}, kJ·mol^{-1}	-2200...-500	-450...+100	- 800...- 400	-1000...-800
EE_{BS} , %	< 70%	~ 85%	~ 90%	~ 95%
ΔG_{BS}^{sp}, MJ·kg^{-1}	16,0-17,0	16,6-21,2 MJ	13,5-28,2	38,4-39,1

Increasing energy efficiency, decreasing exergonic efficiency

Table 21 demonstrates that fat biosynthesis has low exergonic efficiency. Vegetative reproductive organs (tubers, buds) accumulate "diluted" energy in the form of exergonic efficient carbohydrates.

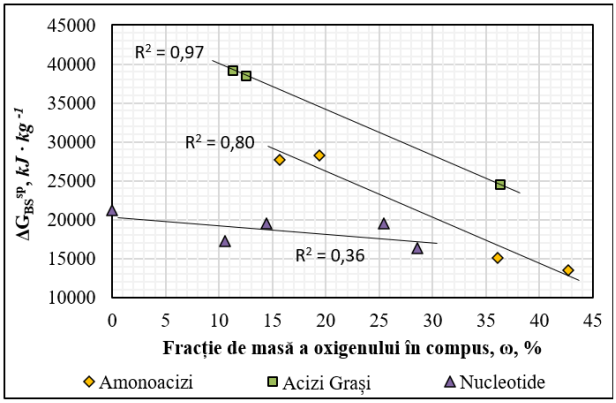

Fig.47. Specific biosynthesis work, $\Delta G_{BS}^{sp} = f\{\omega(O)\}$

The R^2 values for fatty acids (≈ 0.97) and amino acids (≈ 0.80) indicate a linear relationship between ω(O) and ΔG_{BS}^{sp}, suggesting a simple structural control of the energy variation. For nucleotides, $R^2 < 0.50$, requiring a multivariate approach. The specific summary work of biosynthesis, $\boldsymbol{\Sigma\Delta G_{BS}^{sp}}$, is the useful work consumed for the biosynthesis of one kg of (modeled) plant feedstock:

$$\Sigma\Delta G_{BS}^{sp} \approx \Delta G_{BS(Palm)}^{sp} \cdot \Omega_{(fats)} + \Delta G_{BS(Phen)}^{sp} \cdot \Omega_{(proteins)} \qquad (6.5)$$

where $\Omega_{(fats)}$, $\Omega_{(proteins)}$ are the mass fractions of lipids and proteins in the biological object or food, expressed in parts per unit.

Summary specific entropy of biosynthesis, $\Sigma\Delta S_{BS}^{sp}$**,** represents the entropy variation of the biosynthesis process of one kg of raw material:

$$\Sigma\Delta S_{BS}^{sp} = \Delta S_{BS(Palm)}^{sp} \cdot \Omega_{(lipide)} + \Delta S_{BS(Phen)}^{sp} \cdot \Omega_{(protein)} \qquad (6.6)$$

The inclusion of water (75...97%) in these models is incorrect, since water **is not obtained through biosynthesis**, entering the cells through spontaneous osmotic mechanisms (59).

The specific mass of oxygen, $\mathbf{m^{sp}(O_2)}$, $g \cdot kg^{-1}$, is the mass of oxygen that is released during the biosynthesis of one kilogram (1000 g) of raw material.

$$m^{sp}(O_2) = \frac{n(O_2) \cdot M(O_2)}{M_{CBA}} \cdot 1000 \qquad (6.7)$$

where: $n(O_2)$ – the amount of O_2, which is formed during the biosynthesis of one mole of CBA according to the reaction, mol; $1000 \cdot M_{CBA}^{-1}$ – the amount of CBA per kg, $mol \cdot kg^{-1}$. Upon the formation of one kilogram of model compounds (palmitic acid, phenylalanine), specific masses $\mathbf{m^{sp}(O_2)}$**,** 2.875 kg and 2.085 kg are released, thus eliminating entropy from the biological system. The removed entropy, $\mathbf{\Delta S_{elim.}(O_2)}$, represents the entropy eliminated from the biological system due to the formation of O_2 during biosynthesis:

$$\Delta S_{elim.}(O_2) = \frac{m^{sp}(O_2) \cdot S(O_2)}{M(O_2)} \qquad (6.8)$$

The self-organization of the organism is by no means proof of its conscious effort (60). Calculations by Equation (6.6) demonstrate that the value of the specific entropy of biosynthesis, ΣS_{BS}^{sp}, which takes into account only the purely chemical part, but not the structural one, increases and reaches a constant maximum value towards the end of ripening, as does the specific entropy eliminated, $\mathbf{S_{elim.}^{sp}}$, being several orders higher. The entropy eliminated during plant growth is much higher than the entropy of biosynthesis.

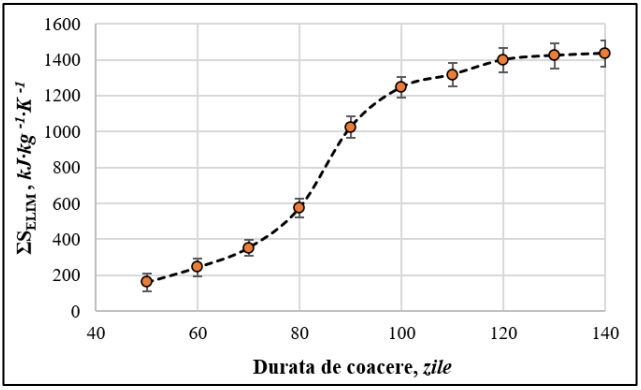

Fig.48. Entropy eliminated during walnut ripening

The error bars in Figure 48 estimate the uncertainty of the model with respect to the variation of the input parameters.

6.2. Structural organization as a stabilizing factor of CBA.

During the transfer from the primary producer organism, CBA undergoes different stages of structural reorganization, which are carried out within different technological processes (7*,21*,43*). The transfer of CBA to the solution phase can be interpreted as a transition to a state with increased configurational freedom, increasing the probability of reactive contacts and irreversible events. For Carthamin, the transition from the CCC to solution leads to an increase in the degradation rate by **α** times, which reaches the value $(9.4 \pm 1.7) \cdot 10^2$ at 70ºC (Table 9). For irreversible events, the rate of entropy production, **σ**, is proportional to the rate constant (61):

$$\frac{dS}{d\tau} = \sigma \sim \frac{k_I \cdot (-\Delta G)}{T} \qquad (6.9)$$

Eq. (6.9) highlights the connection between the reaction rate and the irreversibility. Structural destabilization results directly from the increase in the value of **k**, which indicates the irreversibility amplification. The stability control of the food system is expressed by the decrease in the rate of entropy production (↓**σ**) within the technological processes. Freezing generates water crystallization and leads to the destruction of cellular structures, including the phenomenon of isothermal sublimation (62). Grinding induces accelerated oxidation (14*, 34*). Pressing *Linum* seeds with different degrees of grinding (figure 49) takes place according to different kinetics (25*). The aforementioned require rethinking of technological processes to limit **σ**: optimizing the degree of dispersion, minimizing contact between incompatible phases and ensuring storage conditions that limit interactions (6*).

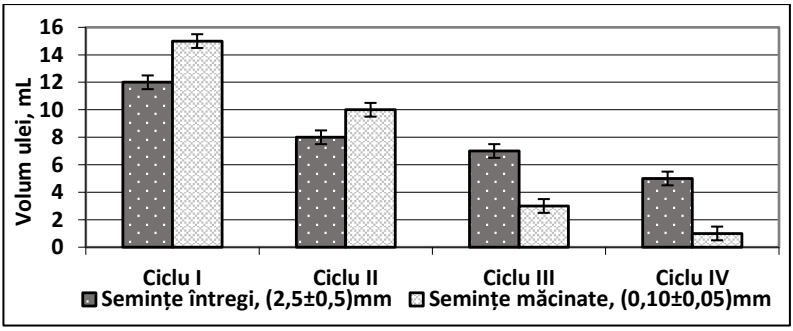

Figure 49. Kinetics of flaxseed oil extraction

The increase in contact accessibility during grinding can be estimated by the specific areas of the particle's ratio. For spherical particles, the area and volume are related as A / V ≈ 6 / D, representing the inverse of the

characteristic particle size. For flax seeds, the size reduction from d_{whole} = (2.5 ± 0.5) mm to d_{ground} = (0.10 ± 0.05) mm, leads to an increase in contact accessibility $\chi_{cont.}$ Taking into account the experimental ranges of the pressed particle sizes (2.0...3.0 mm and 0.05...0.15 mm), the contact accessibility, $\chi \in$ (13...60). This amplification of the interfacial surface explains the potential for intensification of reactive contacts, favoring the increase in the constant of degradation **k**. Under comparable conditions of temperature and associated thermodynamic force (−ΔG) from (6.9), they lead to an increase in the entropy production rate **σ**.

In the walnut kernel there are several groups of compounds from different classes, chemically incompatible. These are free amino acids and sugars, as well as various glucosides of phenolic compounds (24*), which can enter the Maillard reaction (2). Under structurally intact conditions, amino acids (AMA) and reducing carbohydrates (RC) are located in distinct compartments, and the probability of reactive contact is almost zero. The rate of the Maillard reaction, $\mathbf{r_M}$, is equal to:

$$r_M = k \cdot [AMA] \cdot [RC] \tag{6.10}$$

In a geometric approximation, increasing the degree of grinding increases the specific surface area (A/V∼1/d), which increases the probability of contact between AMA and RC, accelerating the reaction. The process continues in food compositions, which contain the pressed core.

In three-phase O/W/G systems, a probabilistic distribution function can be used - the Shannon information entropy, H, which is not identical to the thermodynamic entropy S. Small values of H indicate a concentrated and directed distribution, while larger values reflect a more uniform dispersion and a diminished functional efficiency. For spreads with three types of interfaces (O/W, O/G, W/G), the information entropy H is defined by the relation:

$$H = -\sum_{i=1}^{3} P_i \cdot lnP_i \tag{6.11}$$

where: $\mathbf{P_i}$ – is the relative fraction of the surface active agent, distributed at interface **i**; H – is expressed in natural units (“nat”). This quantity characterizes the probability of the SAA distribution at interfaces. The maximum possible value for three equiprobable events, H_{max} = ln3 = 1.099 nat.

Table 22. Shannon information entropy for a O/W/G system

Oil / Water / Gas	H (nat)	Useless SAA (%)
72 m : 28 m : 1 v	0.224	5
72 m : 28 m : 3 v	0.476	14
82 m : 18 m : 1 v	0.277	7
82 m : 18 m : 3 v	0.553	18

Increasing the air fraction from 1% to 3% leads to an increase in information entropy, through a more chaotic distribution of SAA. There is a strong correlation, $R^2 \approx 0.99$, between the Shannon entropy and the useless AAS. Excessive aeration determines a less efficient use of AAS, a significant part of which is consumed for stabilizing the O/G interface, without a direct contribution to the protection of PUFA. In the combinatorial model, the O/G contact is proportional to the product of the volumetric fractions:

$$P_{U/G} = \Phi_U \cdot \Phi_G \quad (6.12)$$

The Φ_G increase leads to an increase in the probability of U/G contact and to of the information entropy of the AAS distribution, indicating a more dispersed distribution of AAS at the O/W interface. Under these conditions, the reduction of the local protection of the lipid phase and the amplification of the contact with O_2 may favor the increase in the PUFA oxidative susceptibility. The Φ_G fall is equivalent to the system ordering, favoring PUFA oxidative stability.

6.3. Structural organization and entropic cost of MC systems.

Oxygen in emulsions represents the third component, and its distribution constant between phases is equal to the ratio of concentrations (63):

$$K_{distr.} = \frac{C_U(O_2)}{C_A(O_2)} \approx 5 \quad (6.13)$$

The contact area between the emulsion phases, 104...105 $m^2 \cdot kg^{-1}$, and the high solubility of O_2 in the lipid phase ensure rapid diffusion of O_2 from water into oil, and the interaction of oxygen with PUFA residues in the lipid composition will occur in diluted colloidal systems faster than in pure lipids. Therefore, "water" does not represent an obstacle to the diffusion of O_2 molecules to fat. According to studies of the diffusion phenomenon, the diffusion rate of O_2 through agar-agar gels is about 5...10 times slower than through liquid, ceteris paribus (64). Agar-agar contains in its structure a tertiary carbon atom and a -CH_2 group, being less polar than alginate. Therefore, in the MC, the gel based on the GelAlg system, with the upper alginate layer, represents an even greater obstacle for O_2, due to its high polarity.

The energy consumption for food production is at least 4...7 $MJ \cdot kg^{-1}$, and for some products it reaches 10...17 $MJ \cdot kg^{-1}$ (65). In the energy efficiency paradigm, when manufacturing innovative food products, energy consumption should not increase significantly compared to standard values (66) (67). It is possible to estimate the entropic flux of different processes, using the specific energy consumption (SEC):

$$SEC \approx \frac{W}{m} \quad (6.14)$$

where: **W** - total energy consumed, (kWh), **m** - mass of processed material (kg) or mass of removed water (kg H_2O). The reference unit depends on the nature of the dominant process: (1) for mechanical and liquid phase methods (coacervations, Layer-by-Layer, liposomal entrapment, extrusion) - per 1 kg

of dispersion; (2) for drying processes - per 1 kg of removed water, since the energy is mainly determined by the phase transition. The comparison of technologies is carried out according to the physical nature of the dominant operation, not only by the type of equipment. Assuming that the consumed energy is finally dissipated in the ambient environment at the reference temperature T^{Θ}, the entropy produced by the process can be estimated as:

$$\Delta S_{proces} \approx \frac{W}{T^{\Theta}} \quad (6.15)$$

$$\Delta S_{proces} \approx \frac{SEC \cdot 3600}{T^{\Theta}} \quad (6.16)$$

At $T^{\Theta} = 298K$: $$\Delta S_{proces} \approx 12{,}08\ SEC \quad (6.17)$$

This quantity does not represent the thermodynamic entropy of the substance, but an engineering estimate of the entropic cost of the technology, the level of energy dissipation associated with the process. The order of magnitude differences in energy consumption between microencapsulation methods are determined by the dominant physical process: mechanical operations (mixing, pumping, homogenization) are characterized by mechanical work of the order of $10...10^2$ of $kJ \cdot kg^{-1}$ and low entropic cost. Cooling and crystallization require moderate heat flows and generate intermediate SEC. Evaporation requires the supply of latent heat, causing a significant increase in SEC and produced entropy. Lyophilization consists of thermodynamic penalty: the cold production. The highest SEC and ΔS values are obtained. Quantification of SEC and entropy produced allows the classification of microencapsulation technologies according to the "entropic cost", as well as highlighting the fact that the increase in entropy production is associated with water removal operations, and not with the microencapsulation itself. In this context, structural microencapsulation methods, such as complex coacervation, are characterized by a lower entropy production compared to technologies based on evaporation or sublimation. Specialized literature does not provide direct values of SEC; the estimate was made by an analysis of the dominant operation in each technology. The process was decomposed into fundamental components: work (pumping, homogenization, mixing), heating or cooling and phase transitions. The SEC values were estimated per 1 kg of dispersion or per 1 kg of water removed by the phase transition according to the dominant operation. The consumed energy is finally dissipated in the environment at the temperature T^{Θ}, the entropy produced can be estimated by the relationship:

For processes dominated by fluid pressure:

$$e \approx \frac{\Delta P}{\rho} \quad (6.18),$$

where: **e** – specific energy ($J \cdot kg^{-1}$); **ΔP** – difference of pressure ($Pa = N \cdot m^{-2}$); **ρ** – liquid density ($kg \cdot m^{-3}$).

For mixing operations:

$$e \approx \frac{N \cdot t}{m} \quad (6.19),$$

where: **N** – equipment power ($W = J \cdot s^{-1}$); **t** - operating time (s);
m - mass of processed material (kg).

For thermal processes:

$$q \approx C_p \Delta T \quad (6.20).$$

The estimates, although of an order of magnitude nature, allow the ranking of methods from an energetic and entropic point of view (Table 23).

Table 23. Estimation of the value of $\Delta S_{process}$ when obtaining MC

Method, Type	Operations	SEC, kWh·kg⁻¹	ΔS_{pr}, kJ·K⁻¹·kg⁻¹	Estimated
CS, D	Mix + pH	0.005...0.050	0.06...0.60	Ec. 6.19
CC, D	Mix + pH + Cnd	0.01...0.10	0.12...1.21	Ec. 6.19
LL, D	Mix + Ads + Wsh	0.01...0.20	0.12...2.42	Ec. 6.19
EX, D	Pres + Form + Str	0.03...0.30	0.36...3.62	(68), Ec. 6.18
CD, D	Disp + Cl + Cri	0.05...0.40	0.60...4.83	Ec. 6.20
LE, D	Flu + Cl	0.08...0.40	0.97...4.83	Ec. 6.18
FB, DP	Flu + Disp + Usc	0.33...0.74	4.0...8.9	(69)
SD, DP	Disp + Ht + Vap	1.35...1.85	16.3...22.3	(70), (71)
SC, DP	Con + Vac + Subl	16.9...25.3	204...306	(72)

Note: Mix – mixturing; Cnd – condensation; Ads – adsorption; Wsh – washing, Pres – pressing; Form – formation; Str – structurization; Disp – dispersing; Cl – cooling; Cr – crystallization; Flu – fluidization; Dry – drying; Ht - heating, Vap – vaporization; Con – congelation, Vac – vacuumation; Subl – sublimation; D – Dispersion; DP – Dry Powder.

The extrusion method requires low energy consumption. Despite the fact that the extrusion process of large capsules (d = 0.1...3.0 cm) is relatively easy and fast, the industrial production of MC with d = 2...100 μm by extrusion becomes very problematic. Reducing the size of capsules from 1 cm to 10 μm requires $\approx 2 \cdot 10^6$ single extrusion operations. The expensive extrusion matrix determines the price of the entire installation. The development of 3D printing technologies allows obtaining monolith matrices, containing up to 1000 nozzles. However, such engineering solutions remain valid only for small laboratory volumes. Intensive structuring processes, such as extrusion or pressure homogenization, assume a very large number of local deformation and rearrangement events, estimated at the order of $10^6...10^7$ elementary operations for a representative volume of material. Even though each individual event is microscopic, their accumulation gives the process an irreversible character. Thus, the associated energy dissipation results not only from the total energy consumption, but also from the multiplication of small-scale structural transformations. Recently, significant progress has been made in the development of technologies for obtaining monodisperse emulsions

(73). These advanced processes may soon favor the development of microencapsulation technologies with emulsification.

The introduction of microcapsules into the formulation of food products causes a proportional increase in production cost, depending on the mass fraction used and the specific price of the microencapsulated ingredient. For an addition of MC, which will correspond to the mass fraction **ω** in the product, the direct increase in the cost of the raw material, $\Delta C_{\%}$, is estimated by the relationship:

$$\Delta C_{\%} = \frac{\omega \cdot C_{MC}}{C_{PR}} \cdot 100\% \qquad (6.21)$$

where: $\mathbf{C_{MC}}$ – MC price, € · kg^{-1}; $\mathbf{C_{PR}}$ – product price, € · kg^{-1}.

Equation (6.21) shows that the relative effect on the final price depends on the cost of the microcapsules and the initial value positioning of the food product, and the optimization of microencapsulation technologies by limiting the entropy production has economic significance (74). Reducing the energy dissipation of the process decreases the specific energy consumption and the technological cost of the microencapsulated ingredient. Entropic control becomes an integrating criterion, with structural, energetic and economic relevance (22*, 29*). From the existing microencapsulation methods, simple (C) and complex coacervations (CC) have a real perspective for the manufacturing of food-grade MC, which will also be economically feasible.

Conclusions to Chapter 6

1. Understanding the thermodynamics of the CBA biosynthesis process in plants allows optimizing the harvesting of plant raw materials, so as to maximize the content of functionally active compounds in the relatively steady state, which are nutritionally useful. It is advisable to time the harvesting to the stabilization of water content, when CBA biosynthesis becomes thermodynamically favored.
2. Assessing the energetic and exergonic efficiency of CBA biosynthesis provides a valuable tool for raw material selection and functional food design. From the perspective of the living organism, lipid and amino acid biosynthesis, although thermodynamically disadvantaged compared to that of carbohydrates, is activated only in cases where it is necessary to store a large amount of energy and biologically active compounds in a small volume, as in seeds. In the absence of this constraint, plants "prefer" the accumulation of more exergonic efficient carbohydrates.
3. The stability of bioactive compounds can be prolonged by preserving the structural organization of the plant raw material during processing. Thus, classical methods (grinding, pressing, freezing) must be corrected with anti-entropic measures, which involve avoiding direct contact between chemically incompatible components, preventing degradation processes, such as enzymatic browning or radical oxidation of lipids.

4. The implementation of modern microencapsulation technologies with exergy efficiency, such as complex coacervation or liposomal encapsulation, represent efficient and lucrative solutions for protecting CBA in food products. The use of monodisperse emulsions and the control of internal entropy are critical for obtaining stable functionally useful MC.
5. The formulation of food products enriched with CBA must consider the chemical and structural compatibility of the components. A step-by-step approach to the extraction, separation and valorization of bioactive fractions can lead to the production of functional foods of high stability and nutritional value, avoiding the compromise of ingredients.

GENERAL CONCLUSIONS

1. Using experimental, combinatorial and thermodynamic models, it has been demonstrated that the stability of natural dyes from different classes: anthocyanins, betaine, quinochalcones, ω3 and ω6 fatty acids is compromised due to the presence of free water, which does not constitute a barrier for dissolved molecular oxygen. To overcome the existing limitations of protection procedures, strategies have been proposed to prolong the BAC activity by creating MC and using biopolymers for the physicochemical stabilization of dyes by mutual complexation [1,2,4,5,13].
2. Experimental procedures of high scientific value were developed and approved, including modifications and synergistic use of UV-Vis spectroscopy and HPLC with PDA detection, original electrochemical methods for controlling the microencapsulation process, a method for determining the polydispersity of emulsions and microcapsules, an accessible method for analyzing the RGB chromatic profile of natural dyes in model systems and in foods, a way to assess the impact of biopolymers in the colloidal state on the optical properties of solutions. The newly developed methods and their essential elements allow real-time monitoring of the integrity of BAC, dyes in model systems and in foods [6-12,14,15,18,40].
3. Integrated extraction and purification methods were established, which ensure the preservation of the structure and functional activity of BAC from brown algae, flax seeds, beetroot roots, safflower petals, walnut kernels. Liquid fractions and powders were extracted, rich in dietary fiber - alginates and arabinoxylan, oil with a high content of fat-soluble vitamins and polyunsaturated fatty acids - linoleic and linolenic, dyes - betanin, Carthamin. Processes for obtaining functional biopolymers - inulin, alginate, arabinoxylan were patented, resulting in ingredients for the manufacture of functional foods with added biological value [33,37,42-45,47,49].
4. A process for obtaining a spreadable spread with the phase composition Water/Oil/Air, structurally like cow's butter, having a high content of 30...40% (m) PUFA of vegetable origin was developed and patented. A

combinatorial model was developed, which, in correlation with the principles of statistical thermodynamics, explains the structure of Water/Oil/Air, determining the lower limit of their stability, ~ 68% oil, and the impossibility of the existence of two continuous phases [15,30,36,46].

5. It was demonstrated that biopolymers of various origins – alginate, arabinoxylan, hyaluronic acid, polyvinyl alcohol, microcrystalline cellulose are active agents for structuring and stabilizing BAC. Their specific interactions with natural dyes – anthocyanins, betalains, quinochalcones – provide a protective effect, except for the hyaluronic acid-anthocyanin system, where the biopolymer has a destabilizing role. The results confirm the need to adapt the natural food dye to the biopolymer matrix of the food, which ensures the prolongation of activity and stability of the dye until consumption [14,16,21-25,27,28,39].
6. A comprehensive examination of the properties and testing of the conditions of use of YFDS and CCC was carried out: new, edible, yellow and red food dyes, stable respectively in solution and in the soaked solid state, at pH 1...6, which have the potential for integration into lactic acid products and other structured products with a high water content. The mechanism of stabilization of Carthamin with cellulose includes the reduction of water activity and the protection of the chromophore against hydrolysis, the stabilization of quinochalcone against thermal or oxidative degradation. The Carthamin-cellulose complex presents an edible dietary fiber, an additional physiological value. The processes for obtaining quinochalcone dyes have been patented [8,12,26,32,42,45].
7. A process for obtaining yogurt has been patented, in which the azo dye tartrazine is substituted with a mixture of yellow quinochalcones. Yogurt samples with YFDS have demonstrated sensory stability, including chromatic and sensory compatibility of the dye and yogurt, high functional potential of the product, expressed by its antioxidant activity [4,12,41].
8. The classic model of simple coacervation has been revised, arguing that it includes a complex ensemble of adsorption, electrostatic repulsion and molecular reorganization. This interpretation allows for a more efficient control of the MC morphology in formation and offers viable solutions for maintaining the BAC activity in the microencapsulated form during food storage, ensuring targeted delivery [1,9,13,38].
9. An efficient technology for microencapsulation of lipids with PUFA in the liquid phase by forming gelatin–polyuronate bilayer walls on the surface of lipid droplets was developed and patented. The obtained stable microcapsules represent spheres with a diameter of 2...20 microns, the core of which includes the biologically active lipid phase. The thickness of the bilayer wall of the microcapsule is about 370 nm. The microencapsulation process is electrochemically controlled, excluding intermediate separation

and/or drying stages, which ensures low resource consumption and compatibility of MC with multiphase foods and emulsions [17,19,38,48].

10. It has been experimentally demonstrated that, in lactic acid food products, microcapsules with GelAlg walls can serve for targeted delivery of BAC. They remain intact in the oral cavity, resist gastric juice and release the bioactive lipid content only in the small intestine, at pH > 8. This result validates the use of the proposed technology for prolonging the functionality of BAC, PUFA and carotenoids in foods [9,10,16,17].

11. The results obtained suggested a thermodynamic interpretation of the BAC biosynthesis processes, and the hypothesis regarding the need for entropic control was supported by quantitative indicators [20,29,31,34,35]. BAC stabilization is correlated with measurable parameters: phase polydispersity (PDI < 0.2), increased lipid oxidation stability (decrease in the degradation rate of PUFAs by 20...40% in the presence of synergistic antioxidant systems), color stability (ΔE* < 10%) during storage, indicating that the hierarchical organization of foods: MC formation, complexation with biopolymers and antioxidants synergy - leads to a reduction in structural entropy, and to the BAC functionality prolongation.

RECOMMENDATIONS

It is recommended to continue research on the elucidation of the mechanisms of stabilization of BAC in foods, thermodynamic and combinatorial modeling elucidation of microencapsulation processes and biopolymer-dye interactions. It is appropriate to consolidate research on the role of water in the destabilization of BAC and on the ways to limit the entropy production in food systems. It is recommended to apply complementary instrumental methods (UV-Vis, HPLC, FTIR, electrochemistry, RGB) for monitoring the integrity and functional activity of BAC in real time.

For industry, it is proposed to capitalize on scientific results, patents, on PUFA microencapsulation, the use of natural biopolymers and the development of functional products with targeted delivery of BAC. It is recommended to develop technological lines for the integration of natural quinochalcone-type dyes and the Carthamin-cellulose complex, capable of replacing synthetic additives in fermented dairy products. Pilot projects for the cultivation and industrial exploitation of species rich in pigments and essential fatty acids, such as *Carthamus tinctorius* and *Linum*, are encouraged.

At the institutional and national level, it is considered necessary to support applied research and technology transfer in the field of functional foods, including through funding programs aimed at replacing synthetic additives with natural compounds. It is recommended to harmonize the national regulatory framework with EU policies on reducing the artificial dyes use and stimulating the production of bioactive ingredients. It is appropriate to promote

partnerships between universities and industry for the application of scientific results in safe, sustainable products, contributing to increasing the competitiveness of the food sector in the Republic of Moldova.

Overall, these recommendations outline the directions for the development of food technologies based on the entropic control of food systems and on prolonging the functionality of biologically active compounds.

Selective bibliography:

1. STURZA R., GHENDOV-MOȘANU A. (editori): Ameliorarea calității alimentelor prin biotehnologie și inginerie alimentară. Chișinău, Tehnica-UTM, 2023, 267 p. ISBN 978-9975-45-988-4.
2. TATAROV P.G. Chimia produselor alimentare. Chișinău, „MS-Logo", 2017, 450p. ISBN 978-9975-4264-2-8.
3. GHENDOV-MOȘANU A. Compuși biologic activi de origine horticolă pentru alimente funcționale. 2018, Chișinău, Tehnica-UTM, 236 p. https://repository.utm.md/handle/5014/15286.
4. CHIRSANOVA A., CAPCANARI T., BOISTEAN A., COVALIOV E., RESITCA V., STURZA R. Behavior of Consumers in the Republic of Moldova Related to the Consumption of Trans Fat. International Journal of Food Science, Nutrition and Dietetics, . s.l. : 2020, vol. 9, no. 8, pp. 493-498. ISSN 2326-3350.
5. ZADOROJNÂI L., ZADOROJNÂI A. Procedeu de obţinere a hialuronatului de sodiu, acidului hialuronic şi complexului acid hialuronic-proteină. Patent MD, 3099, C08B 37/08, 2006.01.
6. BADALICA PETRESCU M., DRAGAN S., RANGA F., FETEA F., SOCACIU C. Comparative HPLC DAD ESI(+)MS fingerprint and quantification of phenolic and flavonoid composition of aqueous leaf extracts of Cornus mas and Crataegus monogyna. s.l. : in relation to their cardiotonic potential. Notulae Botanicae Horti Agrobotanici Cluj Napoca, 2014, vol. 42, no. 1, pp. 9-18. DOI 10.15835/nbha4219270.
7. CHO M.H., PAIK Y.S., HAHN T.R. Enzymatic Conversion of Precarthamin to Carthamin by a Purified Enzyme from the Yellow Petals of Safflower. Journal Of Agriculture And Food Chemistry, 2000, 48, pp. 3917. https://doi.org/10.1021/jf9911038.
8. BOX G.E.P., HUNTER J.S., HUNTER W.G. Statistics for Experimenters: Design, Innovation, and Discovery. 2nd Edition. Hoboken: Wiley, 2005. 655 p. ISBN 978 0471718130.
9. LI J., SHI C., SHEN D., HAN T., WU W., LYU L., LI W. Composition and antioxidant activity of anthocyanins and non anthocyanin flavonoids in blackberry from different growth stages. Foods, 2022, vol. 11, no. 18, article 2902. DOI 10.3390/foods11182902.
10. JACKSON C.R., RAJA P.M.V., PRAKASH S.A. Novel electrophoretic deposition device: Effects of alginate viscosity grade on deposition kinetics. Journal of Biotechnology & Biomaterials, 2012, suppl. 6, article S6 002. DOI 10.4172/2155 952X.S6 002.

11. KHAIR A.S., SQUIRES T.M. The influence of hydrodynamic slip on the mobility of a spherical colloidal particle. Physics of Fluids, 2009, vol. 21, no. 4, article 042001. DOI 10.1063/1.3116664.
12. ZELAZKO A. RGB colour model. Encyclopedia Britannica, 21 Oct. 2022. https://www.britannica.com/science/RGB-colour-model. Accesat 01.04.2023.
13. SAVCENCO (BUZESCU) A. Obținerea și utilizarea coloranților naturali din petale de șofrănel (Carthamus tinctorius L.) în tehnologia produselor alimentare. Teza de doctor în tehnică. Chișinău, UTM, 2024. 180p.
14. DELSHAD E., YOUSEFI M., SASANNEZHAD P., RAKHSHANDEH H., AYATI Z. Medical uses of Carthamus tinctorius: a comprehensive review from traditional medicine to modern medicine. Electronic Physician, 2018, vol. 10, no. 4, pp. 6672–6681. DOI 10.19082/6672.
15. OpenStax. College Physics 2e. Section 29.1 OPENSTAX. Quantization of Energy. https://openstax.org/books/college-physics-2e/pages/29-1-quantization-of-energy. Accessed 18.05.2025.
16. SAVCENCO A. Spectral and chromatographic characterisation of the yellow food dye from safflower. Journal of Engineering Science, 2022, vol. XXIX, no. 3, pp. 189–195. ISSN 2587-3474.
17. BENEDUCI A., FURIA E., RUSSO N., MARINO, T. Complexation behaviour of caffeic, ferulic and p-coumaric acids towards aluminium cations: a combined experimental and theoretical approach. . s.l. : New Journal of Chemistry, 2017, vol. 41, pp. 5182–5190. DOI 10.1039/C7NJ00661F.
18. LUKYANOV S.M., KOBLIK A.V. Tautomeric equilibria and rearrangements involving phenols. In: RAPPOPORT Z. (ed.). The Chemistry of Phenols. Chichester: John Wiley & Sons, 2003, pp. 713–838. ISBN 978-0471497370.
19. GUREV A., DRAGANCEA V. Chimie organică. Chișinău: Tehnica-UTM, 2023, 160 p. ISBN 978-9975-64-359-7.
20. SASAKI M., TAKAHASHI K. Complete assignment of the 1 H and 13 C NMR spectra of carthamin potassium salt isolated from Carthamus tinctorius L. Molecules, 2021, vol. 26, no. 16, article 4953. DOI 10.3390/molecules26164953.
21. ERBAȘ S., MUTLUCAN M. Investigation of flower yield and quality in different color safflower genotypes. Agronomy, 2023, vol. 13, no. 4, article 956. DOI 10.3390/agronomy13040956.
22. TATAROV P. Physicochemical changes of walnut oil. In: Modern Technologies in the Food Industry. Chișinău, 1-3 nov. 2012. Vol II, pp. 192-197. ISBN 978-9975-87-428-1.
23. WILLIAMS C.A., CARLUCCI S.A. High dose DL α tocopherol acetate is detrimental to beta carotene levels and does not reduce oxidative stress in exercised horses. Equine Veterinary Journal Supplement, 2006, vol. 36, pp. 617–621. . s.l. : DOI 10.1111/j.2042-3306.2006.tb05614.x.
24. WANG X., CHEN Y., McCLEMENTS D.J., PENG D., CHEN H., XU S., DENG Q., GENG F. Regulation of Microlocalization of Antioxidants by Surfactant Micelles in O/W Emulsions. . s.l. : Journal of Agricultural and Food Chemistry, 2024, vol. 72, no. 45, pp. 25306–25318. DOI 10.1021/acs.jafc.4c08855.
25. RADU O. Compoziţii alimentare pe baza uleiului de nucă (Juglans regia L.) rezistente la degradări oxidative. Teza de doctor în tehnică. Chișinău, UTM, 2020. – 150p. http://www.cnaa.md/thesis/56546/. Accesat 02.01.26.

26. ARELLANO M., NORTON I.T., SMITH P. In: TALBOT G. Chapter 10. Specialty Oils and Fats in Margarines and Low-Fat Spreads, pp 241-270. In: Talbot, G., Ed., Specialty Oils and Fats in Food and Nutrition, Elsevier, 2015. DOI 10.1016/B978-1-78242-376-8.00010-7.
27. WILLIAMS C., BUTTRISS J. Improving the Fat Content of Foods. Woodhead Publishing, 2006, pp. 560. ISBN: 1-85573-965-8.
28. RADU O. Peculiarities of walnut oil state in some food emulsions. Journal of Engineering Science. 2020, Vol. XXVII, no. 1, pp. 69-74. ISSN: 2587-3474.
29. HARRIS J.M., HIRST J.L., MOSSINGHOFF M.J. Combinatorics and Graph Theory. 2nd Edition. Springer, 2008. 381 p. ISBN 978-0-387-79711-3.
30. GOST 32261–2013. Maslo slivochnoe. Tekhnicheskie usloviya. Moscow: Standartinform, 2015. (Standard interstatal).
31. DRAGET K., SMIDSRØD O., SKJÅK-BRÆK G. In: STEINBÜCHEL A., RHEE S.K. (eds.). Polysaccharides and Polyamides in the Food Industry: Properties, Production, and Patents. . s.l. : Wiley-VCH, 2005, pp. 1-30. ISBN 978-3-527-31345-7. https://application.wiley-vch.de/books/sample/3527313451_c01.pdf. Accesat 01.02.26.
32. BAERLE A., GUŢANU V. - Procedeu de obţinere a colorantului roşu din materie primă vegetală. - Brevet de invenţie MD-2796 / BOPI, 2005, No. 6. – p.37.
33. SAITO K., FUKUSHIMA A. On the mechanism of the stable red color expression of cellulose-bound carthamin. Food Chemistry, 1988, vol. 29, no. 3, pp. 161-175. DOI 10.1016/0308-8146(88)90130-6.
34. WOHLERT M., BENSELFELT T., WÅGBERG L., FURO I., BERGLUND L.A., WOHLERT J. Cellulose and the role of hydrogen bonds: not in charge of everything. Cellulose, 2022, vol. 29, pp. 1-23. DOI 10.1007/s10570-021-04325-4.
35. BUSZEWSKI B., NOGA S. Hydrophobicity scales and retention behavior in reversed-phase liquid chromatography. Analytical Chemistry, 2012, vol. 84, no. 2, pp. 1099–1106. DOI 10.1021/ac202573a.
36. HAYNES W.M. (ed.). CRC Handbook of Chemistry and Physics. 97th ed. Boca Raton: CRC Press, 2016. ISBN 978-1-4987-5429-3.
37. BAERLE A.V., GUTSANU V.L., MAKAR A.V., ROSHKA I.G. Vliyanie razlichnykh faktorov na kislotno-spirtovoi sinergizm desorbtsii antotsianov iz sul'fokationita. Zhurnal Fizicheskoi Khimii, 2005, vol. 79, no. 7, pp. 1300–1304. ISSN 0044-4537.
38. LAURSEN, R., MOURI, C. Decomposition and analysis of carthamin in safflower-dyed textiles. In: e-Preservation Science. 2013, nr.10, pp. 35-37. ISSN 1581-9280.
39. MITANI E., OZAKI Y., SATO H. Two types of CO···HO H bonds and OH···OH H bonds in PVA/PMMA blends studied by IR spectroscopy. Polymer, 2022, vol. 246, article 124725. DOI 10.1016/j.polymer.2022.124725.
40. DAI Y., VERPOORTE R., CHOI Y. Natural deep eutectic solvents providing enhanced stability of natural colorants from safflower. Food Chemistry, 2014, vol. 159, pp. 116-121. DOI 10.1016/j.foodchem.2014.02.155.
41. SANDULACHI E. Activitatea apei în produsele alimentare. Chișinău: Tehnica-UTM, 2020. 208 p. ISBN 978-9975-45-622-7.
42. MOKRZYCKI W., TATOL M. Colour difference ΔE - a survey. Machine Graphics and Vision, 2011, vol. 20, no. 4, pp. 383-411. ISSN 1230-0535.

43. XI E., VENKATESHWARAN V, LI L., REGO N. , PATEL A.J. , GARDE S. . s.l. : Hydrophobicity of proteins and nanostructured solutes is governed by topographical and chemical context. Proceedings of the National Academy of Sciences of the USA, 2017, vol. 114, no. 51, pp. 13345-13350. DOI 10.1073/pnas.1700092114.
44. RUBINSTEIN M., COLBY R.H. Polymer Physics. Oxford: Oxford University Press, 2003, 454 p. ISBN 978-0-19-852059-7.
45. MASUELLI M.A., ILLANES C.O. Review of the characterization of sodium alginate by intrinsic viscosity measurements. Comparative analysis between conventional and single point methods. s.l. : International Journal of Biomaterials Science and Engineering, 2014, vol. 1, no. 1, pp. 1-11. https://www.researchgate.net/publication/272785338. Accesat 20.01.26.
46. ZHANG W., SHI L., LIU Y., MENG X., XU H., XU Y., LIU B., FANG X., LI H.B., DIN T. Supramolecular interactions via H-bonding contributing to citric-acid-derived carbon dots with high quantum yield and sensitive photoluminescence. . s.l. : RSC Advances, 2017, vol. 7, pp. 20345-20353. DOI 10.1039/C7RA02160G.
47. MARFIL P.H.M., PAULO B.B., ALVIM I.D., NICOLETTI V.R. Production and characterization of palm oil microcapsules obtained by complex coacervation in gelatin/gum Arabic. Journal of Food Processing Engineering, 2018, vol. 41, no. 4, e12673. s.l. : DOI 10.1111/jfpe.12673.
48. STURZA R., VEREJAN A., HARITONOV S., MUNTEANU D., COVACI E., SCUTARU IU., DRUȚĂ R., SUBOTIN IU., GUREV A., DRAGANCEA V., DRUȚĂ V., BAERLE A. Chimia aplicată pentru ingineri. Chișinău: Tehnica UTM, 2021. 356 p. ISBN 978-9975-45-698-2.
49. SATO A.C.K., ZAGATTO POLASTRO M., DE FIGUEIREDO FURTADO G., LOPES CUNHA R. Gelled double-layered emulsions for protection of flaxseed oil. Food Biophysics, 2018, vol. 13, pp. 316-323. DOI 10.1007/s11483-018-9537-4.
50. ZADOROJNÂI L., ZADOROJNÂI A. Hyaluronic acid: obtaining, properties and application. Chemistry Journal of Moldova, 2012, vol. 7, no. 2, pp. 57–66. ISSN 1857-1727.
51. SHINDE U.A., NAGARSENKER M.S. Characterization of gelatin–sodium alginate complex coacervation system. Indian Journal of Pharmaceutical Sciences, 2009, vol. 71, no. 3, pp. 313-317. DOI 10.4103/0250-474X.56033.
52. STEFANET M. Anatomia omului. Vol. 2. Chișinău, USMF, CEP Medicină, 2008, 524 p. ISBN 978-9975-915-72-4.
53. BELITZ H.-D., GROSCH W., SCHIEBERLE P. Food Chemistry. 4-th edition. Springer-Verlag, 2009, 1070 p. DOI 10.1007/978-3-540-69934-7.
54. PEYRON M.A., MISHELLANY A., WODA A. Particle size distribution of food boluses after mastication of six natural foods. Archives of Oral Biology, 2004, vol. 49, no. 5, pp. 425-435. DOI 10.1177/154405910408300713.
55. BIEHLER E., MAYER F. et al. Comparison of 3 spectrophotometric methods for carotenoid determination. . s.l. : Journal of Food Science, 2010, vol. 75, no. 1, pp. C55-C61. DOI 10.1111/j.1750-3841.2009.01417.x.
56. MÜLLER H. Die tägliche Aufnahme von Carotinoiden aus Gesamtnahrungsproben und die Carotinoidgehalte ausgewählter Gemüse- und Obstarten. Zeitschrift für Ernährungswissenschaft, 1996, vol. 35, no. 1, pp. 45-50. DOI 10.1007/BF01612027.

57. BEJAN A. Advanced Engineering Thermodynamics. 4-th edition. Wiley, 2016, 800 p. ISBN 978-1-119-05209-8.
58. DINCER I., ROSEN M.A. Exergy: Energy, Environment and Sustainable Development. Elsevier, 2012, 576 p. ISBN 9780080970905.
59. RONCO C., BELLOMO R., KELLUM J.A., RICCI Z. Critical Care Nephrology. 3rd edition. Amsterdam: Elsevier, 2019. 1411 p. ISBN 978-0-323-44942-7.
60. NAKAGAKI T., YAMADA H., TÓTH Á. Maze-solving by an amoeboid organism. Nature, 2000, vol. 407, no. 6803, p. 470. DOI 10.1038/35035159.
61. LUCIA U. Entropy generation and cell growth with comments for a thermodynamic anticancer approach. Physica A: Statistical Mechanics and its Applications. 2014, vol. 406, pp. 107-118. DOI 10.1016/j.physa.2014.03.053.
62. LV Y., CHU Y., ZHOU P., MEI J., XIE J. Effects of different freezing methods on water distribution, microstructure and protein properties of cuttlefish during frozen storage. Applied Sciences, 2021, vol. 11, no. 15, article 6866. DOI 10.3390/app11156866.
63. CUVELIER M.E., SOTO P., COURTOIS F., BROYART B., BONAZZI C. Oxygen solubility measured in aqueous or oily media by a method using a non-invasive sensor. Food Control, 2017, vol. 73, Part B, pp. 1466-1473. DOI 10.1016/j.foodcont.2016.11.008.
64. BHUNIA K., SABLANI S.S., TANG J., RASCO B. Non-invasive measurement of oxygen diffusion in model foods. Food Research International, 2016, vol. 89, no. 1, pp. 161-168. DOI 10.1016/j.foodres.2016.07.015.
65. LADHA-SABUR A., BAKALIS S., FRYER P.J., LOPEZ-QUIROGA E. Mapping energy consumption in food manufacturing. Trends in Food Science & Technology, 2019, vol. 86, pp. 270-280. DOI 10.1016/j.tifs.2019.02.034.
66. MONFORTI-FERRARIO F., DALLEMAND J., PINEDO PASCUA I., MOTOLA V., BANJA M. et al. Energy use in the EU food sector. State of play and opportunities for improvement. Publications Office of the EU, 2015, 172 p. DOI 10.2790/158316.
67. FERREIRA S., NICOLETTI V.R. Use of a tubular heat exchanger to achieve complex coacervation in a semi-continuous process: Effects of capsules curing temperature and shear rate. . s.l. : Journal of Food Engineering, 2021, vol. 310, article 110698. DOI 10.1016/j.jfoodeng.2021.110698.
68. BOUVIER J.M., CAMPANELLA O.H. Extrusion Processing Technology: Food and Non-Food Biomaterials. Wiley-Blackwell, 2014. 544 p. ISBN 978-1-118-54172-2.
69. MUJUMDAR A.S. Handbook of Industrial Drying. 4th ed. Boca Raton: CRC Press, 2014. 1348 p. DOI 10.1201/b17208.
70. KUDRA T., MUJUMDAR A.S. Advanced Drying Technologies. 2nd ed. Boca Raton: CRC Press, 2009. 438 p. DOI 10.1201/9781420073898.
71. RATTI C. Chapter 3: Freeze drying for food powder production. In: (Es.) BHANDARI B., BANSAL N., ZHANG M., SCHUCK P. Handbook of Food Powders. Woodhead Publishing, 2013. pp. 57-84. DOI 10.1533/9780857098672.1.57.
72. PISANO R., FISSORE D., BARRESI A.A. Quality by Design in the Secondary Drying Step of a Freeze-Drying Process. Drying Technology. 2012, vol. 30, no. 11-12, pp. 1307-1316. DOI 10.1080/07373937.2012.704466.

73. SCHROEN K., BERTON-CARABIN C., RENARD D., MARQUIS M., BOIRE A., COCHEREAU R., AMINE C., MARZE S. Droplet microfluidics for food and nutrition applications. Micromachines, 2021, vol. 12, no. 8, article 863. DOI 10.3390/mi12080863.
74. INTELWASTES. Ghid de bune practici «Utilizarea complexă a tescovinei de struguri, mere și alte deșeuri agroindustriale». Chișinău: UTM; Iași: UȘV, 2021, 61 p. . s.l. : https://intelwastes.utm.md/wp-content/uploads/2022/02/Ghid-de-bune-practici-Intelwastes.pdf. Accesat 28.04.25.

*** AUTHOR'S WORKS RELATED TO THE THESIS (TOTAL 49)**

Monograph (1):

1. BAERLE A. Prolongarea funcționalității compușilor biologic activi în compozițiile alimentare. Chișinău, Tehnica UTM, 2023. 177 p. ISBN 978-9975-45-950-1.

Chapters in collective monographs (4):

2. SANDU Iu., SAVCENCO A., BAERLE A., TATAROV P., MACARI A. Capitolul II: „Stabilizarea proprietăților senzoriale și activității biologice a substanțelor biologic active din compoziții alimentare", pp. 34-57. In: STURZA R., GHENDOV-MOȘANU A. (eds.). Ameliorarea calității alimentelor prin biotehnologie și inginerie alimentară. Chișinău: Tehnica UTM, 2023, 267 p.
3. GUREV A., CEȘKO T., BAERLE A., DRAGANCEA V., GHENDOV-MOȘANU A., STURZA R., NETREBA N., BOEȘTEAN O., HARITONOV S. Cap. III. Valorificarea substanțelor biologic active si a biopolimerilor din deșeuri agroindustriale. pp. 58-88. – ibidem.
4. BULGARU V., CUȘMENCO P., POPESCU L., CEȘKO T., SAVCENCO A., BAERLE A, ȚĂRNA R, MACARI A., STURZA R., GHENDOV-MOȘANU A., SANDULACHI A., GUREV A. et al. Cap. VI: „Tehnologii de fabricare a produselor lactate fermentate cu adaosuri vegetale". pp. 136-172. – ibidem.
5. GHENDOV-MOȘANU A., SANDU I., MAZUR M., BANTEA V., BAERLE A., CRISTEA E., STURZA R.. Cap. VIII. Substituirea coloranților sintetici în produse de cofetărie cu extracte și pulberi vegetale. pp. 203-229. – ibidem.

Articles in international indexed journals - ISI, WoS, Scopus (5):

6. BULGARU V., GUREV A., BAERLE A., DRAGANCEA V., BALAN G., COJOCARI D., STURZA R., SORAN M.L., GHENDOV MOȘANU A. s.l. : Phytochemical, antimicrobial, and antioxidant activity of different extracts from frozen, freeze dried, and oven dried jostaberries grown in Moldova. Antioxidants, 2024, vol. 13, no. 8, article 890. DOI 10.3390/antiox13080890.
7. GUREV A., DRAGANCEA V. , BAERLE A. , NETREBA N., BOESTEAN O., HARITONOV S., GAINA B. Properties of Winemaking by-Products of Feteasca Neagra Grape Seeds. Chemistry Journal of Moldova. 2022, vol. 17, nr. 2. p. 50-61.
8. BAERLE A., SAVCENCO A., TATAROV P., FETEA F., IVANOVA R., RADU O. Stability limits of a red Carthamin–cellulose complex as a potential food colourant. Food & Functions, 2021 (2), pp. 8037-8043.
9. BAERLE A., DIMOVA O., URUMOGLOVA I., TATAROV P., ZADOROJNAI L. Phase Diagram of Gelatine-Polyuronate Colloids: its Application for

Microencapsulation and Not Only. Chemistry Journal of Moldova, 2016, vol. 16, no. 1, pp. 97-105. . s.l. : ISSN 1857-1727.

10. BAERLE A., DIMOVA O., ZADOROJNAI L., TATAROV P. et al. Electrophoresis of oil-containing edible microcapsules with protein–polyuronic shells. Ukrainian Food Journal, 2014, vol. 3, no. 2, pp. 211-217. ISSN 2304-974X.

Articles in journals recognized by NAQAER - Open Acces, DOAJ, EBSCO (8)

11. BANTEA-ZAGAREANU V., SANDU Iu., BAERLE A., TATAROV P. Quality assessment of the toffee with sweeteners and dye from walnut septum or kernel's pellicle. Journal of Engineering Science, 2023, vol. 30, no. 2, pp. 144-157. ISSN 2587-3474.

12. POPESCU L., GHENDOV MOȘANU A., BAERLE A., SAVCENCO A., TATAROV P. Color stability of yogurt with natural yellow food dye from Carthamus tinctorius L.. Journal of Engineering Science, 2022, vol. 29, no. 1, pp. 142–150. DOI 10.52326/jes.utm.2022.29(1).13.

13. BAERLE A. Microencapsulation of functional components in the food technology: partially optimistic view. Journal of Engeneering Science, 2021, vol. 28, no. 3, pp. 139-157. ISSN 2587-3474.

14. BAERLE A., TATAROV P., SANDU Iu. Polyphenols and naphthoquinones extraction from walnut pellicula: the impact on kernels quality. Journal of Engineering Science, 2020, vol. 27, no. 2, pp. 145-153. ISSN 2587-3474.

15. RADU O., BAERLE A., TATAROV P., POPESCU L. Factors, that determine the shelf life of a butter-like spread, based on walnut oil. Journal of Engineering Science, 2019, vol. 26, no. 3, pp. 119-124. . s.l. : ISSN 2587-3474.

16. DIMOVA O., BAERLE A. Formation of Microcapsule's Biopolymeric Shells: Electrochemical Aspects. Journal of Engineering Science, 2018, vol. 2, no. 1, pp. 90–94. ISSN 2587-3474.

17. DIMOVA O.V., BAERLE A.V., TATAROV P.G., KIRITSA E.N. Fortification of fermented milk products with microencapsulated beta-carotene. Dairy Industry, 2013, no. 9, pp. 42-43. ISSN 1019-8946.

18. STARODUBTSEV S.I., BAERLE A.V., BRESTECHKO A.L., MAKARI A.V. s.l. : Spectrophotometric modelling of greenhouse films properties. Meridian Ingineresc, 2010, vol. 2, pp. 29–31. ISSN 1683-853X.

Other journals from abroad (2):

19. POPOVICI C., BAERLE A., TATAROV P. Biochemical aspects of walnut dairy-free milk. Proceedings of University of Ruse, 2017, vol. 56, book 10.2, pp. 28-33. ISSN 1311-3321.

20. BAERLE A., POPOVICI C., RADU O., TATAROV P. Effect of synthetic antioxidants on the oxidative stability of cold pressed walnut oil. Journal of Food and Packaging Science, Techniques and Technologies, 2016, no. 9, pp. 19–24. ISSN 1314-7420.

International conferences abroad (8):

21. BAERLE A., SANDU IU., MACARI A., RADU O. Three-step strategy for obtaining of biologically active substances and functional biopolymers from oilseed pomaces. OPROTEH 2021, Bacău, 25-27 May. Book of abstracts, p.72.

22. BAERLE A., TATAROV P., SANDU Iu., STURZA R., MACARI A. Process for obtaining dietary fiber from flaxseed pomace. In: European Exhibition of Creativity and Innovation: Proceedings of the 13th ed. EUROINVENT, Iasi, 2021, pp. 169-170. ISSN 2601-4564.
23. SANDU Iu., BAERLE A., FETEA F., STURZA R. Biopolymeric composition of the walnut kernels' pellicle. ModTech International Conference: Modern Technologies in Industrial Engineering, 2021, 23-26 June, Online edition. Iași. Book of abstracts, p. 107. . s.l. : ISSN 2286-4369.
24. SANDU IU., BAERLE A., RANGA F., RUGINA D., PINTEA A., PATRAȘ A. Some identified biologically active compounds from the walnut kernel's pellicle: wastes? . s.l. : Proceedings of the 10th International Symposium Euro-Aliment 2021, 7-8 Oct. 2021, Galați: Book of Abstracts, p. 56. ISSN 1843-5114.
25. BAERLE A., TATAROV P., SANDU Iu., STURZA R., MACARI A. Process for obtaining dietary fiber from flaxseed pomace. In: European Exhibition of Creativity and Innovation: Proceedings of the 13th ed. EUROINVENT, Iasi, 2021, pp. 169-170. ISSN 2601-4564.
26. SAVCENCO A., BAERLE A., TATAROV P., MACARI A., RUGINA D., RANGA F. Chalchonic profile of yellow food powder-form pigment, obtained from safflower petals. Euro-Aliment 2021, Galați, România. p. 56.
27. POIANȘCHII V., OLARI S., BAERLE A. Arabinoxylan – basic polysaccharide of flax seeds. In: 83rd International Scientific Conference "Youth Scientific Achievements to the 21st Century Nutrition Problem Solution", Kiyv, 5–6 April 2017. s.l. : Abstracts, Part 1, p. 32.
28. BAERLE A., DIMOVA O., ZADOROZHNAYA L., DRUTSE R. Matematicheskie modeli ustoichivosti betanina v rastvorakh VMS. Tezisy VIII Mezhdunarodnoi Konferentsii «Tekhnica i Tekhnologii Pishchevykh Proizvodstv», Mogilev, 2011, vol. 2, p. 7. ISBN 978-985-6979-16-9.

Conferințe internaționale în Republica Moldova (7):

29. BAERLE A., TATAROV P., STURZA R. Entropy (negentropy) control as the condition for intelligent valorisation of food raw materials. International Conference „Intelligent Valorisation of Agro-Food Industrial Wastes". . s.l. : 7-8 october 2021, Chișinău, „MS Logo", p. 18. ISBN 978-9975-3464-2-9.
30. RADU O., BAERLE A., TATAROV P., POPOVICI C. Aggregative stability of emulsions containing walnut oil. Proceedings of the International Conference „Modern Technologies in the Food Industry (MTFI)", Chișinău, 18-20.10.2018, pp. 230-231. ISBN 978-9975-87-428-1.
31. VEREJAN A., BAERLE A., TATAROV P., MITINA T. Dynamics of Walnuts Huy and Rehydration, ibidem pp. 236-237.
32. SAVCENCO A., BAERLE A., IVANOVA R., TATAROV P.. Regression Analysis of Carthamin Extraction from Safflower. ibidem, pp. 243-244.
33. SURCHICEANU Olga, BAERLE Alexei, STURZA Rodica. Flax Seed Texture Agents for the Production of Functional Foods. ibidem, p. 284.
34. GORNEȚ V., BAERLE A., TATAROV P., SUBOTIN Iu. Influence of composition and heat treatment on technological parameters of liver pate. Modern Technologies in the Food Industry, MTFI 2016, Chișinău: UTM, 2016, pp. 190-193.

35. MACARI A., ILI V., BAERLE A., MARDAR M. Raw-dried salami: influence of initial composition for acceleration of drying. Proceedings of 3-rd International Conf. "Modern Technologies In The Food Industry". Chișinău, UTM, 2016. pp. 225-228. http://repository.utm.md/handle/5014/6979.

National conferences (5):

36. RADU O., BAERLE A., MIJA N., ROȘCA I. Particularitățile spectrale ale uleiurilor vegetale fortifiate cu substanțe biologic active naturale. s.l. : Conferința Tehnico Științifică a Colaboratorilor, Doctoranzilor și Studenților UTM, Chișinău: Tehnica UTM, 2014, vol. 2, pp. 73–76. ISBN 978-9975-45-208-3.
37. BAERLE A., DIMOVA O., DRAGANCEA V. et al. Noile utilizări ale betaninei – colorantului principal din Sfecla Roșie (Beta Vulgaris L.). Conf. Șt. Colab, Doct. și Stud. UTM, 2012. - p. 8-9. ISBN 978-9975-45-208-3.
38. YUKAL'CHUK Yu., BAERLE A., DIMOVA O., FULGER D. Optimizatsiya sostava zhidkikh sred dlya polucheniya zhirosoderzhashchikh mikrokapsul. Conferința UTM, Chișinău, 2011, vol. 2, pp. 97–99. ISBN 978-9975-45-208-3.
39. ZADOROJNÂI L., VEREJAN A., BAERLE A., GHEȚIU M., ZADOROJNÂI A. Influența acidului hialuronic asupra stabilității unor coloranți roșii naturali. Conferința Științifică a Colaboratorilor, Doctoranzilor și Studenților UTM, 17–19 November 2010, pp. 126–128.
40. BAERLE A., MEREUȚA O., MACARI A., STURZA R. et al. Planirovanie i tekhnika spektral'nogo eksperimenta UV VIS dlya polikomponentnykh i difaznykh model'nykh sistem. Conferința Științifică Colaboratori, Doctoranzi și Studenți UTM, 2007, pp. 126–127. s.l. : ISBN 978-9975-45-208-3.

Patents (9):

41. POPESCU L., SAVCENCO A., BAERLE A., TATAROV P., GHENDOV-MOȘANU A., STURZA R., PATRAȘ A. Procedeu de fabricare a iaurtului. MD-1625, BOPI 2023 (1).
42. SAVCENCO A., BAERLE A., TATAROV P. et al. Procedeu de obținere a colorantului roșu în formă de pulbere din petale. MD-1609. BOPI 2022 (3).
43. BAERLE A., TATAROV P., SANDU IU. Procedeu de eliminare a compușilor fenolici și naftochinonelor din pieliță miezului de nuci. MD-1566. BOPI 2021 (10).
44. BAERLE A., TATAROV P., SANDU IU., STURZA R. et al.Procedeu de obținere a fibrelor alimentare din șrotul de semințe de in. MD-1509 BOPI, 2021 (3).
45. SAVCENCO A., BAERLE A., TATAROV P., IVANOVA R. Process for producing dyes from Safflower petals. MD-1453, BOPI 2020 (8).
46. RADU O., POPESCU L., TATAROV P., BAERLE A. UTM, MD (titular). Procedeu de obținere a amestecului de grăsimi tartinabile pe bază de smântână dulce. MD-1281. BOPI 2018 (9).
47. DIMOVA O., BAERLE A., TATAROV P., VEREJAN A. Procedeu de obținere a alginaților din alge brune. MD-669. BOPI 2013 (8).
48. BAERLE A., TATAROV P., DIMOVA O. et al. Process for microencapsulation of food and cosmetic oil compositions. MD-557, BOPI 2012 (11).
49. BANTEA-ZAGAREANU V., BAERLE A., LUPASCO A. - Procedeu de obținere a inulinei din rădăcini de plante din familia Asteraceae. MD-456. BOPI 2011 (12).